Title
Formation mechanisms and quantification of organic nitrates in atmospheric aerosol

Author
Rollins, Andrew Waite

Publication Date
2010

Peer reviewed|Thesis/dissertation

Formation mechanisms and quantification of organic nitrates in atmospheric aerosol

by

Andrew Waite Rollins

A dissertation submitted in partial satisfaction of the
requirements for the degree of
Doctor of Philosophy

in

Chemistry

in the

Graduate Division

of the

University of California, Berkeley

Committee in charge:

Professor Ronald C. Cohen, Chair
Professor Kristie A. Boering
Professor William D. Collins

Spring 2010

Formation mechanisms and quantification of organic nitrates in atmospheric aerosol

Abstract

Formation mechanisms and quantification of organic nitrates in atmospheric aerosol

by

Andrew Waite Rollins

Doctor of Philosophy in Chemistry

University of California, Berkeley

Professor Ronald C. Cohen, Chair

Nitrogen oxides (NO_y) in Earth's troposphere exert control over the production of ozone (O_3) and particulate matter. In this dissertation the role of NO_y in the formation of secondary organic aerosols (SOA) is investigated using theoretical as well as both existing and new analytical techniques. A number of insights are gained into the process through which SOA is formed, and the chemical composition of SOA formed through oxidation of volatile organic compounds (VOCs) in the presence of NO_x.

In Chapter 2, I review the theoretical basis for understanding the formation of SOA in the atmosphere and the role of NO_y in the context of this theory. Expectations for how the chemistry of NO_x influences SOA formation and composition in the atmosphere are discussed in the context of previously reported laboratory measurements. In Chapter 3, I describe a chamber study quantifying the formation of organic nitrates and SOA through the oxidation of isoprene by the nitrate radical (NO_3) and discuss the importance of this SOA source on a global scale. The importance of multiple stages of isoprene oxidation by NO_3 is investigated and quantified for the first time. In Chapter 4, I investigate the degree to which organic nitrates in aerosols can be quantified using an Aerodyne Aerosol Mass Spectrometer (AMS). How aerosol organic nitrates affect the current understanding of organic aerosol composition obtained via AMS is discussed. In Chapter 5, I describe a new instrument capable of quantifying organic nitrates in particles, representing a significant advance in the analysis of the chemical composition of organic aerosols. This instrument is used in the laboratory to quantify the formation of organic nitrates in particles formed through high-NO_x photooxidation of a number of SOA precursors.

Contents

List of Figures

List of Tables

Chapter 1

Introduction

1.1 Atmospheric particulate matter

Submicron particulate matter (PM) or aerosol in the Earth's atmosphere has significant impacts on Earth's radiation budget and human health. PM interacts with incoming shortwave solar radiation by both scattering and absorbing to varying degrees, depending on the chemical composition and size distribution of the particles (the direct aerosol effect) [*Coakley and Cess*, 1985; *Charlson et al.*, 1991]. Particles also provide surface area onto which water vapor can condense to form the droplets that form clouds. The distribution of atmospheric PM thereby has a significant impact on Earth's albedo through the spatial distribution, lifetimes, and optical properties of clouds (the indirect aerosol effect) [*Albrecht*, 1989; *Ramanathan et al.*, 2001]. Though the basis of these effects are well known, a large uncertainty in the anthropogenic forcing on Earth's radiation budget exists due to the difficulties associated with parameterizing the aerosol effects in climate models. For example, the Intergovernmental Panel on Climate Change Fourth Assessment Report (IPCC AR4) found the anthropogenic forcing due to the direct aerosol effect to be in the range of -0.9 to -0.1 $\mathrm{W\,m^{-2}}$, and that of the indirect effect to be in the range -1.8 to -0.3 $\mathrm{W\,m^{-2}}$. The large range of uncertainty due to these combined effects of aerosols (-2.7 to -0.4 $\mathrm{W\,m^{-2}}$) encompasses the magnitude of the positive forcing due to carbon dioxide (1.5 to 1.8 $\mathrm{W\,m^{-2}}$) and the uncertainty of the sum of all anthropogenic forcings (0.6 to 2.4 $\mathrm{W\,m^{-2}}$) is by far dominated by the uncertainties in the aerosol effects [*Forster et al.*, 2007]. Significant motivation therefore exists to constrain the sources, chemical composition, spatial distribution and hygroscopicity of atmospheric aerosols.

Adverse health effects associated with aerosols are also significant. Submicron particles are capable of penetrating the human airway and depositing directly in the lungs, thereby acting as a medium for the deposition of chemicals into the bloodstream [*Lippmann*, 2009]. Meta-analyses have demonstrated that exposure to high concentrations of these particles leads to an increased risk of premature death due to cardio-pulmonary disease [e.g., *Dockery*

et al., 1993; *Laden et al.*, 2006]. Both long term and acute elevated exposures to PM have been demonstrated to cause an increased risk of mortality. Generally, a short term increase in PM2.5 (total mass of particles with aerodynamic diameters less than 2.5 μm) of 10 $\mu g\,m^{-3}$ is associated with an increased risk of mortality of 1% in the few days immediately following the exposure. Sustained exposures are associated with an increased risk of $\approx$10% / 10 $\mu g\,m^{-3}$. Because most metropolitan areas typically have daytime PM concentrations in the 10 - 30 $\mu g\,m^{-3}$ range, these increased risks have a significant impact and have been estimated to cause 800,000 deaths / year globally [*Cohen et al.*, 2005]. Over 100 independent studies have inferred these effects and an exhaustive review has been compiled by *Pope and Dockery* [2006]. Understanding the human health effects of aerosols from a process-based standpoint is challenging due to the variability of the chemical composition of particles, but a number of materials in PM including Secondary Organic Aerosols (SOA) produced in the presence of NO_x (NO_x = NO + NO_2) have been shown to be toxic to lung cell cultures [*Baltensperger et al.*, 2008].

Due to these climatic and health consequences, an understanding of the sources and human influences on atmospheric PM is desirable. Nitrogen oxides (NO_y) are known to strongly influence organic aerosol production though the effects that NO_x has on the atmospheric processing of organic compounds [e.g., *Kroll and Seinfeld*, 2008; *Hallquist et al.*, 2009]. However, significant gaps remain in understanding the mechanisms underlying these laboratory observations, and ambient atmospheric data has not yet been used to assess these effects. SOA that is formed by the atmospheric oxidation of volatile organic compounds accounts for about half of the submicron PM in the troposphere [*Jimenez et al.*, 2009]. While the majority of the carbon in the aerosols is known to be of biogenic origin, SOA formation is highly correlated with urban chemistry where NO_x concentrations are typically the highest [*Weber et al.*, 2007]. Therefore, NO_x emissions may be the most significant human influence on SOA formation and composition, and as this is the case an understanding of the link between NO_x and SOA is vital to designing successful control strategies for SOA.

1.2 Organic radical chemistry: the link between NO_x and SOA

Nitrogen oxides have natural sources such as lightning, natural wildfires and microbial activity. However, the primary input of oxidized nitrogen to the atmosphere is through anthropogenic combustion processes. The IPCC AR4 recently compiled a global budget of NO_x sources. In that study the anthropogenic fossil fuel, aircraft, agricultural and biomass burning NO_x sources were estimated to be 33.4 TgN / yr (70.9-79.9% of the total), while the natural soil emission and lightning sources were 8.4-13.7 TgN / yr (20.1-29.1%) [*Forster et al.*, 2007]. This additional NO_x leads to a major change in the fate of organic compounds, which are oxidized in the atmosphere via the chemistry of peroxy radicals (RO_2). Most atmospheric

oxidation processes eventually lead to the production of these short lived organic peroxy radicals. In the absence of NO_x, these radicals react with other organic peroxy radicals or with the hydroperoxyl radical (HO_2). The following reactions summarize this chemistry, where R and R' are organic groups:

$$\begin{aligned} RO_2 + R'O_2 &\rightarrow ROOH + R'{=}O && \text{(R1)} \\ &\rightarrow RO + R'O + O_2 && \text{(R2)} \\ &\rightarrow ROOR' + O_2 && \text{(R3)} \\ RO_2 + HO_2 &\rightarrow ROOH + O_2 && \text{(R4)} \end{aligned}$$

When nitrogen oxides are present, a significant perturbation to the fate of the organic peroxy radicals exists:

$$\begin{aligned} RO_2 + NO &\rightarrow RO + NO_2 && \text{(R5)} \\ &\rightarrow RONO_2 && \text{(R6)} \\ RO_2 + NO_2 &\rightarrow ROONO_2 && \text{(R7)} \\ RO_2 + NO_3 &\rightarrow RO + NO_2 + O_2 && \text{(R8)} \end{aligned}$$

Due to reactions (R5) - (R8), the products of organic carbon oxidation in urban environments and other high NO_x environments is significantly different than that of organic carbon in pristine environments. As well, the nitrate radical (NO_3), which is formed via the reaction of NO_2 with O_3

$$NO_2 + O_3 \rightarrow NO_3 + O_2 \qquad \text{(R9)}$$

can react rapidly and directly with alkenes and aldehydes. The differences in chemical composition and total amounts of organic aerosols that are produced in high-NO_x and low-NO_x environments is due in part to this chemistry.

1.3 Aerosol radiative forcing

The differences in aerosol chemical composition produced in high NO_x and low NO_x environments have important consequences for the climate impacts of SOA. Organic nitrates are formed through the oxidation of organic compounds in the presence of NO_x, and the higher molecular weight organic compounds which are more likely to form SOA also have significant yields to form nitrates. The abundance of organic nitrates in ambient aerosols is not well constrained, and the presence of nitrate in aerosols may have important climate impacts via the direct and indirect aerosol radiative effects which are both known to be functions of chemical composition. The absorptive and scattering optical properties of an aerosol are functions of both aerosol size and chemical composition [*Bergstrom et al.*, 2007].

Aerosol optical properties can be parameterized using the Aerosol Optical Depth (AOD), τ, and the Single Scattering Albedo (SSA), ω. AOD is the total light extinction by aerosols in an air parcel ($I/I_0 = e^{-\tau}$), and SSA describes what fraction of the extinction is due to scattering with values of ω ranging from zero to one. Smaller values of ω therefore correspond to more strongly absorbing aerosols while larger values correspond to efficiently scattering aerosol. Laboratory measurements of ω at 532 nm for carbonaceous aerosols range from 0.2 - 1.0, with soot or 'black carbon' having the lowest values, and organic components the highest [*Bergstrom et al.*, 2007]. Urban oxidation of particles has been observed to be correlated to increased ω for ambient aerosols. For example, ω was observed to increase from 0.6 to 0.85 throughout the day in Mexico City, coincident with an increase in oxidized organic aerosol [*Paredes-Miranda et al.*, 2008]. However the extent to which organic oxygen vs. organic nitrogen independently contribute to these changes in ω has not been investigated.

SSA also generally increases with particle size [*Yu et al.*, 2006]. Because hygroscopicity has a strong effect on how particle size will vary with relative humidity, chemical influences on hygroscopicity result in an impact on the aerosol direct effect as well. Organic compounds in ambient particles have been observed to both enhance and suppress aerosol hygroscopic growth [*Pan et al.*, 2009]. The differences between enhancement and suppression of growth by organics is likely due to the degree of aerosol oxidation, and increased oxidation has been shown to be strongly correlated to particle hygroscopicity (κ) [*Chang et al.*, 2009; *Jimenez et al.*, 2009], with κ values [*Petters and Kreidenweis*, 2007] of up to 0.2 observed for ambient oxygenated organic aerosol. Small organic nitrates are systematically $\approx$ 2 orders of magnitude less soluble than the corresponding alcohol, hydroperoxyl or carbonyl, and thus nitrates may be less hygroscopic [*Sander*, 1999]. Cloud Condensation Nucleus (CCN) activity of particles is a function of their hygroscopicity, and therefore the aerosol indirect effect may also be affected by the CCN activity of nitrates.

1.4 Nitrate aerosols and the NO_y budget

Not only does NO_x exert control over the composition and mass of organic aerosol in the atmosphere, but organic aerosols are likely to have an impact on the distribution of the total oxidized nitrogen in the atmosphere as well. Besides its important impact on SOA formation, NO_x plays a critical role in the catalytic formation of tropospheric ozone, which is a breathing hazard [*Jerrett et al.*, 2009] and a significant anthropogenic greenhouse gas (0.25 - 0.65 $W\,m^{-3}$) [*Forster et al.*, 2007]. NO_x also leads to the deposition of reactive nitrogen through the formation of ammonium nitrate particles (NH_4NO_3), nitric acid (HNO_3) and organic nitrates, which can deposit directly onto surfaces via dry deposition and through washout by rain. These nitrogen inputs have significant ecological consequences for nitrogen limited ecosystems [*Matson et al.*, 2002]. Thus, significant motivation exists to understand all significant atmospheric sources and sinks of oxidized nitrogen.

The formation of organic nitrates and peroxy nitrates via reactions (R6) and (R7) consti-

tute either sinks or temporary reservoirs of NO_x, and this can have important implications for long-range transport of NO_x in the atmosphere. For example, molecules of the form $R(O)O_2NO_2$ (peroxy acyl nitrates, PNs), are thermally unstable and are known to effectively transport NO_x leading to the formation of ozone much further downwind than NO_x itself can be transported [e.g., *Wolfe et al.*, 2008]. NO_x export of this nature has been shown to increase O_3 concentrations on the order of ≈10%, and lead to exceedances in the EPA 8-hour ozone standard [*Hudman et al.*, 2004]. In urban outflow, alkyl nitrates (ANs, $RONO_2$) can typically be 10 - 20% of NO_y (e.g. *Day et al.* [2003]), which is comparable to the PN contribution. ANs are thermally stable, but may not be chemically stable. $RONO_2$ may for example recycle NO_x through further oxidations of the organic backbone through a reaction such as

$$RONO_2 + OH \rightarrow R' + NO_X \tag{R10}$$

and this has been shown to have a critical control on surface ozone concentrations [e.g., *von Kuhlmann et al.*, 2004; *Fiore et al.*, 2005]. These uncertainties in the fate of organic nitrates translate to differences in ozone production, for example, in the eastern United States of 4-12 ppb [*Fiore et al.*, 2005]. As the atmospheric fate of AN is not well understood, incorporation into aerosol leading to transport and potential downwind release of NO_x is an unconstrained possibility.

1.5 Overview of this work

In this dissertation a number of developments are made towards understanding the control that NO_x has on PM formation, as well as the ability that organic nitrates have to partition to atmospheric aerosols. Chapter 2 outlines the theoretical basis for understanding the effects that NO_x is expected to have on the formation of organic PM. Equilibrium partitioning theory is used in the context of an explicit chemical oxidation mechanism to examine how varying NO_x concentrations should effect the formation of SOA from photooxidation. α-pinene which is a significant atmospheric SOA precursor is used as a model system for this because its photochemistry is currently more well constrained than that of most other SOA precursors. I show that NO_x can lead to increased or decreased formation of SOA, depending on the NO:NO_2 ratio. This allows for an understanding of the apparent 'NO_x-saturated' and 'NO_x-limited' regimes of SOA formation which have been observed in chamber experiments. The prior laboratory experiments which have studied the SOA / NO_x system are reviewed and discussed in this context.

Chapter 3 discusses a laboratory experiment which was used to understand the formation of SOA and organic nitrates through the reaction of isoprene with the nitrate radical (NO_3). Isoprene is by far the most significant source of non-methane organic carbon to Earth's atmosphere. The potential of isoprene to form SOA has been debated significantly in the literature, though the isoprene + NO_3 channel has received little study. I show that, while

the initial stable products of the isoprene + NO_3 reaction are a poor source of aerosol, these initial products will react with NO_3 to form significant SOA. The total yield to form organic nitrates through both of these stages of oxidation is also constrained, and the importance of the isoprene + NO_3 reaction as a global SOA source is discussed. It is found that in the atmosphere these doubly oxidized products are likely to be formed, resulting in an SOA mass yield of 14%.

While organic nitrates are likely to be important components of ambient aerosols, the existing aerosol measurement techniques are not capable of quantifying them with high time resolution. Aerosol mass spectrometry (AMS) is likely to be the most widespread technique currently used for quantification of aerosol chemical composition with high time resolution. Its ability to measure organic nitrates has been discussed in the literature, but not studied directly. In Chapter 4, I use a series of organic nitrate SOA proxy molecules including monoterpene hydroxynitrates to evaluate the response of an AMS to organic nitrates. I show that organic nitrates are unlikely to be distinguishable from inorganic nitrates in atmospheric aerosols using an AMS. Also, I show that the presence of aerosol organic nitrate may lead to a significant error in the calculation of the elemental composition of OA with the AMS, which is a technique that has been employed in a number of recent publications.

Chapter 5 describes a new measurement technique developed at Berkeley to quantify aerosol organic nitrate directly. The theory of operation and laboratory evaluation are discussed. This instrument is shown to have the potential to detect aerosol organic nitrate in ambient environments with time resolution on the order of ≈ 1 min. Further, the instrument is used to measure the contribution of organic nitrates to SOA generated in the lab via photooxidation of VOC's.

1.6 Suggestions for future research

Based on modeling and laboratory studies, the work in this dissertation suggests that organic nitrates may be more widespread sources of atmospheric SOA than previous observations have indicated. As well, an important fraction of NO_y may exist in the form of aerosol organic nitrates, which likely has implications for air quality and nitrogen deposition. Direct observations of aerosol organic nitrates using the technique described in Chapter 5 may lead to a significantly improved understanding of this open question. The arguments made in Chapter 2 suggest that the handle that NO_x has over SOA formation may be more complicated than previously thought. Chamber experiments which have been used to evaluate the SOA yields from photooxidation of VOCs have typically been performed in NO:NO_2 regimes which are not atmospherically relevant. A reexamination of key species such as α-pinene with careful independent controls over NO and NO_2 may reveal important, previously unobserved effects. Finally, if organic nitrates are not as ubiquitous in atmospheric aerosols as the conclusions in this dissertation might suggest based on modeling and laboratory experiments, the discrepancy should be addressed more directly. Ambient aerosol organic nitrate

may be converted to volatile nitrate or NO_x through aqueous or heterogeneous chemistry, processes which may result in lower ambient concentrations than modeling and laboratory measurements suggest. The new measurement technique described here could be used both to probe the formation of organic nitrate aerosol and its atmospheric fate.

Chapter 2

Theory and modeling of the effects on NO_X on organic aerosol formation

2.1 Introduction

The formation of submicron organic particles in the atmosphere is currently understood through the framework of an equilibrium partitioning theory. In this picture, individual organic compounds exist in equilibrium between the gas and condensed phases and the existing liquid organic particles act as a medium for the solvation of the semi-volatile organic compounds. Due to Raoult's law, an individual compound can be found in the condensed phase, even if its gas phase concentration is below the saturation vapor pressure of the pure compound. This theory is believed to be an accurate description and predictor of the processes that determine atmospheric OA concentrations. Most of the experimental evidence to support this theory comes from a number of laboratory smog chamber experiments performed over the previous two decades. In general the observations in these experiments support partitioning theory, and have provided data (equilibrium partitioning coefficients) to allow partitioning theory to be used to calculate the expected OA concentration in the atmosphere based on the known inputs of organic carbon. In the last few years, motivated by differences between the OA observed in the atmosphere and in the chambers, a number of possible chemical perturbations to the original simple theory have emerged. While these perturbations suggest that the compounds engaged in the gas/particle partitioning are essentially not as chemically static as the original picture treats them, the basic theory still stands and is the best way that we have to think about organic aerosols in the atmosphere.

In this chapter I will briefly introduce partitioning theory and use it to discuss the effects that NO_x is expected to have on the formation of organic aerosols. The experimental observations which have been made to test these theories will be reviewed. I will draw attention to a few key gaps in the current knowledge and outline the uncertainties which may limit our ability to predict partitioning. The role of organic nitrates is highlighted and

some calculations based on a near-explicit chemical mechanism are made to suggest how important the formation of organic nitrate aerosols may be to the SOA and NO_y budgets.

2.2 Atmospheric submicron aerosol

The formation of submicron aerosols (particulate matter or PM) in the atmosphere is initiated through nucleation of very low volatility gases to form nucleation mode particles ($\leq$10 nm). Only very low volatility compounds are capable of overcoming the Kelvin effect and forming the small critical clusters from which almost all submicron particles originate. While organic compounds are believed to be involved in the formation of new particles in the atmosphere, sulfuric acid (H_2SO_4, vapor pressure = 9.9 μtorr at 296 K) is the only compound for which the physics of nucleation has been observed to be in good agreement with observations of nucleation in the atmosphere. After new particles have formed and grown to $\approx$ 10 nm, they grow rapidly through the condensation of non-volatile and semi-volatile inorganic and organic compounds which constitute the majority of the condensed phase mass [*Seinfeld and Pandis*, 1998].

By mass, submicron tropospheric particles are on average $\approx$ 1/2 inorganic and 1/2 organic compounds [*Murphy et al.*, 2007; *Zhang et al.*, 2007a]. The concentration of inorganic compounds (mostly ammonium sulfate (NH_4HSO_4), ammonium bisulfate ($(NH_4)_2SO_4$) and ammonium nitrate (NH_4NO_3)) can typically be accurately predicted given knowledge of the gas phase precursor (H_2SO_4, NH_3, and HNO_3) concentrations and the temperature (e.g. *Fountoukis et al.* [2009]). This is useful from an air quality standpoint because the formation of PM can be controlled indirectly through regulating the emissions of the precursor gases SO_x, NH_3 and NO_x.

While the mass of inorganic compounds in tropospheric PM can be explained with knowledge of only a few equilibrium constants, a useful and accurate parametrization of organic aerosol formation continues to elude current efforts. Organic aerosol formation and fate is difficult to model because both the sources of material for organic aerosols and the underlying physics and chemistry of their formation and transformation in the atmosphere are orders magnitude more complicated than that for the inorganics.

2.3 Partitioning theory

The simplest useful theory of organic aerosols is one in which organic particles in the atmosphere are pictured as liquid droplets which act as a solvent for the dissolution of each individual organic compound [*Pankow*, 1994a, b]. In this view each individual compound i partitions between the gas and condensed phases, with the fraction of the compound in the condensed phase given by

$$Y_i = \frac{M_0/C_i^*}{1 + M_0/C_i^*} \tag{2.1}$$

where Y_i is the condensed phase fraction, M_0 is the total concentration of all condensed phase organics, and C_i^* is a gas/particle partitioning coefficient specific to species i [*Donahue et al.*, 2006]. Because partitioning theory has been developed by atmospheric scientists with a history of measuring the total mass of PM, the equations most commonly used have a mass centered view. As a result, units for M_0 and C^* are typically μg m^{-3} (μg of particulate matter per m^{-3} of air). Using the units most commonly encountered in the literature, the partitioning coefficient for a species is related to its vapor pressure by

$$\frac{1}{C^*} = \frac{760RT}{MW_{\text{om}} 10^6 \zeta_i P_{L,i}^0} \tag{2.2}$$

Here, R is the gas constant, T is the temperature, MW_{om} is the average molecular weight (g mol^{-1}) of the condensed phase organic mass (M_0), ζ_i is the activity coefficient, and $P_{L,i}^0$ (torr) is the liquid vapor pressure of compound i. Equations (2.1) and (2.2) are straight-forward applications of Raoult's law [*Pankow*, 1994a, b]. Figure (2.1) shows the condensed phase partitioning predicted by Equations (2.1) and (2.2) assuming $MW_{\text{om}} = 150$ μg m^{-3} (an approximate average molecular weight of atmospheric OA) and $T = 298$ K. The observed ambient submicron organic aerosol concentrations are typically in the range of $\approx$ 2-3 μg m^{-3} in remote locations and $\approx$ 5-20 μg m^{-3} in urban locations, with up to 80 μg m^{-3} being observed recently in very polluted regions such as Beijing [*Jimenez et al.*, 2009]. As shown in Figure (2.1), at these ambient concentrations compounds with C^* values less than ≈ 0.1 μg m^{-3} are typically mostly partitioned to the particle phase, while compounds with C^* greater than 1000 μg m^{-3} are almost completely in the gas phase. As a rule of thumb, if $C_i^* = M_0$, than species i is half in the condensed phase and half in the gas phase. The compounds with C^* values in the range between 0.1 and 1000 are likely to be found in either the condensed or vapor phases depending on the ambient organic aerosol loading, and Figure (2.1) shows that the partitioning can be quite sensitive to the C^* value at a given loading. For example, with $M_0 = 10$ μg m^{-3} a compound with $C^* = 100$ would be found 9% in the condensed phase, while a compound with $C^* = 1$ would be 91% condensed. This means that for an accurate prediction of ambient organic aerosol concentrations based on a bottom-up approach, errors in the presumed C^* values on the order of $\log_{10} C^* = \pm 1$ for compounds in this semi-volatile category can lead to large errors in the calculated partitioning. Further examples of partitioning errors of this kind are explored in section (2.7).

In many cases partitioning theory has been shown to be in good agreement with observations in chamber SOA experiments. Usually this has been done by showing that the yield to form SOA by oxidizing a VOC in a chamber can be fit with Equation (2.1). A comprehensive list of the various experimental facilities used for these experiments is included in *Hallquist et al.* [2009]. The other key predictions of partitioning theory which have been observed both in chamber and ambient SOA is that the partitioning is sensitive to dilution (controlled reductions in M_0) and temperature, which has a strong impact on vapor pressure and therefore C^* [*Grieshop et al.*, 2007; *Cappa and Jimenez*, 2010]. These basic observed thermodynamic behaviors of ambient aerosols which are predicted by partitioning theory are

the basis for belief that the physical picture behind this theory describes atmospheric OA, and furthermore that the mechanism by which SOA is produced in chamber experiments is the same as that in the atmosphere.

2.4 Applying partitioning theory

The application of partitioning theory in chemical transport models has been the basis of most bottom-up approaches which attempt to calculate ambient organic aerosol loadings. Frequently, the only quantity that has been measurable in the atmosphere is the total organic aerosol loading (M_0) and this is the quantity which most model outputs have been compared to. For a set of semi-volatile compounds, each with a total (gas + particle) concentration of c_i, M_0 is given by the sum of the condensed phase concentrations of the individual species. Because Y_i is the fraction of compound i that is in the condensed phase, M_0 is given by

$$M_0 = \sum_i Y_i \, c_i \tag{2.3}$$

Because M_0 itself appears in Equation (2.1) which is used to calculate the Y_i values, using Equation (2.1) we have

$$M_0 = \sum_i \frac{M_0/C_i^*}{1 + M_0/C_i^*} \, c_i \tag{2.4}$$

To find M_0 given the C^* and c values, an iterative approach seeking a self-consistent value for M_0 can be taken. In this approach, gas/particle equilibrium at all times is implicit. Alternately, equation (2.2) can be cast into a kinetic framework where condensation and evaporation are calculated and used to track the change in particle mass over time. Either way, the fundamental quantities required to calculate M_0 in the atmosphere are the concentrations (c_i) and saturation concentrations (C_i^*) of the organic compounds.

Unfortunately, a comprehensive set of measurements of the concentrations of semi-volatile compounds in the atmosphere are not sufficiently available to calculate M_0, in fact semi-volatile compounds are rarely if ever quantified. One reason for this is that the number of compounds likely to participate in the partitioning process is much too great (100's to 1000's) for measurements of them to be a reasonable undertaking [*Goldstein and Galbally*, 2007]. Further, direct measurements of semi-volatile compounds is challenging from an instrumental standpoint and hence data using chromatographic techniques which can measure these compounds are only beginning to be reported. However, semi-volatile compounds present in the atmosphere mostly originate from the gas phase oxidation of a much smaller set of directly emitted volatile and semi-volatile compounds which are more easily and routinely quantified. For this reason the basic strategy of SOA modeling is to accurately quantify the emissions, and then use laboratory data and presumed gas phase oxidation schemes to calculate the concentrations (c_i) of the semi-volatile organic compounds that can form aerosol.

The C^* values required for calculating M_0 have been typically acquired in two different ways. One way is to calculate them directly through knowledge of the vapor pressure and activity coefficient and application of Equation (2.2). Few direct measurements of activity coefficients ζ_i have been made and these are almost universally assumed to be 1. Vapor pressures for semi-volatile organics are also not routinely measured, but in recent years a number of methods have been developed to estimate vapor pressures for arbitrary organic compounds [*Hilal et al.*, 2003; *Clegg et al.*, 2008; *Pankow and Asher*, 2008]. It should be noted that these methods use measured vapor pressures of known compounds to estimate those of structurally similar compounds. While the compounds of interest are semi-volatile and non-volatile ($P_L^0 \approx \mu$torr), the data are heavily weighted by measurements of volatile compounds ($P_L^0 >$ mtorr).

The second and more common strategy to find partitioning coefficients is to calculate effective C_i^* and c_i values simultaneously by measuring the observed aerosol mass produced through oxidation of the precursor VOC's in the lab. To do this a series of experiments are performed where the total mass of oxidation products ($\sum_i c_i$) are known, M_O is measured, and Equation (2.4) is applied to calculate the C_i^* values [*Odum et al.*, 1996]. This strategy is advantageous in that it results in a direct measurement of the C_i^* and c_i values required for modeling, but problematic because it will result in errors if for some reason the laboratory conditions used in the experiment result in a much different production of total aerosol than would be observed in the atmosphere from oxidation of the same VOC. This is a notorious problem in the literature due to for example unrealistic relative concentrations of radicals such as OH : NO or OH : NO_2, temperature, effects from chamber walls, and extent of reaction. Also, typically these values are calculated from a set of measurements where $M_0 >$ 100 μg m^{-3} and then used to predict concentrations in the range 1 - 10 μg m^{-3}. This can be a problem because Equation (2.4) is highly non-linear in M_0. Finally, while in principle, the use of effective C_i^* and c_i values allows for a calculation of M_0, because the partitioning of specific semi-volatile compounds is not considered, aerosol chemical composition is not addressed with this method and therefore this scheme does not lend itself to considering the importance of further chemistry of the initial oxidation products. All general circulation model studies of SOA production to date [e.g., *Heald et al.*, 2005; *Volkamer et al.*, 2006] have used the parameters derived from chamber studies of this kind to calculate SOA.

2.5 Sources of semi-volatile compounds

The vast majority of organic carbon emitted to the atmosphere by humans and vegetation is volatile, with vapor pressures greater than 1 torr [*Guenther et al.*, 1995; *Olivier et al.*, 2005; *Guenther et al.*, 2006]. The gas phase oxidation of these species generally leads to a suite of compounds with a wider distribution of vapor pressures than the precursor. Some of the products are more condensible due to the addition of functional groups, while other products are more volatile due to fragmentation of the carbon-carbon bonds. In the atmosphere, OH,

NO_3 and O_3 are the primary gas phase oxidants which initiate oxidation processes. OH oxidation mostly happens during the day because its largest source is from photolysis of O_3 (generally termed 'photooxidation') while NO_3 is only active in the dark due to its rapid photolysis by visible light, and O_3 is active both at day and night. Generally, OH oxidation is thought to be responsible for the largest fraction of oxidation due both to it's rapid reaction with saturated and unsaturated compounds, and its diurnal cycle which parallels that of biogenic carbon emissions. The distribution of stable oxidation products resulting from the oxidation of any VOC is a strong function of the chemical environment in which oxidation takes place. For example, OH oxidation of alkanes and alkenes in the atmosphere produces organic peroxy radicals as key intermediates. Peroxy radicals are short lived, reacting rapidly with most other radicals. In the absence of NO_x, their primary fate is to react with other organic peroxy radicals and hydroperoxyl radicals. If NO_x is present, typically the concentration of NO in the atmosphere is much greater than that of the peroxy radicals, so reaction with NO is the primary pathway. Peroxy radicals also will react with NO_3 though few rate constants have been measured for RO_2 + NO_3 reactions. RO_2 can react with NO_2 to form peroxy nitrates ($ROONO_2$), but these molecules have short thermal decomposition lifetimes (minutes - hours at T > 287K) and exist in equilibrium with NO_2. Consequently they have not typically thought of as important aerosol precursors.

Figure (2.2) shows the reaction scheme that is generally thought to dominate atmospheric peroxy radical chemistry. Here, the formation of an organic peroxy radical is shown from hydrogen abstraction from an alkane followed by addition of O_2. Analogous organic peroxy radicals are formed from reactions of OH, O_3 and NO_3 with alkenes and aldehydes. The RO_2 + RO_2 reactions are thought to either immediately produce closed shell products with hydroxyl and carbonyl functionalities, or produce unstable organic alkoxy radicals. Alkoxy radicals either decompose or react with O_2 to produce carbonyls. RO_2 + HO_2 reactions produce organic hydroperoxyl compounds.

$$RO_2 + HO_2 \rightarrow ROOH \tag{R11}$$

A number of studies have also produced evidence in a number of ways that RO_2 + HO_2 may also produce some OH, perhaps through a reaction such as

$$RO_2 + HO_2 \rightarrow RO + O_2 + OH \tag{R12}$$

though these products have not been measured directly [*Thornton et al.*, 2002]. One very recent study (Wennberg et al., unpublished) has demonstrated that further chemistry of the organic hydroperoxides may be the important OH recycling step through a reaction such as

$$ROOH + OH \rightarrow R' + OH \tag{R13}$$

Reactions of organic peroxy radicals with NO produce organic nitrates and alkoxy radicals which eventually result in more volatile carbonyl and fragmented compounds. Although

peroxynitrates formed from RO_2 + NO_2 reactions are thermally unstable, one very recent study has shown that these may be important intermediates in the formation of the SOA from e.g. isoprene oxidation (Seinfeld, unpublished).

Generally, because of the chemistry shown in Figure (2.2) NO_x is thought to exert an important control on how much SOA will be formed from the oxidation of a VOC. Next to the stable products, Figure (2.2) shows the approximate multiplicative changes in vapor pressure resulting from the addition of the various functional groups to the starting VOC. Vapor pressure changes are estimated using the SIMPOL (SIMplified P_L^0) method of *Pankow and Asher* [2008]. In the absence of NO_x the products are expected to be mostly hydroperoxides, hydroxyl and carbonyl compounds. NO will shift the product distribution towards a larger fraction of carbonyl and fragmented compounds, as well as organic nitrates and preoxynitrates. Measured yields to form organic nitrates vs. alkoxy radicals from the RO_2 + NO reaction for SOA relevant VOC's range from 8% (isoprene) up to $\approx$ 35% (long chain alkanes) [*Arey et al.*, 2001; *Paulot et al.*, 2009], generally increasing with the size of the carbon backbone. While the organic nitrates are estimated to be approximately as low in vapor pressure as the alcohols, the higher probability of forming carbonyls and fragmented compounds in high-NO_x oxidation has generally been thought to shift the product distribution towards more volatile products overall than in the NO_x free case.

2.6 NO_x dependence of SOA yields

Figure (2.3) illustrates the consequences of the general oxidation scheme depicted in Figure (2.2) on the volatility of organic compounds in the atmosphere. This figure tracks both the oxygen/carbon ratio (O:C) and volatility (C^*) of the oxidation products of low-NO_x and high-NO_x α-pinene photooxidation. To generate this figure, the Master Chemical Mechanism[1] (MCM) [*Saunders et al.*, 2003] was used to predict the distribution of products in a box model simulation. The MCM is a near-explicit oxidation scheme for analyzing gas-phase processing of atmospherically relevant organic compounds. The α-pinene mechanism used here consisted of a total of 310 organic species, and 899 reactions. The simulation was initiated with 10 ppb α-pinene, an important OA precursor, and the OH concentration was held fixed at 6×10^6 molecules cm^{-3} OH, an average daytime OH concentration. SIMPOL was used to estimate the vapor pressures of all species in the model at 298 K. To convert P_L^0 to C^* using Equation (2.2) the activity coefficients (ζ_i) were assumed to be 1, and the average weight of the organic aerosol was assumed to be 150 g mol^{-1}. in Figure (2.3) the O:C is used as a general indicator of atmospheric oxidation. Most VOC's are emitted with O:C = 0, and in general atmospheric oxidation increases the O:C by adding functional groups and breaking carbon-carbon bonds until O:C = 2 (CO_2). Thus, time in the atmosphere necessarily moves upwards on the O:C axis.

[1] `http://mcm.leeds.ac.uk/MCM/`

In reading this figure one should keep in mind that the MCM predicts the formation of many compounds which have not specifically been measured in the laboratory oxidation of e.g. α-pinene. The modeling of explicit chemistry of unmeasured reactions is based on generalized reaction schemes for oxidation of organic compounds for which there is a significant amount of data from studying simpler compounds. The MCM output has also been tuned primarily to accurately predict O_3 production as opposed to organic aerosol. However, the MCM does predict the production of some important contributors to SOA which have been measured directly. Figure (2.3) illustrates both the spread in volatility of products as oxidation occurs, as well as the strong control that NO_x has on the product distribution. The top panel shows where α-pinene lies in the O:C - volatility space. The middle panel shows the product distribution after 1 hour of reaction at 6×10^6 molecules cm^{-3} OH (the lifetime of α-pinene to OH at this concentration is 0.87 hours). The bottom panel shows the products after 5 hours of reaction time. The intensity shown in the figure is weighted by total carbon, so one α-pinene molecule would appear the same as 10 CO molecules. The left two panels are for the NO_x free simulation, and the right panels were initiated with 100 ppb NO. After 1 hour, a small fraction of the carbon is below the $\log_{10} C^*$ range of 0 - 1 which Figure (2.1) indicates is required for condensation under atmospheric conditions. A larger fraction of the carbon is below this threshold after 5 hours. It is evident that the product distribution in the NO_x-free and high-NO_x cases are significantly different. In general, the NO_x-free case produces a lot of material in the $\log_{10} C^*$ range of 0 - 6. The high NO_x case appears more bi-modal, with a larger fraction of products at the lower volatility range ($\log_{10} C^* < 0$) than the NO_x free case, but also produces more very volatile material such as CO, CO_2 (CO_2 is not tracked in the model or figures) and acetone. Figure (2.6) provides an alternate representation of the α-pinene oxidation model output. Here, the products are weighted by carbon (top two panels) and nitrogen (bottom panel) and the C^* distributions are shown at 5 different times during the model run. The bottom panel clearly shows that the organic nitrogen produced in α-pinene oxidation is likely to be all condensible, while the carbon is spread over the entire volatility range.

Figures (2.3) and (2.6) show that in general with very high concentrations of NO present during the oxidation of α-pinene, the volatility distribution of the products can be shifted significantly relative to the NO_x-free case. To asses the quantitative effect of NO_x on SOA formation, box model simulations were run with the α-pinene MCM oxidation scheme using different initial concentrations of NO. SIMPOL was used to estimate the vapor pressures of the products, and Equation (2.4) was used to calculate the OA mass concentration after 99% of the α-pinene was reacted away. The resulting SOA mass yield is shown in Figure (2.7). Two sets of simulations were run, one with an initial α-pinene concentration of 10 ppb, and the other with 50 ppb. OH concentration was held fixed at 6×10^6 molecules cm^{-3}. The NO_x concentration was varied by changing the initial concentration of NO in the simulation. Adding NO to the simulation also increases the NO_2 concentration through the reaction of

NO with organic peroxy radicals

$$RO_2 + NO \rightarrow RO + NO_2 \tag{R14}$$

which occurs with a yield of 77% for the α-pinene peroxy radicals. In the simulations with NO_x, the photolysis rates have an important impact on the result, primarily because the photolysis of NO_2 decreases the NO_2/NO ratio, and leads to the formation of ozone (O_3) through the following reactions:

$$NO_2 + h\nu \rightarrow NO + O \tag{R15}$$
$$O_2 + O \rightarrow O_3 \tag{R16}$$

To simulate the chemistry under ambient conditions, typical daily maximum photolysis rates were used for all species (for a complete list of the photolysis reactions, see the MCM web page on photolysis reactions[2]). The SOA mass yield is defined as the increase in OA mass divided by the reacted α-pinene mass:

$$Y = \frac{\Delta M_0}{\Delta \alpha\text{-pinene}} \tag{2.5}$$

Because the yield is defined in this way, yields greater than one are possible due to the increased molecular weight of some of the products.

Figure (2.7) illustrates the significant impact that NO_x can have on the mass of SOA that is formed from the photooxidation of a VOC. For the 10 ppb α-pinene case, the mass yield increases from 21% at 0 NO to a maximum of 80% at 8 ppb NO (shown as initial NO / initial α-pinene of 0.8 on figure). Increasing the NO / α-pinene above 0.8 leads to a monotonic decrease in the yield, down to 55% at the maximum modeled NO concentration of 100 ppb. The non-linear dependence observed in these simulations is due to two different effects of increasing NO. One effect is that the addition of NO leads to the production of O_3 through reactions R14 - R16. Ozone itself reacts directly with α-pinene and thus can change the product distribution. The more important effect of NO on SOA yield is due to the competition between HO_2, RO_2, NO and NO_2 for the α-pinene peroxy radicals as discussed in Section (2.5). This peroxy radical competition is itself a nonlinear effect. At low NO concentrations the increases in NO input lead to increased NO and NO_2 which lead to increases in the rates of RO_2 + NO and RO_2 + NO_2 relative to RO_2 + HO_2. However, in the NO_x saturated regime where all of the organic peroxy radicals react with either NO or NO_2, further increases in NO decrease the importance of RO_2 + NO_2 relative to RO_2 + NO. One reason that this is important in the α-pinene MCM model is because the MCM predicts the formation of a large peroxy acyl nitrate molecule as one of the low vapor pressure, high yield products. These molecules are only formed through the RO_2 + NO_2 channel and thus in the very high NO regime the yield of this product decreases.

[2] `http://mcm.leeds.ac.uk/MCM/parameters/inorg.htt`

As discussed above the MCM reaction scheme for α-pinene is based on some products have not been measured, but are presumed to be produced based on analogs to other similar reaction systems. Thus, both the yields and vapor pressures for some of the important SOA forming molecules in the model have not been measured. However, the yields predicted here are within reason of those that have been measured in chamber experiments. For the reaction of 12.6 - 13.8 ppb α-pinene with OH *Ng et al.* [2007b] observed SOA mass yields of 6.6% - 39.7% with a strong NO_x dependence. The reaction of 47.5 ppb α-pinene resulted in a mass yield of 45.8%. The yields shown in Figure (2.7) are in this range, and show that higher concentrations of VOC reacted lead to the expected higher yield due to the increased OA available for partitioning. While the specific products produced in the model may not actually be those existing in ambient OA, the simulations do capture an important aspect of the NO_x dependence of SOA: Both NO and NO_2 concentrations can have important impacts on the product distributions and consequently NO_x may have a non-linear effect on SOA mass yields in the atmospherically relevant range of VOC:$NO_x \approx 1$.

2.7 The volatility of organic nitrates

The model calculations described in Section (2.6) used approximate organic nitrate vapor pressures. While a number of studies have observed organic nitrates in aerosols, only a very limited amount of vapor pressure data is available from direct measurements of organic nitrates. The group contribution method SIMPOL used to generate Figure (2.3) uses the available data from hundreds of organic compounds (nitrates and non-nitrates) to allow for the estimation of vapor pressure of an arbitrary compound [*Pankow and Asher*, 2008]. SIMPOL is an empirical method which finds and applies non-linear relationships between vapor pressure and structural components of a molecule (e.g. number of carbon atoms, hydroxyl groups, etc.). Figure (2.4) shows all of the vapor pressure data available on organic nitrates that was used to compile SIMPOL. In general the analysis of these data by *Pankow and Asher* [2008] leads to the conclusion that at 298K the addition of a nitrate group to a molecule reduces its vapor pressure by a factor of ≈ 0.0065. This change in pressure is comparable to changes due to the addition of a hydroxyl group (0.0065) or a hydroperoxyl group (0.0036). However, it is clear from Figure (2.4) that the vapor pressure data used to determine these properties is mostly that of completely volatile compounds. Only one of the compounds measured ($C_4H_6N_4O_{11}$) is expected to be have a low enough volatility to contribute to SOA at room temperature.

SIMPOL is not the only method currently available to estimate vapor pressures for compounds for which P_L^0 is unknown. SPARC[3] (SPARC Performs Automated Reasoning in Chemistry) is a different tool which uses calculated intermolecular interaction strengths (e.g. dipole-dipole interactions) and the molecular volume to estimate the enthalpic and entropic free energy changes due to evaporation. The free energy change is then used to calculate P_L^0

[3] `http://sparc.chem.uga.edu/sparc`

[*Hilal et al.*, 2003]. Both SIMPOL and SPARC have been individually evaluated by comparing the predicted and measured P_L^0 for hundreds of compounds. Both models perform well, with the SIMPOL model being reported as reproducing most P_L^0 values within a factor of 2, and the SPARC model having an RMS deviation of 0.0096 atm between measurements and predictions. As noted previously, the model/measurement comparison is not generally performed for the semi-volatile organic nitrates that are of interest here because little data is available. To evaluate the skill of these models to predict the P_L^0 values for semi-volatile organic nitrates, in Figure (2.5) the vapor pressure predictions for a few volatile and semi-volatile organic nitrates in the temperature range 273 - 313 K as calculated using the two different models are compared. Without prior knowledge that one method is more accurate, the results of this comparison suggest that the vapor pressure of an arbitrary organic nitrate may be estimated with the accuracy of $\approx \pm 1$ order of magnitude. While this is a significant achievement considering that the vapor pressures of interest span more than 10 orders of magnitude, this level of uncertainty results in a significant spread in the predicted partitioning. For example, using equation Equation (2.1) if $M_0 = 5$ μg m^{-3} and $\log_{10} C^* = 0 \pm 1$, the calculated range of how much of a compound is in the condensed phase is 98% - 33%. This result suggests that explicit chemical box models and estimated vapor pressures should not be expected to provide extremely accurate calculations of SOA concentrations when a significant fraction of the SOA mass lies in the semi-volatile C^* range of 0.1 - 1000 μg m^{-3}.

2.8 Experimental chamber measurements

2.8.1 Effects of NO_X on SOA yield

Due to its expected importance from a regulatory standpoint with respect to air quality, a number of studies have to measured the effect of varying NO_x concentrations on SOA mass yields in chambers [*Hatakeyama et al.*, 1991; *Pandis et al.*, 1991; *Zhang et al.*, 1992; *Song et al.*, 2005; *Presto et al.*, 2005; *Kroll et al.*, 2005, 2006; *Zhang et al.*, 2006; *Ng et al.*, 2007b, a]. Almost all studies have attempted to quantify SOA yield by measuring the total OA mass produced by reacting a known amount of VOC. Typically a series of these experiments is carried out with varying initial concentrations of NO_x. NO_x is typically controlled either by adding NO directly to the chamber, or using a 'high-NO_x' OH precursor such as HONO or methyl-nitrite which produce both NO and OH through photolytic reactions. An important aspect of these experiments is that they are chamber reactions carried out with OH radical and NO_x precursors that vary from study to study. While NO and NO_x are frequently measured, OH, HO_2, RO_2 and NO_3 are rarely measured, and must be inferred. As well, different chambers are likely to have different rates of chemical loss to the chamber walls. Thus, OH concentrations may be significantly different between experiments and sometimes the competing roles of OH, O_3 and NO_3 are not clear.

Here, the main observations of these chamber studies are summarized. Though these

studies are termed as looking at the 'NO_x' dependence, with few exceptions they have been looking at the NO dependence. 'High-NO_x' is typically defined as a chemical environment in which NO is in large enough excess over HO_x such that almost all organic peroxy radicals react with NO. In the atmosphere due to the steady state between NO and NO_2, high-NO_x' during the day necessarily implies substantial concentrations of NO and NO_2 with an NO:NO_2 ratio that is on the order of 1 (1.4 - 0.4 for O_3 of 20 - 80 ppb). However in chamber studies which may be initiated without O_3, the NO_x may be completely NO or NO_2 making chamber high-NO_x substantially different than ambient high-NO_x.

Isoprene is the largest single source of non-methane organic carbon on Earth *Guenther et al.* [2006] and hence a significant body of research has focused on understanding its atmospheric fate. *Kroll et al.* [2006] summarize a series of studies looking at the NO_x dependence of isoprene SOA. These studies used hydrogen peroxide (H_2O_2) as the OH precursor and NO as the source of NO_x. The SOA yield was observed to increase as NO concentration increased from 0 to a ratio of NO_x:isoprene of ≈ 3. Further increases in NO_x lead to decreasing yields. *Kroll et al.* [2006] believe that the decreasing yield with high NO_x is due to the fragmentation of carbon-carbon bonds due to RO_2 + NO reactions.

Ng et al. [2007b] examined the NO_x dependence of SOA formation from photooxidation of α-pinene and two sesquiterpenes (biogenic $C_{15}H_{24}$ molecules). In these experiments HONO H_2O_2 and NO were used as radical precursors for high-NO_x experiments, and H_2O_2 was used for low-NO_x. For α-pinene, the low-NO_x experiments produced significantly more SOA (39.7% - 45.8% for 13.8 - 47.5 ppb α-pinene) than the high-NO_x experiments (6.6% - 21.2% for 12.6 - 46.6 ppb α-pinene) which had a minimum initial NO_x:initial α-pinene of 15. With the sesquiterpenes a monotonic increase in the SOA yield was observed with increasing NO_x. *Ng et al.* [2007b] attribute the differences in the α-pinene and sesquiterpene NO_x trends to differences in the peroxy and alkoxy radical chemistry of the different size organic compounds, suggesting that larger alkoxy radicals may isomerize while the α-pinene radicals fragment.

Presto et al. [2005] performed a study examining the effects of NO_x and NO_2 on SOA from α-pinene ozonolysis. While photooxidation and ozonolysis of alkenes produces different specific products, both reactions produce organic peroxy radicals and thus might be expected to have similar dependencies with respect to NO_x. *Presto et al.* [2005] observed a generally decreasing SOA yield with increasing NO_2 and NO_x relative to α-pinene. Though the NO_x and NO_2 SOA yields that were reported were essentially the same, they did observe that the presence of NO completely inhibited SOA formation for NO_x:α-pinene greater than 0.22, suggesting that the compounds produced in the presence of NO are too volatile to condense.

Almost all studies have reported observing either monotonic increases or monotonic decreases in SOA yield with increasing NO_x. The only notable exceptions to this are that of *Kroll et al.* [2006] for the study of isoprene SOA, and that of *Pandis et al.* [1991] for β-pinene. These studies both observed maximum SOA yields for NO_x:VOC of $\approx$1.5 - 3. Observations of decreasing SOA yields with NO_x have generally been attributed to increased fragmentation of alkoxy radicals produced in RO_x + NO reactions. The reasons for increases in the yield with NO_x in the low NO_x limit are less certain.

One significant complication to the interpretation of the chamber data, is that the SOA yields are almost always parameterized by the ratio of initial NO_x:initial VOC. While this would seem to allow for a reasonable comparison to the chemistry in the atmosphere, the mechanism that is believed to control the SOA yield is the peroxy radical chemistry which is a function of the relative concentrations of RO_2, HO_2, NO_2, NO_3 and NO. While the relative concentrations of e.g. NO : HO_2 will depend on NO_x : VOC, it is also a strong function of the initiating oxidant concentration. For example, HO_2 is primarily produced via hydrogen abstraction from alkoxy radicals by O_2:

$$R(H)O^{\cdot} + O_2 \rightarrow RO + HO_2 \tag{R17}$$

This reaction is fast enough ($k \approx 9 \times 10^{-15}$ molecule cm^{-3} [*Atkinson*, 2007]) that at 21% O_2 the overall production rate of HO_2 in a chamber is limited by the rate of the VOC + oxidant reaction which leads to alkoxy radical production. Furthermore, the steady state concentration of HO_2 is a function of OH, H_2O, H_2O_2, NO and photolysis frequencies, so that the resulting OH:HO_2 in a chamber can be much different than that in the atmosphere. Thus, while the OH concentration can typically be inferred in a chamber study by measuring the decay rate of a hydrocarbon, the HO_2 concentration can not necessarily be accurately calculated relative to OH. The result is that even though various chamber studies may have similar NO_x : VOC, and OH, the HO_2 : NO_x may vary significantly. Without more specific knowledge of the radical concentrations in various investigator's experiments, it is difficult to directly compare the results.

2.8.2 Organic nitrates in chamber aerosol

If NO_x does lead to an increased formation of organic aerosol mass, the formation of low volatility organic nitrates is expected to be one of the sources of this mass. Aerosol organic nitrates has been observed in virtually all chamber experiments that have attempted to measure it. Various analytical detection techniques have been used providing qualitative analysis of their importance. These techniques include Fourier Transform Infrared Spectroscopy (FTIR) of particles on filters, mass spectral analysis of liquid extractions from filter samples, as well as online Aerosol Mass Spectrometry (AMS) techniques.

FTIR analysis of particles collected on quartz fiber filters was used by *Palen et al.* [1992] to study products of high-NO_x photooxidation of isoprene. For isoprene, they detected on average 0.1 - 0.34 organic nitrate groups / organic molecule in the aerosol depending on both the NO_x and total organic aerosol concentrations, as well as the particle size. For β-pinene they observed a range of 0.07 - 0.48. *Presto et al.* [2005] used FTIR to observe aerosol organic nitrates from the high-NO_x ozonolysis of α-pinene.

Aerosol mass spectrometry is an increasingly common technique for probing the chemical composition of atmospheric aerosols [*Canagartna et al.*, 2007]. AMS instruments use the aerodynamic properties of particles in the 50 - 1000 nm range to concentrate the particles

relative to gas. The particles are then rapidly vaporized, typically at 600°C and detected with 70 eV electron impact mass spectrometry, though variations of the vaporization and ionization techniques have been implemented (e.g. *Tobias et al.* [2000], *Northway et al.* [2007]). Nitrates are known to yield signals at m/z 30 and 46 (NO^+ and NO_2^+). AMS nitrate signals attributed to organic nitrates have been observed in a number of chamber studies, including *Lim and Ziemann* [2005], *Zhang et al.* [2006], *Ng et al.* [2007b], *Ng et al.* [2008], *Fry et al.* [2009], *Rollins et al.* [2009]. These measurements suggest that organic nitrate molecules are always some, if not all [*Lim and Ziemann*, 2005] of the OA produced in high-NO_x SOA experiments.

Electrospray ionization mass spectrometry (ESI-MS) is a much less destructive analytical technique than is AMS, and allows for the detection of SOA molecules intact. ESI-MS was used by *Surratt et al.* [2006] to identify specific multifunctional organic nitrates in aerosols collected on filters during photooxidation of isoprene and by *Ng et al.* [2008] to analyze aerosols from the reaction of isoprene with NO_3. These measurements demonstrated that the multifunctional nitrates predicted by explicit VOC oxidation schemes do exist in OA. As well, these studies emphasized the importance of multiple stages of oxidation that produce highly functionalized isoprene oxidation products which form aerosol.

2.9 Ambient atmospheric aerosol measurements

While the NO_x dependence of SOA formation rates and composition has not been evaluated directly from ambient measurements, observations suggest that high-NO_x environments may produce SOA more efficiently than low-NO_x environments. Measurements of the radiocarbon ($^{14}C/^{12}C$) content of aerosols suggest that although in urban areas SOA concentrations are generally much higher than in rural areas (e.g. [*Zhang et al.*, 2007a]), the organic carbon in the particles is typically mostly of biogenic origin [*Lewis et al.*, 2004; *Szidat et al.*, 2004] with sources typically not located in cities. As well, some of these studies have provided evidence that the SOA production is correlated to high-NO_x photochemical activity [*de Gouw et al.*, 2005; *Weber et al.*, 2007]. The mechanism by which biogenic SOA production is enhanced in urban air remains an unresolved paradox in the literature.

The only unambiguous measurements of organic nitrates in ambient aerosols has been achieved via ESI-MS and FTIR. Using ESI-MS *Surratt et al.* [2008] detected organic nitrates with isoprene and monoterpene backbones in ambient samples taken in the southeastern United States. FTIR was used to identify organic nitrates in Los Angeles [*Mylonas et al.*, 1991; *Allen et al.*, 1994] and in Houston [*Garnes and Allen*, 2002]. Aerosol mass spectrometry however is not capable of reliably quantifying organic nitrates in presence of ammonium nitrate [*Burns et al.*, 2010; *Rollins et al.*, 2010; *Farmer et al.*, 2010]. Because of the ubiquity of ammonium nitrate concentrations in tropospheric aerosols, the large amount of AMS data that has been compiled around the globe has not been used to attempt to quantify organic nitrates.

2.10 Conclusions

Chamber experiments have shown that depending on the organic precursor used and oxidizing conditions of the experiment, NO_x can either enhance or suppress organic aerosol production. Observations in the atmosphere suggest that OA production is much more efficient in urban plumes than places where NO_x : VOC is low. Modeling suggests that peak SOA production may occur near NO_x : VOC ≈ 1, however the NO : NO_2 ratio is likely to play an important role and the peak production may vary between precursors. Measurements of organic nitrates in atmospheric aerosols are not yet sufficient to make a strong statement about their widespread importance in the OA or NO_y budgets. However, the results so far suggest that organic nitrate oxidation products of large anthropogenic and biogenic hydrocarbons are readily condensible, and these are likely to be found mostly in the condensed phase.

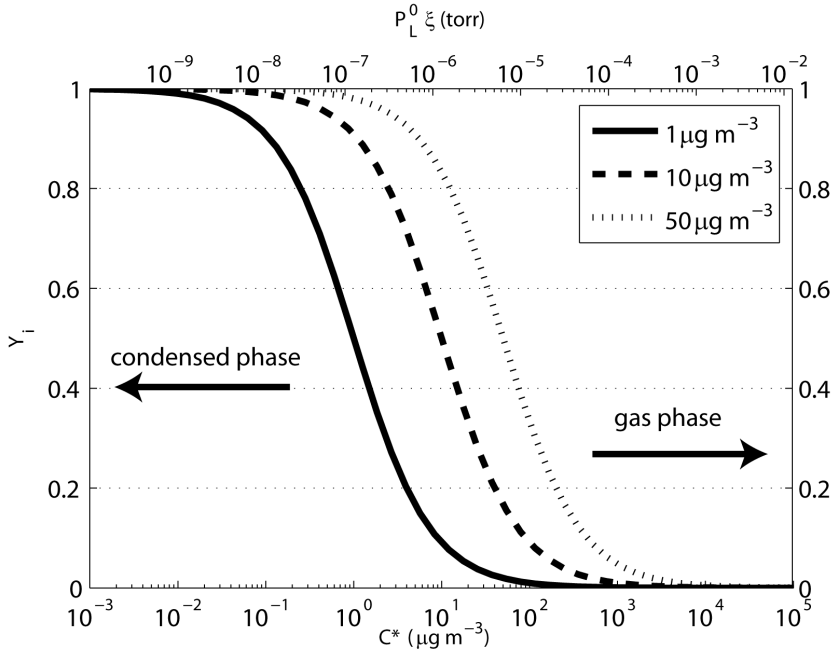

Figure 2.1: The gas/particle partitioning predicted using Equations (2.1) and (2.2) assuming $MW_{\mathrm{om}} = 150$ μg m^{-3}. Here, the fraction of a compound in the condensed phase is plotted as a function of the compound's C^* value(bottom axis) and the product of the vapor pressure (P_L^0) and activity coefficient ζ at 1, 10 and 50 μg m^{-3} total organic aerosol (M_0).

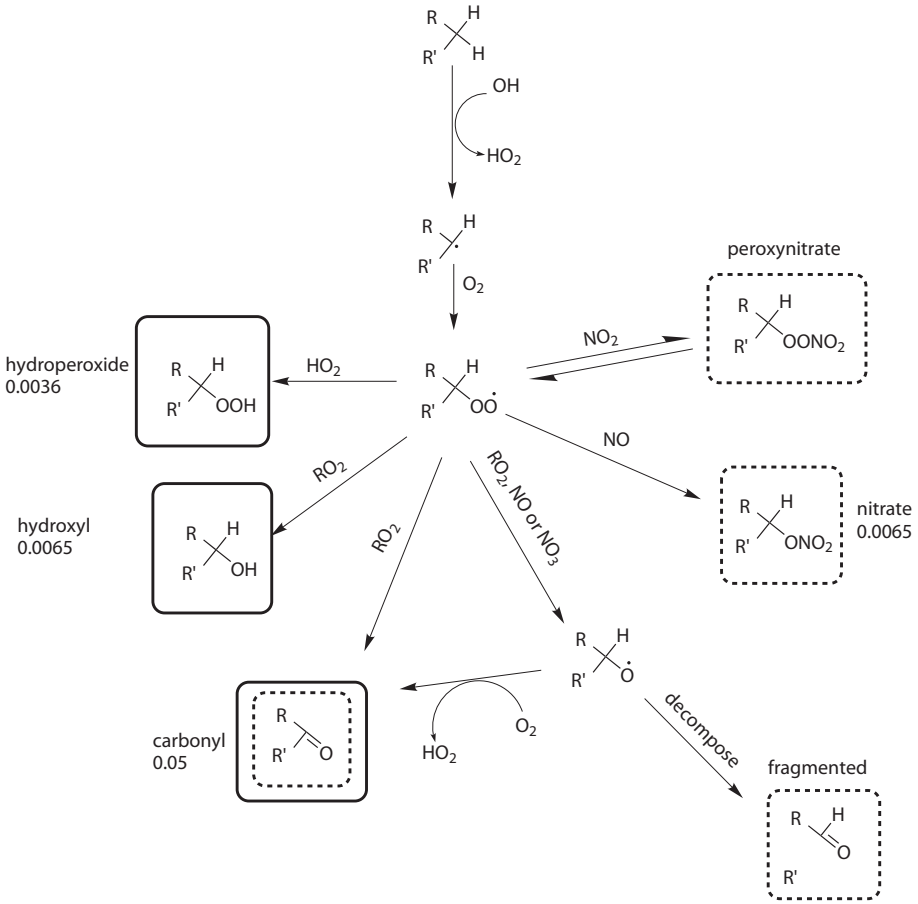

Figure 2.2: A generalized scheme representing the NO_x dependence of VOC oxidation products. Here is shown the formation of a peroxy radical from the OH oxidation of an alkane. Analogous peroxy radicals are formed from the oxidation of alkenes by OH and by NO_3. Peroxy radicals react with other organic (RO_x) or hydro (HO_x) peroxy radicals to form stable products which may condense to existing or to form new particles. The stable first generation oxidation products are shown in boxes. Solid boxes show products from 'low NO_x' oxidation and dashed boxes show those from 'high NO_x' oxidation. Where available, the multiplicative factors are shown which represent the change in vapor pressure from the initial compound to the respective product as predicted by the SIMPOL model. Fragmentation increases volatility, by a factor of ≈3 / carbon atom lost. SIMPOL does not predict change in vapor pressure for peroxynitrates, but the addition of an acyl-peroxy nitrate group ($R(O)O_2NO_2$) leads to a vapor pressure factor reduction of 0.0047.

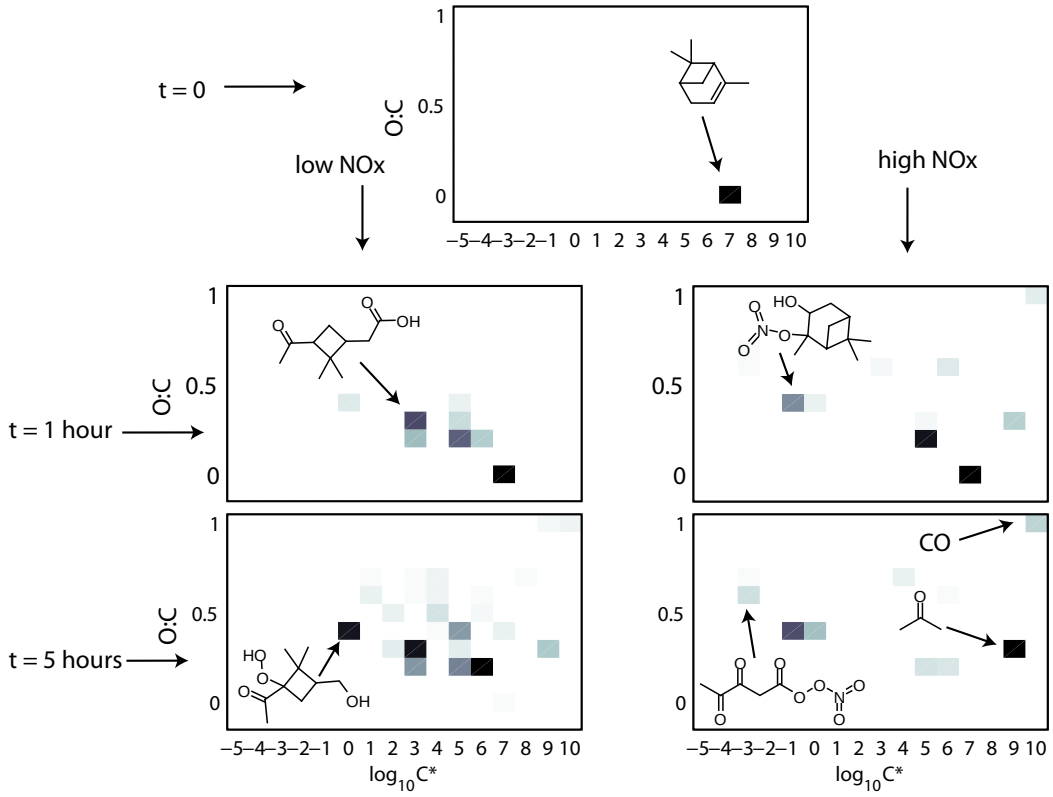

Figure 2.3: Evolution of O:C and volatility of products from the low NO_x photooxidation of α-pinene. OH concentration is fixed at 6×10^6 molecules cm^{-3}. The top panel shows α-pinene. The middle panel shows the product distribution after 1.7 hours (2 $\times$ the α-pinene lifetime to OH). Bottom panel is after 4.4 hours (5 OH lifetimes).

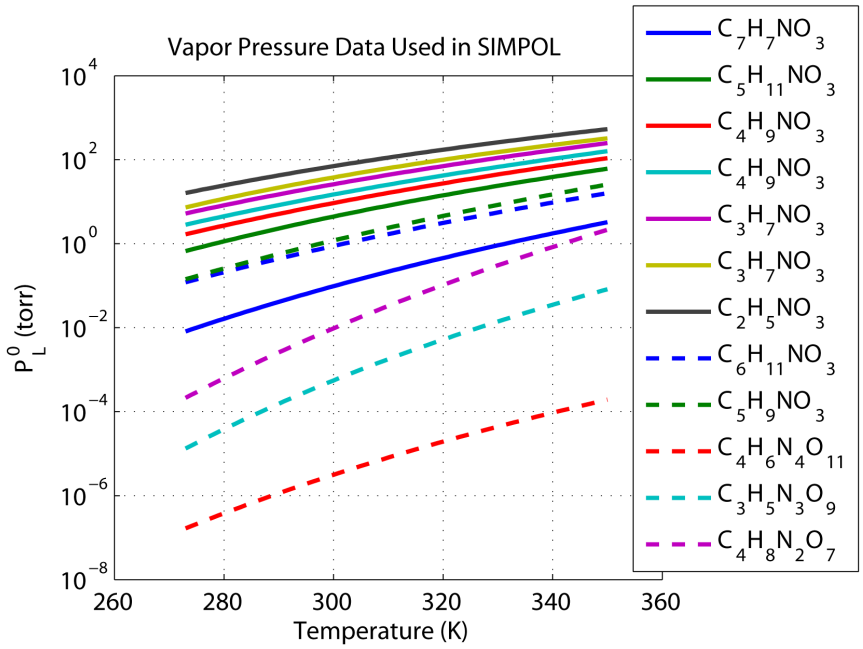

Figure 2.4: Data used in the SIMPOL group contribution method of calculating vapor pressures of organic nitrates.

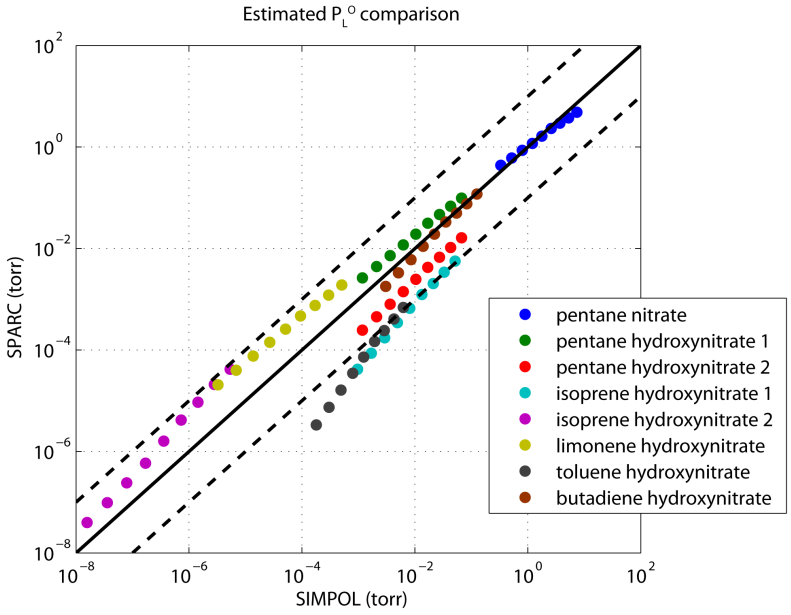

Figure 2.5: SIMPOL and SPARC models compared for some hydroxynitrates T=273 - 313K.

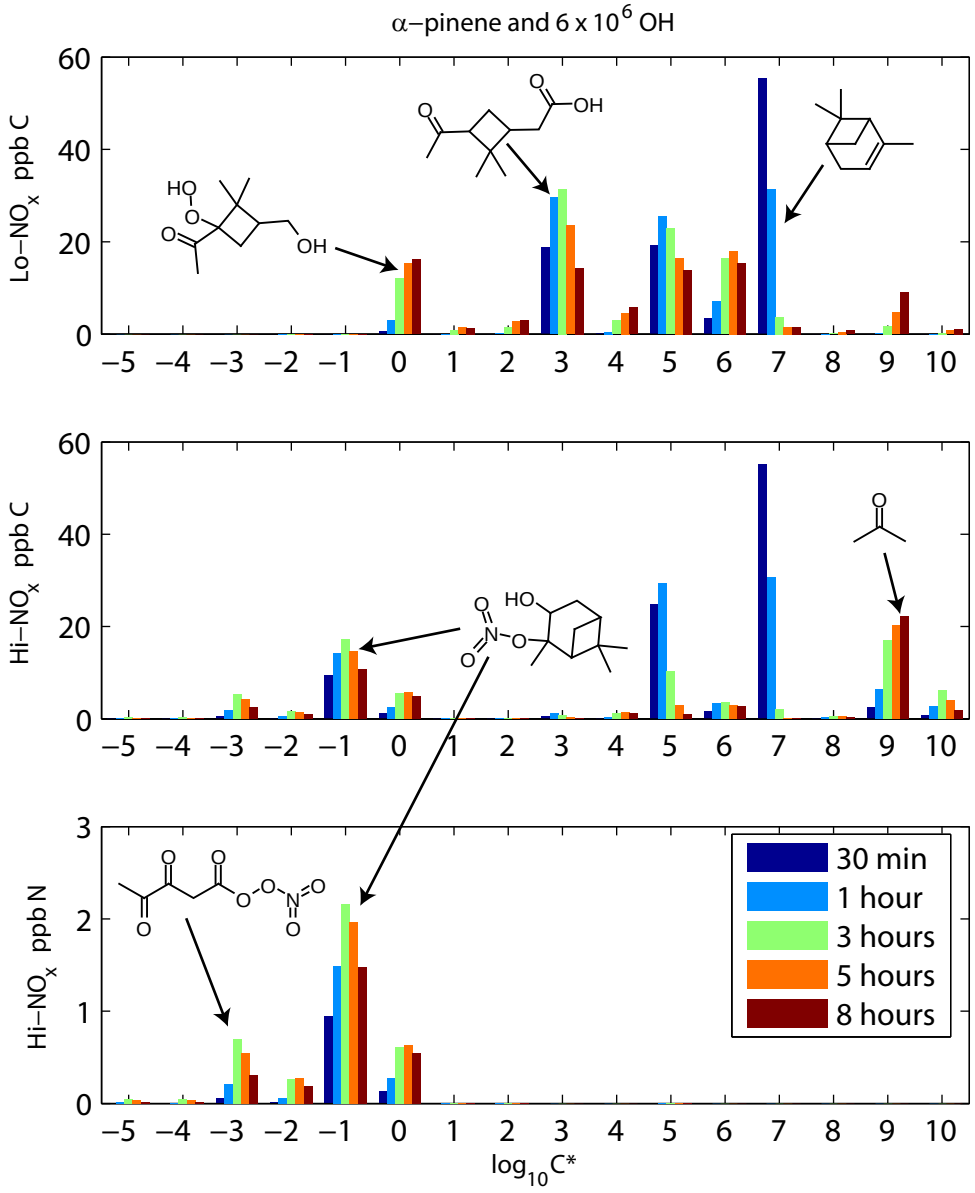

Figure 2.6: Calculated distribution of nitrogen and carbon in the α-pinene photooxdation model. The top panel shows the carbon weighted molecular distribution in the NO_x-free simulation. The middle panel shows the carbon weighted molecular distribution in the high-NO_x simulation. The bottom panel is the nitrogen weighted molecular distribution in the high-NO_x simulation. Bar colors correspond to different run times of the model. The α-pinene lifetime to OH at this concentration is 0.87 hours.

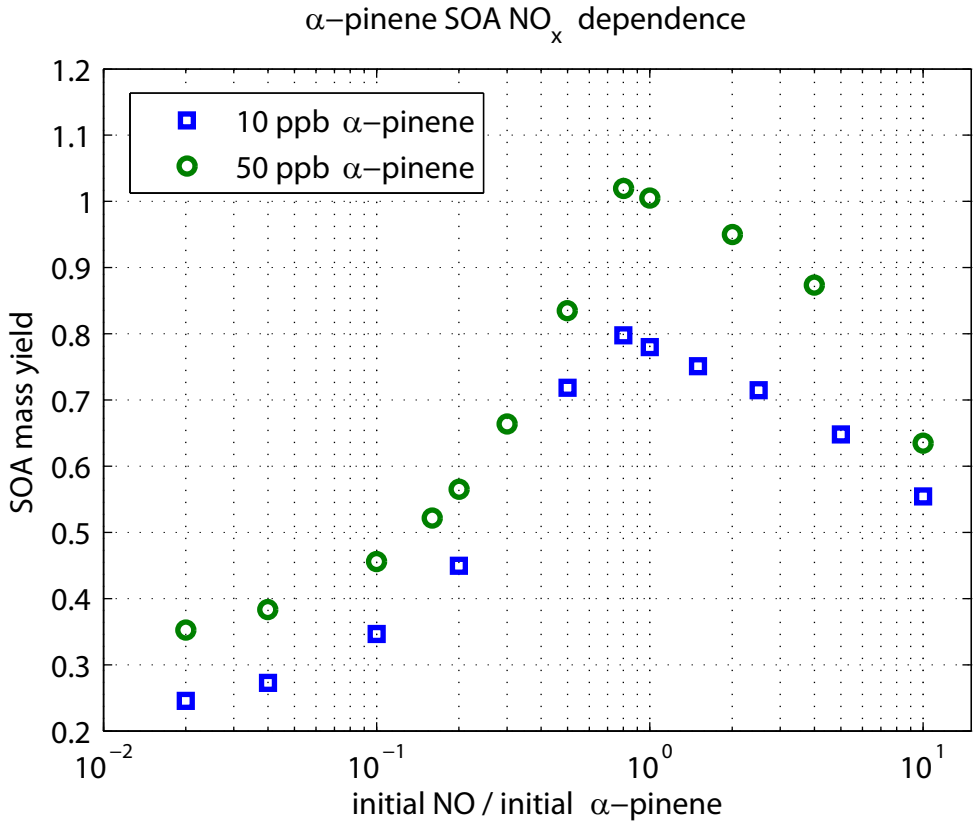

Figure 2.7: A model evaluation of the NO_x dependence of the SOA yield from α-pinene photooxidation. In this model OH is fixed at 6×10^6 molecules cm^{-3}. NO_x is added to the simulation by the addition of NO, which is the common practice in SOA chamber experiments.

Chapter 3

Isoprene oxidation by nitrate radical: alkyl nitrate and secondary organic aerosol yields

3.1 Introduction

Isoprene (2-methyl-1,3-butadiene) is globally the most abundant non-methane volatile organic compound (VOC), with an estimated emission of 440-660 Tg C / year [*Guenther et al.*, 2006]. Total non-methane VOC emissions are estimated at 1150 Tg C / year biogenic [*Guenther et al.*, 1995] and 186 Tg C / year anthropogenic [*Olivier et al.*, 2005] making isoprene the source of 34% - 51% of the non-methane organic carbon emitted to Earth's atmosphere. The combined factors of its source strength and high reactivity to atmospheric oxidants (OH, O_3, and NO_3), make isoprene a major factor in the chemistry of the troposphere. As a result, tropospheric O_3 and aerosol burdens and distributions are highly sensitive to the products of isoprene chemistry [e.g., *Chameides et al.*, 1988; *Thornton et al.*, 2002; *Henze and Seinfeld*, 2006; *Wu et al.*, 2007]. Recent field studies have provided mass spectroscopic evidence for the existence of isoprene oxidation products in ambient aerosol [*Gómez-González et al.*, 2008a; *Surratt et al.*, 2008]. The identified tracer molecules include tetrols and hydroxynitrates, which mostly appear to be produced by the oxidation of both double bonds in isoprene either through photooxidation (OH) of isoprene or through mixed NO_3/OH oxidation, and organosulfates which are believed to be produced by the subsequent reaction of tetrols or hydroxynitrates with acidic particles (NH_4HSO_4).

Isoprene emissions are near zero at night when nitrate radical chemistry is typically thought to be of primary importance. However, isoprene emitted during the day is observed to persist after sundown when NO_3 concentrations begin to increase [*Starn et al.*, 1998; *Stroud et al.*; *Steinbacher et al.*, 2005], and theoretical arguments suggest that NO_3 can be important in shaded forest canopies near NO_X (NO_X = NO = NO_2) sources even during

daytime [*Fuentes et al.*, 2007]. NO_3 has been measured during the day in polluted urban areas [*Geyer et al.*, 2003a] and new developments in NO_3 instrumentation allowing for sub-ppt sensitivity are beginning to reveal the potential importance of NO_3 - VOC chemistry during the day [*Brown et al.*, 2005]. Global estimates made with GEOS-Chem suggest that $\approx 6\%$ of the total isoprene oxidation occurs by NO_3 [*Ng et al.*, 2008]. Regionally however, in areas such as cities and power plants surrounded by forest where high NO_X emissions are collocated with isoprene sources, NO_3 has been shown to oxidize 22% or more of the total daily isoprene emission [*Brown et al.*, 2009].

Alkyl nitrates ($RONO_2$) formed from reactions of isoprene with NO_3 represent $\approx 50\%$ of the total nitrate production in isoprene rich regions, with likely consequences for tropospheric O_3 production [*Horowitz et al.*, 1998; *von Kuhlmann et al.*, 2004; *Fiore et al.*, 2005; *Horowitz et al.*, 2007; *Wu et al.*, 2007]. Photochemical oxidation of isoprene has been shown in chamber studies to produce aerosol with mass yields that are small (1 - 3%) [*Kroll et al.*, 2005, 2006] compared to yields from other biogenic VOC's, but due to the source strength of isoprene this could be the single most significant source of SOA on Earth [*Henze and Seinfeld*, 2006; *Zhang et al.*, 2007b; *Ng et al.*, 2008]. SOA from the reaction of isoprene with NO_3 has been recently studied [*Ng et al.*, 2008], with significant yields observed (4.3 - 23.8% for 2.2 - 68.1 $\mu g/m^3$ isoprene reacted). The nitrate radical reacts primarily with unsaturated VOC's and therefore is a particularly effective oxidant for many biogenic compounds. Isoprene which has two double bonds, can react with NO_3 at each bond, and the products of both oxidation steps can affect both NO_X and NO_y (NO_y = NO_X + organic nitrates + NO_3 + N_2O_5 + HNO_2 + HNO_3 + particulate nitrate) partitioning as well as SOA formation. There is little detailed information about the fate of the initial oxidation products, which are primarily alkenes and aldehydes. Both functional groups may have important roles in the reactivity of the initial products.

Kinetics of the first step in isoprene oxidation by NO_3 are well established. The rate constant has been measured by a number of investigators using various methods [*Atkinson et al.*, 1984; *Benter and Schindler*, 1988; *Dlugokencky and Howard*, 1989; *Barnes et al.*, 1990; *Berndt and Boge*, 1997; *Wille et al.*, 1991; *Suh et al.*, 2001] and the recommended rate constant at 298 K is 6.8×10^{-13} molecule^{-1} cm^3 s^{-1} [*Atkinson et al.*, 2007]. The mechanism for the reaction is addition of NO_3 to one of the double bonds, mainly at the C_1 position. Theoretical and experimental studies are in good agreement that the main product of the reaction in the presence of oxygen will be a C_5 nitrooxycarbonyl. Minor products include C_5 hydroxynitrates, C_5 nitrooxyhydroperoxides, methyl vinyl ketone (MVK) and methacrolein (MACR) [*Barnes et al.*, 1990; *Skov et al.*, 1992; *Ng et al.*, 2008]. *Ng et al.* [2008] also identified many other gas and particle phase products from isoprene + NO_3. SOA was observed to form from both first generation and second generation products. Reaction of the C_5-hydroxynitrate with NO_3 was more correlated with production of SOA than was the reaction of the other major C_5 products. Highly functionalized C_{10} peroxides were also identified in the gas and particle phases. *Ng et al.* [2008] concluded that SOA in this system is produced more efficiently by RO_2 + RO_2 reactions than by RO_2 + NO_3 reactions.

In this work we report a chamber experiment on the reaction of isoprene + NO_3 performed with isoprene (max 11 ppb) O_3 (max 62.4) and NO_X (max 31.1 ppb) where NO_3 is generated in situ via the reaction of O_3 + NO_2. To date, the isoprene + NO_3 experiment with the lowest reported reactant concentrations is that of *Ng et al.* [2008] who used a lower limit of 18.4 ppb isoprene and added N_2O_5 directly to the chamber. In this experiment high precision measurements of both gas phase and particle phase products have been made, including especially detailed observations of nitrogen oxides. NO, NO_2, NO_3, N_2O_5, and total alkyl nitrates ($\Sigma RONO_2$) were observed. This unique set of measurements provides a new measure of the alkyl nitrate yield and allows us to estimate the reactivity of the initial oxidation products, strengthening our understanding of the mechanism by which gas and aerosol products are produced in the ambient environment.

3.2 Experimental

The experiment was conducted in the SAPHIR chamber in Jülich, Germany. The reaction chamber is a double walled 120 μm Teflon-FEP cylindrical bag, 5 m in diameter and 18 m long providing a volume of $\approx 270\,m^3$. The chamber is housed in an aluminum structure with shutters that can be left open to outside lighting, or closed to simulate nighttime chemistry. For this experiment the shutters were always closed. During experiments the chamber is overpressured by 40 - 60 Pa with respect to the ambient pressure, and the space between the two FEP sheets is continually flushed with high purity N_2. These measures isolate the air inside the chamber from outside air. Air sampled from the chamber during experiments is replaced with synthetic dry air to maintain the positive pressure. A mixing fan inside the chamber continuously stirs the gas in the chamber to maintain a spatially uniform mixture with a mixing time of 2 - 3 minutes. SAPHIR has been described in further detail elsewhere [*Bossmeyer et al.*, 2006; *Rohrer et al.*, 2005; *Wegener et al.*, 2007].

3.2.1 Instrumentation

This experiment was conducted on 18-Jul-2007 during an intercomparison campaign focused on measurements of NO_3 [*Dorn et al.*, 2009] and N_2O_5 [*Apodaca et al.*, 2009], during which ten different instruments for measurement of NO_3 and / or N_2O_5 were co-located at the SAPHIR chamber. NO_3 and N_2O_5 measurements were found to be in agreement to $\pm$10% for almost all of the instruments throughout the campaign. Figures and analysis in this paper make use of Cavity Ringdown Spectroscopy (CaRDS) measurements reported by Brown and coworkers [*Brown et al.*, 2001; *Dubé et al.*, 2006] with accuracies of +12% / -9% for NO_3 and +11% / -8% for N_2O_5 [*Fuchs et al.*, 2008]. Measurements of isoprene were obtained by Proton Transfer Reaction - Mass Spectrometry (PTR-MS), and Gas Chromatography with Flame Ionization Detector (GC-FID). Volatile organic compounds (VOC) including MVK, MACR and methyl ethyl ketone (MEK) were also measured with GC-FID. NO and NO_2 were

measured with a Chemiluminescence (CL) instrument equipped with a photolytic converter (ECO Physics CLD TR 780). NO_2 as well as the higher nitrogen oxide classes total peroxy nitrates (ΣPNs), total alkyl and multifunctional nitrates ($\Sigma RONO_2$) were also measured by Thermal Dissociation - Laser Induced Fluorescence (TD-LIF) [*Thornton et al.*, 2000; *Day et al.*, 2002]. The TD-LIF $\Sigma RONO_2$ measurement includes alkyl nitrates only, not peroxy nitrates or HNO_3. Ozone was measured with a UV Photometer (ANSYCO O341M), as well as with a CL detector (ECO Physics CLD AL 700) modified as described by *Ridley et al.* [1992]. Both O_3 instruments were in good agreement and figures in this paper show the CL measurements.

Aerosol size distribution, surface area, volume, and total number density were obtained with a Scanning Mobility Particle Sizer (SMPS) (TSI model 3936L85) and Condensation Particle Counter (CPC, TSI model 3785) with time resolutions of 7 minutes and 20 seconds respectively. A high resolution ($\Delta m / m = 250$ ppm at $m / z = 100$, [*DeCarlo et al.*, 2006]) aerosol mass spectrometer (Aerodyne HR-ToF-AMS) was operated to measure the chemical composition of the non-refractory aerosol, providing data every 2 minutes. The AMS was connected to the SAPHIR chamber via a stainless steel tube designed to minimize losses in the sampling line. Details of the AMS are described in [*Canagartna et al.*, 2007]. The high resolution (HR) capabilities of the AMS can distinguish between chemically different fragments at the same nominal mass (i.e. NO^+ and CH_2O^+ at $m / z = 30$) when signal to noise is high enough. In this manuscript we use the AMS to quantify aerosol organic nitrate content, following *Fry et al.* [2009]. The AMS measures nitrate at m/z 30 (NO^+) and m/z 46 (NO_2^+). NH_4NO_3 is characterized by a ratio of NO_2^+/NO^+ of 0.35 with the instrument employed in this study, and is consistent with the reported ranges of this value of 0.33 - 0.56 which have been observed using the Aerodyne AMS [*Alfarra et al.*; *Cottrell et al.*, 2008]. In this experiment we found a much lower ratio of 0.156 which is taken as indication of organic nitrate. For the reported AMS nitrate, HR analysis was used to exclude the non nitrogen containing fragments from the nominally nitrate peaks at m/z = 30 and 46, as well as to ensure the other major peaks normally considered organic did not contain nitrogen. The signal at m/z 30 was observed to contain NO^+ and CH_2O^+. No significant contribution of organic ions was observed at m/z 46. The measured SMPS mode diameter grew from initial 50 nm to 90 nm during the course of the experiment, and a transmission efficiency of 1 was assumed through the aerodynamic lens of the AMS. The collection efficiency, CE, was assumed to be 0.5 for $(NH_4)_2SO_4$ and 1 for organics and nitrate. It is assumed at this point that the Relative Ionization Efficiency (RIE) for the nitrate is 1.1. Under these assumptions AMS and SMPS agree well when deriving a mass loading from SMPS size distributions with a density of 1.4 for Ammonium sulfate and 1.2 for the organic fraction.

3.2.2 Experiment Description

The chamber was prepared by flushing for 12.5 hours with clean synthetic air at a rate of 75 m^3/h. Starting at 6:20 UTC, the dark chamber was loaded with trace gasses to meet the

intended experimental conditions (relative humidity = 57%, ethane 5.5 ppb as a tracer for dilution, CO 500 ppm as an OH scavenger, isoprene 9.6 ppb, and NO_2 16 ppb, see Figure 3.1). In addition we added ammonium sulfate seed aerosol (3.5 $\mu g/m^3$). At 8:50, O_3 (37 ppb) was added initiating the production of NO_3. After 5 hours of reaction time the chemistry was accelerated by injecting an additional 23 ppb NO_2 and 43 ppb O_3, and then approximately 1 hour after the isoprene was fully consumed another 11 ppb of isoprene was added. The slow reaction of O_3 and NO_2 generated NO_3 radicals throughout the experiment, consuming the majority of the isoprene. Using a chemical kinetics box model we calculate that throughout the experiment $\approx$90% of the isoprene reacted with NO_3 and $\approx$10% with O_3. The GC-FID measurements of ethane were fitted to an exponential decay with a rate constant of $k_{dil} = 1.39 \times 10^{-5}\,s^{-1}$, which was applied to all species in the box model to account for dilution.

3.2.3 Modeling

The Kinetic PreProcessor (KPP V2.1) [*Sandu and Sander*, 2006] was used to produce code for kinetic box model simulations of the chamber experiment. Two sets of simulations were run. In one set KPP input was provided by the Master Chemical Mechamism (MCM V3.1) [*Saunders et al.*, 2003]. In another set of simulations the MCM isoprene + NO_3 degradation scheme was modified and optimized to reproduce the chamber observations, leaving the isoprene + O_3 scheme identical to that in the MCM. The full reaction set used in this second scheme is listed in Table 3.1, and both mechanisms are shown schematically in Figure 3.2 for comparison. This second mechanism includes two main deviations from the MCM: Firstly, the yield to form alkyl nitrates as the first generation oxidation products of isoprene + NO_3 is less than 100%, and secondly, these initial oxidation products retain a double bond to which NO_3 can add electrophilically, eventually forming additional multifunctional nitrates. Both sets of simulations used the same rate constants for chamber wall loss of NO_3, N_2O_5 and $\Sigma RONO_2$. NO_3 and N_2O_5 loss rates were determined to be 1.0×10^{-3} s^{-1} and 1.1×10^{-4} s^{-1} from a VOC/particle free experiment. The loss rate of $\Sigma RONO_2$ is determined to be 2.2×10^{-5} s^{-1} by a best fit of the $\Sigma RONO_2$ data and model at the end of the experiment when changes in $\Sigma RONO_2$ are mostly due to dilution and wall loss.

Details of the chemistry included in the modified model are as follows:

- **Inorganic Chemistry:** The inorganic reactions and rates are taken directly from the MCM website.[1]
- **VOC Chemistry:** MVK and MACR are assumed to be produced with yields of 3.5% each from isoprene + NO_3, as was previously reported [*Kwok et al.*, 1996] and these yields are held fixed in the simulations. HO_X (as HO_2) is assumed to be produced

[1] `http://mcm.leeds.ac.uk/MCM/`

by 80% of the RO_2 reactions, which is a rough approximation consistent with the semi-explicit model used by *Horowitz et al.* [2007].

The only measurement we made of the other carbon products of isoprene oxidation is the $\Sigma RONO_2$. We reduce the model complexity by only distinguishing these oxidation products by their -ONO_2 content and whether they have undergone a second oxidizing reaction with NO_3 or O_3. NIT1 (Table 3.1, Figure 3.2) is representative of all first generation oxidation products which have one -ONO_2 group. The branching ratio to form NIT1 is a tunable parameter in the model. The group of species represented by NIT1 is reactive towards NO_3 and O_3. The effective rate for reaction of NO_3 with this group of unsaturated species is also tunable, and is fit to be 7.0×10^{-14} molecules^{-1} cm^3 s^{-1} to achieve the best agreement between modeled and measured NO_3 and N_2O_5 (see section 3.3.1). The nitrate radical which reacts with NIT1 is presumed to lead to the production of additional -ONO_2 functionality (NIT3, either di-nitrate or 2 organic nitrate molecules), or be converted to NO_2 or HNO_3 leaving the original -ONO_2 group attached to a different carbon backbone (NIT2). The branching ratio between formation of NIT2 and NIT3 is the final tunable parameter in the model. The reaction of NIT1 with O_3 makes NIT4 which is also treated as an unspecified $RONO_2$. Example structures of NIT1-4 are shown in Figure 3.2c. The lumped species NIT1-4 include, but are not limited to the molecules shown in the figure. The modeled $\Sigma RONO_2$ is therefore NIT1 + NIT2 + 2 × NIT3 + NIT4 + NISOPO2 + NIT1NO3OO.

Because the primary oxidation product of isoprene + NO_3 is believed to be 4-nitrooxy-3-methyl-2-butanal, we use the reaction rates of the structurally similar 2-methyl-2-butene as a reference for the ratio of the reaction rates with O_3 and NO_3 (both rates taken from MCM). Thus, $k_{O_3} = 4.3{\times}10^{-5}{\times}\ k_{NO_3}$. The choice to use 4-nitrooxy-3-methyl-2-butanal as the reference compound for these rates has a small impact on the outcome of the model because the O_3 reaction is much slower than the NO_3 reaction. The O_3 reaction (R9) accounts for 7% of the consumption of the NIT1 species throughout the entire model run, while during the short SOA growth period (14:30 - 16:15) it is only 4%. Using methacrolein as the reference compound increases these values to 26% and 17% respectively.

- **Peroxy Radicals:** Peroxy radicals in the model are generated by reactions of each double bond of isoprene with NO_3. All peroxy radical (RO_2) reaction rates are taken directly from MCM. The initial isoprene nitrate peroxy radical + RO_2 rate is 1.30×10^{-12} molecule^{-1} cm^3 s^{-1}, and this rate is used also for all second generation RO_2 + RO_2 reactions. All RO_2 + NO_3 and RO_2 + HO_2 reactions proceed at standard MCM rates of 2.5×10^{-12} molecule^{-1} cm^3 s^{-1} and 2.3×10^{-11} molecule^{-1} cm^3 s^{-1} respectively (see Table 3.1). The yield for product formation is modeled to be the same regardless of the peroxy radical reaction partner, and the products of all peroxy radical reactions are only distinguished by whether a stable alkyl nitrate or NO_2 is formed. For example,

two isoprene peroxy radicals could form a C_{10} peroxide, or two C_5 products. These product channels are not tracked in the model because the only observable and therefore modeled quantities are NO_X, NO_3, N_2O_5 and $\Sigma RONO_2$.

3.3 Gas Phase Products

We first describe the observations from the chamber and show that different time periods uniquely constrain some of the model parameters. Two distinct chemical environments dominated the chemistry in the chamber at three different time periods. These time periods are referred to by their UTC hour and are most obvious in the observations of NO_3 and N_2O_5 (Figure 3.1c). In what follows, the stated production rates of NO_3, the fraction of isoprene reacted with NO_3, and the peroxy radical fate are all calculated using the box model which is more extensively described in section 3.2.3.

1. 8:00 - 14:30, Isoprene oxidation: During the initial phase the isoprene concentration was high and isoprene dominated the consumption of nitrate radicals. The NO_3 production rate ranged from 0.56 ppt s^{-1} (2.0 ppb hr^{-1}) at 8:00 to 0.16 ppt s^{-1} (0.58 ppb hr^{-1}) at 14:30. At any given time $> 90\%$ of the NO_3 loss was due to reaction with isoprene, with the majority of the balance being to reaction with oxidation products. Reaction of peroxy radicals is predominately with other peroxy radicals and hydroperoxy radicals. RO_2 + NO_3 accounts for $< 5\%$ of RO_2 reactions.

2. 14:30 - 16:15, Secondary oxidation: During this second phase, the isoprene concentration decreased rapidly to zero and reaction with the initial oxidation products was a much more important sink for NO_3. Between UTC 15:18 and 16:15 reaction with these initial oxidation products accounted for more than half of the total NO_3 reactivity. Second generation oxidation products rapidly accumulated through the reaction of NO_3 with the initial isoprene oxidation products. RO_2 + NO_3 also accounted for a larger fraction of the peroxy radical reactions, peaking at ≈ 40 - 50% of total peroxy radical loss.

3. 16:15 - 24:00, Isoprene oxidation: During the third phase additional isoprene was added to the chamber, bringing the concentration to 11 ppb. Isoprene again was the dominant sink of NO_3, suppressing both the production of the doubly oxidized products of isoprene and RO_2 + NO_3 reactions.

3.3.1 Optimized Model Parameters

As previously discussed, three of the model parameters have been adjusted to minimize differences in the model-measurement comparison. These are: 1) Branching ratios for the formation of alkyl nitrates vs. NO_2 from the isoprene + NO_3 reaction, 2) reaction rate of

first generation oxidation products with NO_3, and 3) branching ratios for formation of alkyl nitrates and NO_2 from the reaction of NO_3 with the first generation oxidation products. Model optimization of the free parameters was achieved in the following order:

1. **Branching ratio #1:** Stable nitrates result from addition of NO_3 and O_2 to isoprene followed by a radical-radical reaction that produces a closed shell product through either an abstraction reaction followed by a cleavage, or a recombination of the radicals (Figure 3.2). The branching ratio (Y_{AN1}) to form alkyl nitrates from isoprene + NO_3, is defined as the fraction of isoprene + NO_3 reactions that eventually form stable nitrates:

$$Y_{AN1} = \frac{\Delta\Sigma\mathrm{RONO_2}}{\Delta\mathrm{isoprene}} \tag{3.1}$$

   An initial attempt was made to evaluate this branching ratio directly from changes in the isoprene, NO_3, N_2O_5 and $\Sigma RONO_2$ observations during second addition of isoprene to the chamber. This addition lead to a prompt consumption of a known amount of NO_3 and N_2O_5, and subsequent production of alkyl nitrates and NO_2. The measurements did not however resolve the isoprene consumed in this rapid reaction. This was because the time scales of chamber mixing and reaction were comparable such that the initial concentration of isoprene added was not measured precisely, resulting in no stepwise decrease observed in the isoprene concentration at 16:15 (see Figure 3.1e). The branching ratio Y_{AN1} would be equal to $\Delta\Sigma RONO_2/\Delta NO_3$ if $\Delta NO_3 = \Delta$isoprene, i.e. in the absence of another NO_3 sink. However, because the NO_3 concentration was high relative to RO_2, we calculate that $RO_2 + NO_3 \rightarrow RO + NO_2 + O_2$ accounted for $\approx$15 - 25% of the total RO_2 reactions, meaning that on the order of 20% of the sudden change in NO_3 radicals was due to the reaction with peroxy radicals, not isoprene. Due to the uncertainty in the reaction rate for the specific peroxy radicals with NO_3 it is not possible to precisely calculate the contribution of this reaction to the ΔNO_3. For the initial phase of the experiment however the concentration of NO_3 was so low that the rate of $NO_3 + RO_2$ is minor compared to $RO_2 + RO_2$ and $RO_2 + HO_2$, and uncertainties in the reaction rates other than NO_3 + isoprene result in a small uncertainty in the branching ratio.

   To evaluate the yields of alkyl nitrates and NO_2 we therefore varied this yield in simulations run over the time period 7-13 UTC (Figure 3.3). A yield 70 $\pm$ 8% alkyl nitrates and 30% NO_2 was found to minimize the accumulated residuals between model and measurements of $\Sigma RONO_2$ and NO_2 over this time period.

2. **Alkyl nitrate + NO_3 reaction rate:** With the branching ratios for the first generation products fixed at 70% and 30% for alkyl nitrates and NO_2 respectively, the time period 14 - 16:15 UTC was used to fit the rate coefficient for reaction of the lumped species NIT1 + NO_3. A rate coefficient of $7\times10^{-14} \pm 3\times10^{-14}$ molecules^{-1} cm^3 s^{-1} was found to be optimal (Figure 3.3) based on minimizing residuals in comparison of modeled and observed $NO_3 + N_2O_5$.

3. **Alkyl nitrate + NO_3 products:** Using the optimized branching ratios for isoprene + NO_3 and the optimized reaction rate, the branching ratio to form alkyl nitrates or NO_2 from the second oxidation step was investigated. Focusing on the time period 14 - 16:15 UTC when the isoprene was depleted so that $RONO_2$ + NO_3 was the primary sink of NO_3, we examined the yield in 20% increments (Figure 3.4). The model and measurements are in best agreement for a yield of 40% ± 20%. We note that a yield of greater than 0% for NO_2 results in modeled NO_2 which is significantly greater than the measurements. This implies that the second oxidation step has a high yield to form HNO_3 directly.

Figure 3.5 shows a comparison between the MCM model, and the model optimized in this work for modeled $\Sigma RONO_2$, NO_2 NO_3 and N_2O_5. Generally, the MCM overpredicts NO_3, N_2O_5 and alkyl nitrates, and underpredicts NO_2.

Table 3.2 summarizes the results of studies in the literature that report quantifying the yield of total alkyl nitrates from the isoprene + NO_3 reaction. Our observation of alkyl nitrate formation (70 ± 8%) is equivalent to previously reported yields (65% - 80%), within the combined experimental errors [*Skov et al.*, 1992; *Perring et al.*, 2009]. The fact that multiple experiments conducted under different conditions (concentrations of isoprene and oxidants differing by more than a factor of 100) have all produced high yields of alkyl nitrates implies that the yield is robust and relatively insensitive to the peroxy radical chemistry, and supports findings that the isoprene + NO_3 reaction is possibly the single strongest source of alkyl nitrates in the atmosphere [*Horowitz et al.*, 2007].

MACR, MVK and methyl ethyl ketone (MEK) were observed in small yields. Approximately 70% of the observed MVK and 80% MACR were calculated to be from the reaction of isoprene with ozone, and the remainder is consistent with yields of 2 - 4% for both MVK and MACR from NO_3 + isoprene. Production of 0.9 ppb MEK was also observed by 24:00 UTC. The observations of the yields of MACR and MVK are consistent with previous observations. *Barnes et al.* [1990] reported an observable but small yield of MACR. *Skov et al.* [1992] report MACR below their FTIR detection limit (<5%). *Kwok et al.* [1996] measured the production of MVK and MACR with GC-FID and reported yields of 3.5% for both MVK and MACR. *Perring et al.* [2009] observed a 7% yield of the sum of MVK and MACR using PTR-MS. *Skov et al.* [1992] and *Perring et al.* [2009] measured product yields by adding isoprene to a chamber that was initially charged with ppm levels of N_2O_5. *Kwok et al.* [1996] added isoprene first as we did, but then injected N_2O_5 in ppm steps. All of these experiments would have resulted in a much larger NO_3/RO_2 ratio than in the experiment reported on here. These similar yet small yields of MVK and MACR observed in vastly different radical regimes are not surprising, supporting the conclusion that the yields of these products are primarily determined by the position at which O_2 adds to the alkyl radical adduct generated by isoprene + NO_3 as opposed to the peroxy radical reaction partner. The observation of 0.9 ppb MEK at the end of the experiment is surprising. It seems that this product would have appeared in the FTIR detection scheme of *Skov et al.* [1992], however they do not

report observing it. The mechanism responsible for the MEK in our experiments is unclear and might have been an interference from a different compound with the same GC retention time.

The rate constant that we find for the reaction of the first generation oxidation products with NO_3 ($7{\times}10^{-14}$ molecules^{-1} cm^3 s^{-1}) can be compared to known rate constants for compounds that are likely to be structurally similar. The observations that $40 \pm 20\%$ of this reaction generates an alkyl nitrate, while $60 \pm 20\%$ of the nitrogen does not reappear in any of our measurements indicates that the reaction occurred by $\approx 40\%$ addition of NO_3 to a double bond, and $\approx 60\%$ abstraction of an aldehydic hydrogen to produce HNO_3, with rate constants of $0.4 \times 7 \times 10^{-14} = 2.8 \times 10^{-14}$ molecules^{-1} cm^3 s^{-1} and $0.6 \times 7 \times 10^{-14} = 4.2 \times 10^{-14}$ molecules^{-1} cm^3 s^{-1} for these two respective reactions. Both of these reaction channels are reasonable considering that multiple studies have found the C_5-hydroxycarbonyl to account for most of the initial product yield. Though a significant amount of HNO_3 may have been produced from this reaction, the increase in particulate nitrate appears to be due to the organic nitrates, indicated by the low NO_2^+/NO^+ ratio observed with the AMS.

We compare the addition reaction to the reaction of NO_3 with 3-methyl-2-butene-1-ol (MBO), which is a unsaturated alcohol structurally similar to the C_5 nitrates produced by isoprene + NO_3. The reaction rate constant for MBO has been measured as 1×10^{-12} molecules^{-1} cm^3 s^{-1} [*Noda et al.*, 2002]. While the effect of nitrate substitutions has not been studied on the reactions of alkenes with NO_3, the electronegative nitrate group should be expected to slow the reaction. For example, in the case of the electrophilic OH addition to a double bond, the C_5-hydroxynitrate reaction rate constant would be predicted to be a factor of 5 slower than that for MBO [*Kwok and Atkinson*, 1995]. Scaling the MBO reaction by a factor of 5 yields a rate constant of 2×10^{-13} molecules^{-1} cm^3 s^{-1}, ten times faster than our fitted value of 2.8×10^{-14} molecules^{-1} cm^3 s^{-1}. The presumed rate constant for hydrogen abstraction of $4.2{\times}10^{-14}$ molecules^{-1} cm^3 s^{-1} is on the fast end of the range that has been measured for aldehydes with NO_3. *D'Anna et al.* [2001] measured a rate constant of 2.68×10^{-14} molecules^{-1} cm^3 s^{-1} for the reaction of 2-methylbutanal, which differs from the C_5 hydroxycarbonyl only by a nitrate substitution at the δ carbon. We caution that these comparisons are intended only to be rough, as we only are considering what are believed to be the highest yield isomers of the isoprene + NO_3 reactions. Further, the measured products from the initial reaction only account for 77% of the primary products ($\Sigma RONO_2$ + MVK + MACR) and it may be reaction of one of the unresolved initial products that consumes most of this NO_3 and produces SOA.

3.3.2 Peroxy radical fate

The relative concentration of peroxy radical reaction partners RO_2, HO_2 and NO_3 can lead to differences in observed yields of i.e. peroxides, hydroperoxides and nitrates between experiments. We used the MCM based model described in this paper to calculate the relative

importance of the three possible peroxy radical reaction partners, and the model includes HO_2 enhancements due to the OH + CO $\rightarrow$ HO_2 reaction. Figure 3.6 shows the modeled contributions of these three radicals to the total RO_2 reactions throughout the experiment. For the majority of the experiment the RO_2 fate is almost entirely dominated by reaction with peroxy and hydroperoxy radicals. NO_3 is modeled to be a significant reaction partner for peroxy radicals for a brief period of time in the middle of the experiment when the isoprene concentration was zero and the nitrate radical production rate was high ($\approx 1.5\,\mathrm{ppt\,s^{-1}}$). During this time, a large concentration of NO_3 accumulated ($\max \approx 150\,\mathrm{ppt}$) at the same time that RO_2 and HO_2 production decreased.

While it would be interesting to use this experiment to help clarify the role of nighttime peroxy radical reactions in tropospheric chemistry, direct comparison of the modeled peroxy radical chemistry to the nighttime atmosphere is not conclusive. Box models simulating nighttime chemistry are in disagreement as to whether or when NO_3 + RO_2 reactions can compete with RO_2 + RO_2 and RO_2 + HO_2 as a sink for RO_2. At least two studies have concluded that in polluted environments NO_3 can be an important sink for RO_2 [*Geyer et al.*, 2003b; *Vaughan et al.*, 2006], while *Bey et al.* [2001] conclude that this process is insignificant. One of the reasons for this discrepancy may be the lack of detailed knowledge surrounding RO_2 + RO_2 and RO_2 + NO_3 reaction rates. Our experiment does not address constraints to these rates

We do note that model calculations (both the modified model and MCM) suggest that HO_2 dominates the fate of peroxy radicals in the chamber. If all RO_2 + HO_2 reactions formed a hydroperoxide via RO_2 + HO_2 $\rightarrow$ ROOH, than the majority of the oxidation products would be hydroperoxides instead of carbonyls. *Ng et al.* [2008] conducted a chamber study with higher total radical concentrations, but presumably similar ratios between HO_2 and RO_2. They observed a ratio of carbonylnitrate : nitrooxy hydroperoxide of $\approx$4 - 5. These combined results suggest that either the rate of RO_2 + RO_2 is much faster relative to RO_2 + HO_2 than used in our calculations, or that the yield for hydroperoxides from RO_2 + HO_2 may be significantly less than 100%. Laboratory [*Hasson et al.*, 2004; *Jenkin et al.*, 2007; *Crowley and Dillon*, 2008] and theoretical [*Hasson et al.*, 2005] studies have shown that while the hydroperoxide yield from small peroxy radicals such as methyl peroxy and ethyl peroxy is near 100%, larger more substituted peroxy radicals especially of the form R(O)OO may form alcohols or OH in high yields from the reaction with HO_2. Photochemical box models have also been shown to more accurately reproduce field data if RO_2 + HO_2 reactions are not chain terminating sinks of HO_X [e.g., *Thornton et al.*, 2002; *Lelieveld et al.*, 2008]. Thus, the yield of ROOH from RO_2 + HO_2 reactions is currently an open question.

3.4 Aerosol

Figure 3.1 shows the raw AMS signal. The AMS indicated some brief initial increase in SOA with the injection of O_3, but this production did not continue throughout the experi-

ment and our analysis focuses on the more significant growth between 14:00 and 17:00 UTC. The number density of particles followed a monotonic exponential decay with a lifetime of 3.7 hours throughout the experiment, presumably due to wall losses and chamber dilution. We assume that the observed OA at some time t is due the combined effects of SOA production $P(t)$ and loss $L(t)$. The loss between AMS data points separated by Δt is assumed to be proportional to the observed OA at some time ($C(t)$), such that losses alone would yield

$$C(t + \Delta t) = C(t)e^{-\Delta t/3.7h} \tag{3.2}$$

Therefore, the production between data points is the difference between the observed OA at time $t + \Delta t$ and the concentration that would have been observed from wall losses alone

$$P(t) = C(t + \Delta t) - C(t)e^{-\Delta t/3.7h} \tag{3.3}$$

To correct the AMS data for these losses we calculated the sum of the production terms for all previous time steps, so that the corrected OA is

$$C_{corrected}(T) = C(0) + \sum_{t=0}^{T} P(t) \tag{3.4}$$

In Figure 3.7 we show the SOA corrected for this loss with $t = 0$ being 7:23.

Secondary organic aerosol was observed to increase rapidly during the phase of the experiment when the isoprene concentration was low and the NO_3 concentration was at its peak. In Figure 3.1 panels a, c, and f it can be observed that the increases in organic and nitrate aerosol were correlated to NO_3 concentration, not O_3. SOA production ceased immediately when the NO_3 concentration decreased within minutes from >150 ppt to <5 ppt, while O_3 concentration was smoothly and slowly decreasing. The rapid growth of SOA observed uniquely in the presence of high NO_3 concentration indicated that SOA formation was initiated by NO_3 oxidation rather than O_3. The fact that this growth also took place when isoprene concentration was at a minimum indicated that this SOA was generated upon reaction of NO_3 with one of the initial isoprene oxidation products as opposed to isoprene itself. A final mass yield in the traditional sense

$$Y = \frac{\Delta\text{organic aerosol mass}}{\Delta\text{isoprene mass}} \tag{3.5}$$

of 2% was observed.

Figure 3.7 shows the change in AMS organic aerosol corrected for chamber dilution and wall loss (green), the modeled net amount of isoprene consumed by NO_3 (blue), and the modeled net amount of isoprene nitrates (produced by the isoprene + NO_3 reaction with a 70% yield) consumed by reaction with NO_3 (extent of reaction R5 from Table 3.1, red line). The blue curve shows Δisoprene (μg / m^3) and the red curve shows the moles of second

generation oxidation products multiplied by the molecular weight of isoprene. We define this quantity as $\Delta\text{isoprene}^{2X}$ because it is the mass concentration of isoprene which reacted two times with NO_3.

Mass yields with respect to isoprene can be read for the first and second oxidation steps by comparing these lines to the AMS data. We consider the time period between 10:00 UTC and 14:30 UTC as the isoprene oxidation period and use this time to calculate the SOA yield for isoprene. The period between 14:30 and 16:30 was when the secondary chemistry became much more important, and therefore we use this time period to calculate SOA from this secondary chemistry. In Figure 3.7 these periods are distinguished with vertical dashed lines, and the calculated concentrations of the oxidation products are noted at these times. The change in isoprene consumed from 10:00 - 14:30 is $\Delta\text{isoprene} = 13.2 - 4.2 = 9\,\mu\text{g}\,\text{m}^{-3}$, and from 14:30 - 16:30 the change in $\Delta\text{isoprene}^{2X} = 4.5 - 0.47 = 4.03\,\mu\text{g}\,\text{m}^{-3}$. Using 15 minute averages, we calculate that at 10:00, 14:30 and 16:30 the loss corrected OA concentrations were 0.56 ± 0.04, 0.56 ± 0.04, and $1.08 \pm 0.02\,\mu\text{g}\,\text{m}^{-3}$ respectively. Therefore from 10:00 - 14:30 $\Delta\text{OA} = 0.00 \pm 0.06$ and from 14:30 - 16:30 $\Delta\text{OA} = 0.52 \pm 0.04$. Using the error in the ΔOA from 10:00 - 14:30, we calculate the upper limit of SOA from isoprene by mass as $0.06 \,/\, 9 = 0.7\%$. For the second oxidation step we calculate $0.5 \,/\, 4.03 = 14\,\%$. The error however in the estimate of yield from second generation products is large and is dominated by the error in our fitting of the reaction rate for the first generation products with NO_3, which we estimated at 43% of the reaction rate (Section 3.3.1) so that the SOA yield would be $14 \pm 6\%$.

The TD-LIF instrumentation observes the sum of gas and aerosol organic nitrates. Figure 3.8 shows the changes in TD-LIF signal and AMS nitrate, with both measurements averaged to 15 minute resolution. We observed an increase of $\approx 4\,\mu\text{g}\,\text{m}^{-3}$ total organic nitrate coincident with 0.12 μg m^{-3} aerosol nitrate. This indicates that $\approx 3\%$ of the organic nitrate produced in the second oxidation step partitioned to the particle phase. Of the final SOA products which exist in gas / particle equilibrium, the molecular yield can be calculated by scaling the mass yield (14%) by the relative molecular weights of isoprene and of the SOA. For example, assuming particle/gas equilibrium if the primary SOA component were a C_5-dinitrate-diol ($C_5H_{10}O_8N_2$) with MW = 226, the fraction of this molecule in the particle phase would be $14 \pm 6\% \times 68 \,/\, 226 = 4 \pm 2\%$ which is in agreement with our nitrate partitioning observation of 3%.

3.4.1 SOA Composition

The design of the gas phase model used in this study was primarily motivated by accurately calculating the partitioning of NO_y throughout two stages of isoprene oxidation, and thus species were lumped according to their nitrate content. However, other studies [*Barnes et al.*, 1990; *Skov et al.*, 1992; *Ng et al.*, 2008; *Perring et al.*, 2009] have distinguished hydroxynitrates, carbonylnitrates, and peroxynitrates as the majority of the oxidation products. In Figure 3.9 we consider physical properties including expected SOA yields of some of the spe-

cific molecules that may be responsible for SOA produced from the isoprene + NO_3 system. These expected yields are then compared to the calculated $14 \pm 6\%$ mass yield, and $4 \pm 2\%$ molar yield from the second oxidation step.

This figure depicts the evolution of isoprene oxidation products through two stages of oxidation by nitrate radical, assuming that in each step the reaction takes place by addition of NO_3 to one of the C=C bonds. For simplicity, we consider secondary oxidation products produced by the reaction of NO_3 with the C_5 hydroxynitrate, as the consumption of this product was highly correlated with SOA formation in the study of *Ng et al.* [2008]. We note that sulfate esters of i.e. the diol-dinitrate (MW = 226) have been measured in particles both in labratory [*Ng et al.*, 2008] and field [*Surratt et al.*, 2008] samples, supporting these as likely candidates for SOA formation here. Similar second generation structures to those depicted could be arrived at from reactions of the C_5 carbonylnitrate, and the predicted vapor pressures of these products are a factor of 6 - 8 higher than for the analogous hydroxynitrate. Although multiple isomers of each molecule are possible, we show only one of each for simplicity. The vapor pressure of these molecules is determined primarily by the number of carbon atoms and the molecular functionalities, various isomers should have similar vapor pressures. For the first generation products we calculate vapor pressures for the C_5 compounds of 13 - 0.97 Pa, and for the C_{10} peroxide, 4.1×10^{-3} Pa. For the second generation products with 4 functional groups, we calculate 5.2×10^{-5} - 9.7×10^{-5} Pa for the C_5 compounds, and 1.3×10^{-11} Pa for the C_{10}. Also in Figure 3.9 for each molecule we show the molecular weight (Da, black), and effective saturation concentration C^* (μg m^{-3}, green). From the effective saturation we calculate the fraction of this molecule residing in the particle phase in the presence of 0.52 μg m^{-3} organic aerosol (red), which was the actual (not dilution corrected) OA at 16:30. Vapor pressures are estimated using the group contribution method [*Pankow and Asher*, 2008] which has been demonstrated to estimate these values to within a factor of 2 for 456 atmospheric compounds spanning 14 orders of magnitude in P_L^0. The vapor pressure is related to an equilibrium partitioning coefficient (K) and to the effective saturation concentration (C^*) by

$$K = \frac{1}{C^*} = \frac{760RT}{MW_{\mathrm{om}} 10^6 \xi P_L^0} \tag{3.6}$$

with R being the ideal gas constant (8.206×10^{-5} m^3 atm mol^{-1} K^{-1}), T is the temperature (K), MW_{om} is the mean molecular weight of the organic aerosol (g mol^{-1}) and ξ is the activity coefficient of the species in the organic aerosol phase, which is typically assumed to be 1 [*Odum et al.*, 1996]. For these calculations we assume $MW_{\mathrm{om}} = 226$ g mol^{-1} which is the molecular weight of the C_5 dinitrate-diol. The fraction of a given molecule i which is residing in the OA phase (Y_i) is then calculated under these assumptions using the relationship between C^*, the particle phase (C_p) and gas phase (C_g) concentrations of species, and the ambient OA concentration (M_0):

$$\frac{1}{C^*} = \frac{C_p}{C_g M_0} \tag{3.7}$$

$$Y_i = \frac{M_0/C^*}{1 + M_0/C^*} \tag{3.8}$$

At low concentrations of aerosol, the yield calculated as a function of vapor pressure is highly sensitive to both M_0 and MW_{om}. For example, in Fig. 3.9 we state that for $MW_{\mathrm{om}} = 226$ and $M_0 = 0.52$ μg m^{-3}, $Y_i = 5.6\%$. Varying M_0 from 0.4 - 0.6 μg m^{-3} with MW_{om} fixed at 226 g/mol we calculate $Y_i = 4$ - 6% for this compound. If instead we hold M_0 fixed at 0.52 μg m^{-3} and vary MW_{om} in the range 150 - 300 g/mol, we calculate $Y_i = 4$ - 8%. Generally, given uncertainties in MW_{om} and M_0 we find that equilibrium partitioning predicts yields of <<1% for the first generation products, $\approx$4 - 20% for the second generation C_5 products, and >95% for the C_{10} peroxides. Considering the factor of two uncertainty in the vapor pressures of the oxidation products and the assumption that $\xi = 1$, we find these predicted yields reasonably close to the $4 \pm 2\%$ molar yield observed and conclude that the primary components of the aerosol are most likely C_5 second generation oxidation products. The yields that would have been observed if the aerosol was primarily composed of first generation oxidation products or highly functionalized peroxides are well outside of this range. Figure 3.10 shows the AMS nitrate vs AMS organic signals from UTC 14:15 - 24. A linear fit to the data indicates that the ratio of nitrate:organic of the SOA (on a mass basis) was approximately 0.18. The production of SOA with a nitrate:organic ratio of 0.18 could in principle be due to condensation either of a single nitrate containing organic compound with this ratio, or by co-condensation of multiple oxidation products. In Fig. 3.9 (purple numbers) we have estimated the nitrate:organic mass ratio that would be observed for the presumed second generation products, assuming that $RONO_2$ fragments in the AMS as R (organic) and ONO_2 (nitrate) and each are detected with equal efficiency. The calculated values are shown in purple. All molecules have nitrate:organic mass ratios >1, much too large to explain the observations. Fragmentation of organic nitrates $RONO_2 \rightarrow RO + NO_2$ on the AMS heater is likely, which would reduce these ratios somewhat by reducing the nitrate mass and increasing the organic mass by 16 g/mol (one O atom) for each nitrate group. For example, the dinitrate-diol structure of MW 226 would in this case have a nit:org ratio of 0.69 instead of 1.2. This however is still much higher than our observed 0.18. The discrepancy here could be explained by a number of mechanisms, including: 1) co-condensation of nitrate and non-nitrate organics, 2) polymerization of the nitrate peroxy radicals with non-nitrate containing species, or some other addition of non-nitrate functional groups to the isoprene oxidation products, 3) underestimation of the nitrate content in the aerosol, or 4) release of nitrogen upon condensation of organic nitrates.

Isoprene (C_5H_8) and nitrate radical (NO_3) respectively have molecular weights of 68, and 62. If a single molecule is forming the SOA through the addition of one nitrate radical followed by the polymerization of isoprene units, this would be somewhere between 5 and 6 isoprene units (0.18 and 0.15 nitrate / organic mass respectively). Even if we assume that oxidation of each double bond of isoprene adds 2 oxygens to the mass ($C_5H_8O_4$, MW = 132) this would require at least two fully oxidized isoprenes per nitrate group. Laboratory

studies have observed the formation of polymers in SOA from isoprene [*Surratt et al.*, 2006] and other precursor VOC's [*Jang et al.*, 2002; *Kalberer et al.*, 2004; *Muller et al.*, 2008] by various mechanisms some of which may be possibilities here.

An internal isomerization of the δ-alkoxy radical formed by NO_3 addition to isoprene at the 1 position via a 6 membered ring is also a possibility for adding non-nitrate functionality to the oxidation products (Figure 3.11). Such isomerizations have been suggested as responsible for observed products from the isoprene + NO_3 reaction in the studies of *Kwok et al.* [1996] and *Ng et al.* [2008]. This could lead to a slight decrease in the nitrate:organic ratio: 0.93 vs the 1.2 for example if the second double bond of the two products shown in Figure 3.11 reacts again with NO_3. *Atkinson* [2007] recommends estimated rates of internal isomerization vs. reaction with O_2 for alkoxy radicals based on a structure-reactivity relationship and these rates can in principle be used to estimate the relative importance of the products formed from these two different alkoxy reaction channels. The recommended reaction rate with O_2 at 298 K is $k_{O_2} = 9 \times 10^{-15}$ molecule^{-1} cm^3 s^{-1} so that at 21% O_2 standard conditions, $k_{O_2}[O_2] = 4.6 \times 10^4$ s^{-1}. The recommended isomerization rate is $k_{isom.} = 3.2 \times 10^5$ s^{-1}, nearly 7 times as fast as the reaction with O_2, suggesting that molecules formed from the rearrangement might be expected to account for a significant fraction of the carbon balance. The production of this molecule as a main product of the isoprene + NO_3 reaction would not be in conflict with previous product studies for which organic nitrate standards were not available and for which the product chemical structure has been deduced based on the existence of carbonyl and nitrate peaks in FTIR spectra. *Ng et al.* [2008] however do not report significant yields of this product, even though it would have been likely to be detected by their CIMS with comparable efficiency to other products that are reported. *Perring et al.* [2009] do not report this either, though carbon closure in that experiment is reported to be within 10%.

Ng et al. [2008] reported observing many multifunctional organic nitrates and dinitrates in both the gas phase, and on filter samples produced in their isoprene + NO_3 experiment. Although an AMS nitrate:organic ratio for this experiment was not reported, and it is possible that there were many unidentified products, all of the structures observed with their CIMS and filter extraction TOFMS have much higher nitrate:organic ratios than we measured. Furthermore, as we have observed in the initial reaction, and as is well founded for many alkene NO_3 reactions, the yield of organic nitrate formation from these reactions is high. The continued oxidation of double bond containing isoprene oxidation products is expected to lead to the formation of organic nitrates. Therefore it seems most reasonable that the condensing species were similar to the C_5 dinitrate species in Figure 3.9. Our data can neither confirm nor deny the possibility of release of NO_X during SOA formation due to rapid changes in total NO_2 which would have been only contributed to in a minor way from this process. While AMS nitrogen:carbon and oxygen:carbon ratios have been verified for nitrogen containing compounds including amines, amides and phenols, [*Aiken et al.*, 2007] similar results have not been reported for molecules containing $RONO_2$ groups, leaving open the possibility that organic nitrate content is underestimated.

3.5 Atmospheric Implications

Our observations indicate that the formation of SOA from isoprene + NO_3 under typical concentrations of OA will rely on the extent to which both double bonds of isoprene are oxidized. Here, we observed oxidation of both bonds via reaction with NO_3. However, the exchange of a nitrate group with a hydroxy group has a minor affect on the effective saturation concentration, thus we expect that reaction with NO_3 followed by reaction with OH or vice versa would produce a similar aerosol yield. To consider the extent to which these second oxidation steps will take place in the atmosphere, we compare the lifetime of the initial oxidation products to reaction with OH and NO_3 to their lifetimes with respect to wet and dry deposition.

MCM uses a rate constant for 4-nitrooxy-3-methyl-2-butanal with OH of 4.16×10^{-11} molecules^{-1} cm^3 s^{-1}. This rate is roughly consistent with those measured by *Treves and Rudich* [2003] for unsaturated hydroxyalkyl nitrates. At an average daytime concentration of 2×10^6 molecules / cm^3 this would give a lifetime to OH of 3.3 hours, indicating these compounds generated at night by NO_3 chemistry remaining through the next morning would be consumed by reaction with OH early in the day.

We found an effective rate constant for the initial oxidation products with NO_3 of 7.0×10^{-14} molecules^{-1} cm^3 s^{-1}. Nighttime NO_3 concentrations are highly variable ranging from 0 to hundreds of pptv, and depend on the availability of NO_X. In a recent study *Brown et al.* [2009] show that the first generation daytime isoprene oxidation products MVK and MACR, are found at ppb levels along with 50-100 ppt NO_3. This range of NO_3 concentrations would yield 3.1 - 1.6 hours for lifetimes of isoprene nitrates.

We use the method of *Brimblecombe and Dawson* [1984] to estimate the wet deposition rate of the first generation oxidation products. This method has been used previously to estimate the wet removal rate of hydroxy-nitrate isoprene oxidation products [*Shepson et al.*, 1996]. Henry's law coefficients at 283K of 4-nitrooxy-3-methyl-2-butanal (2.3×10^4 M/atm) and 4-nitrooxy-3-methyl-2-butanol (3.3×10^5 M/atm) were calculated using the SPARC online calculator [*Hilal et al.*, 2003, 2004]. Using the same assumptions for mid-latitude meteorology as *Shepson et al.* [1996] and *Brimblecombe and Dawson* [1984], we use these Henry's law constants to calculate rainout rates of 2.3×10^{-6} s^{-1} for the carbonyl-nitrate and 5.5×10^{-6} s^{-1} for the hydroxy-nitrate. These rates imply rainout lifetimes of these species of 5 and 2.1 days respectively, both which are too slow to compete with the lifetime to reaction.

Lifetimes to dry deposition are perhaps less well constrained, although we note that loss to dry deposition is unlikely at night because most of the isoprene + NO_3 reaction will take place above the nocturnal boundary layer. Dry deposition velocities (v_d) of HNO_3 have been reported in the range of 2 - 4 cm s^{-1} [*Seinfeld and Pandis*, 1998; *Farmer and Cohen*, 2008], while reported PAN deposition velocities range from 0.25 - 0.8 cm s^{-1} [*Turnipseed et al.*, 2006; *Garland and Penkett*, 1976; *Farmer and Cohen*, 2008; *Wolfe et al.*, 2008]. Multi-functional nitrate deposition velocity have been measured by *Shepson et al.* [1996] and *Farmer and Cohen* [2008] at 0.4 cm s^{-1} and 2.0 cm s^{-1} respectively, and inferred from NO_y fluxes by

Munger et al. [1996] ranging from 0.5 cm s^{-1} at night to 2 cm s^{-1} during the day. Assuming the same scale height as we use for the wet deposition calculation (2.3 km) the lifetime ($\tau = Z/v_d$ where Z = scale height) for v_d of 0.25 - 2.0 cm s^{-1} would be 10 - 1.3 days if it were important.

These estimates of wet and dry deposition lifetimes of the carbonyl- and hydroxy-nitrate first generation oxidation products of isoprene are significantly longer than lifetimes to chemical reaction by average daytime OH concentrations, and NO_3 concentration greater than 10 ppt. For NO_3 above 10 ppt the first generation oxidation products are likely to react with NO_3 at night converting them to condensible species, but on timescales longer than the rapid reaction of isoprene with NO_3 that has been observed immediately after sunset. For much smaller NO_3 concentrations, transport at night, daytime deposition or OH oxidation will dominate the fate of these nitrates.

3.6 Summary and Conclusions

We have observed the reaction of isoprene with nitrate radicals at atmospherically relevant concentrations of VOC and oxidants (9.6 ppb isoprene, 16 ppb NO_2, 37 ppb O_3). A modified version of the MCM was used to evaluate the yields for alkyl nitrates from the reaction of isoprene with NO_3 (70%) and for the subsequent reaction of the first generation oxidation products with NO_3 (20-60%). Alkyl nitrate observations which were significantly lower than predicted by the MCM were used to determine an effective rate constant for reaction of the group of first generation oxidation products with NO_3. We observed that SOA is formed from the isoprene / NO_3 system, but at low organic aerosol concentration (<1 μg / m^3), only when both double bonds of isoprene are oxidized. Using the modified MCM, we estimate that the SOA mass yield of isoprene which reacts two times with NO_3 is 14% and show that this yield is consistent with equilibrium partitioning of the expected oxidation products. Modeling also indicates an inconsistency between the current estimations of the relative magnitudes of the rate constants for RO_2 + RO_2 vs RO_2 + HO_2, and the expectation that RO_2 + HO_2 $\rightarrow$ ROOH with a 100% yield. The AMS data reported much less nitrate content than would be expected from these structures, and we therefore conclude that either some additional chemistry was responsible for the chemical content of the SOA, or the aerosol nitrogen content is higher than measured.

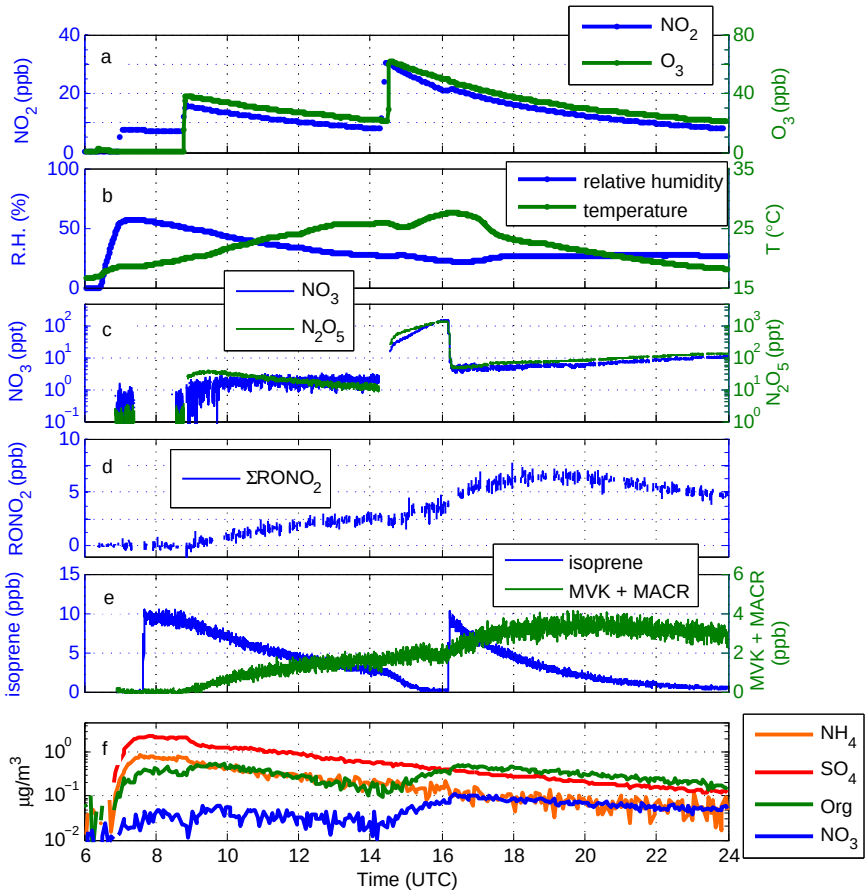

Figure 3.1: Descending top to bottom, measurements of (a) NO_2 and O_3 (CL measurement), (b) chamber temperature and relative humidity (RH), (c) NO_3 and N_2O_5 (CaRDS), (d) organic nitrates ($RONO_2$, TD-LIF), (e) isoprene and the sum of methacrolein and methyl vinyl ketone (PTR-MS), and (f) AMS measurements of aerosol composition.

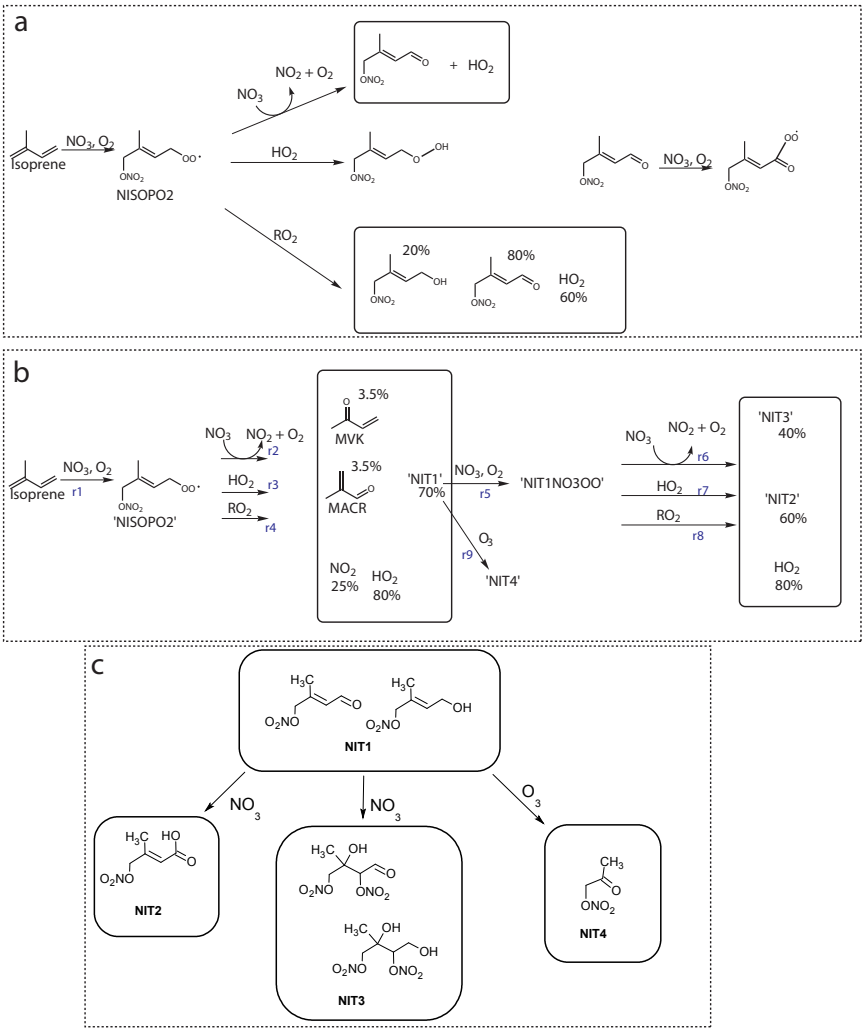

Figure 3.2: a: Schematic of isoprene + NO_3 mechanism MCM V3.1. 100% of first generation oxidation products are alkyl nitrates. The only first generation product which is reactive towards NO_3 is the carbonyl nitrate, which reacts in an aldehyde + NO_3 mechanism at a rate of 1.1×10^{-14} molecule^{-1} cm^3 s-1. b: The modified mechanism used in this study. NIT1 - 4 are lumped species representing organic nitrates produced by the first (NIT1) and second (NIT2, NIT3, NIT4) oxidation steps. NIT1 has one $RONO_2$ group and one carbon-carbon double bond. Oxidation of the second double bond by NO_3 is presumed to either leave the original nitrate functionality (NIT2) or add an additional $RONO_2$ group (NIT3). Oxidation of NIT1 by O_3 is presumed to leave the nitrate functionality (NIT4). NIT1NO3OO is the peroxy radical generated by reaction of NIT1 with NO_3 followed by O_2. c: Some example likely structures of the lumped species NIT1 - 4 used in the modified mechanism.

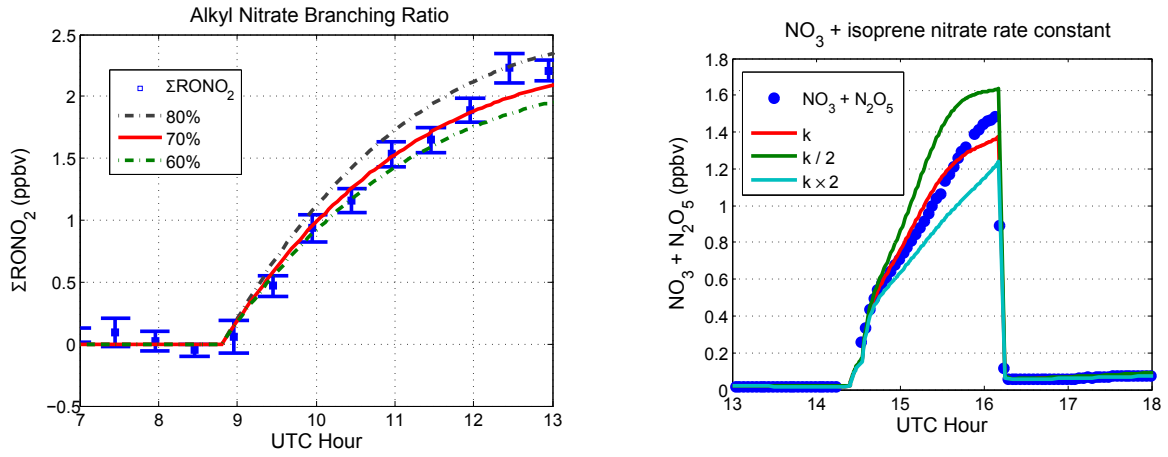

Figure 3.3: Left: Model with varying branching ratios for production of alkyl nitrates from the initial isoprene + NO_3 reaction. Error bars represent $\pm 2\sigma$ of TD-LIF measurement. Right: NOAA N_2O_5 and model calculations using k = 7.0 $\times 10^{-14}$ molecule^{-1} cm^3 s-1 for NO_3 + NIT1.

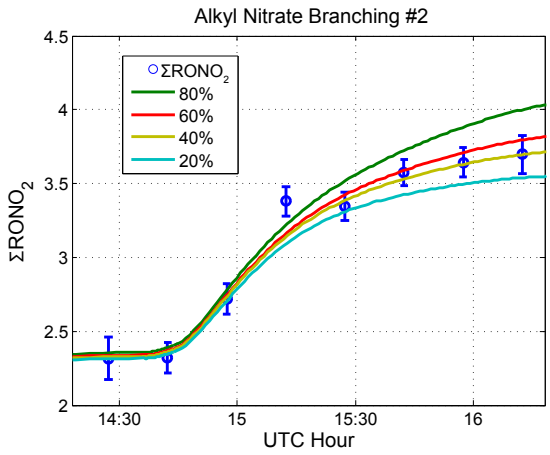

Figure 3.4: Model runs varying the branching ratio to form alkyl nitrates from the oxidation of isoprene's second double bond.

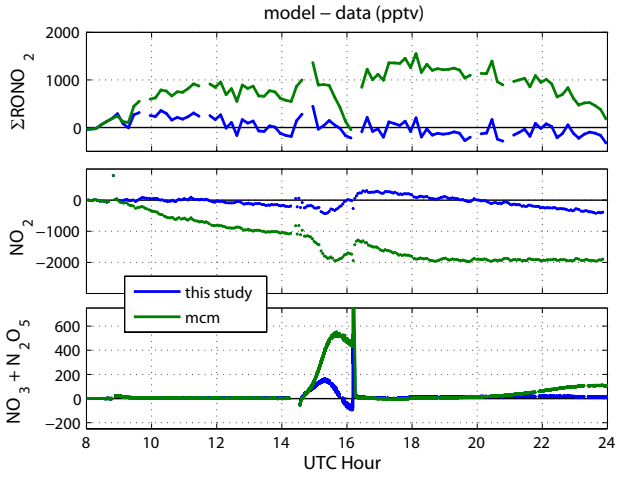

Figure 3.5: Differences between data and model (data - model) for (top) $\Sigma RONO_2$, (middle) NO_2, and (bottom) NO_3 + N_2O_5. Green lines are calculations from MCM V3.1 and blue lines are the modified model from this work.

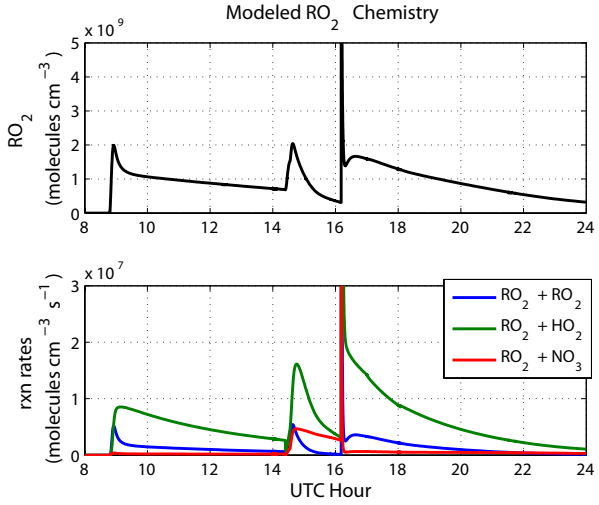

Figure 3.6: Modeled calculations of (top) total peroxy radicals concentrations, and (bottom) sum of the rates of all RO_2 + RO_2 reactions (blue), all RO_2 + HO_2 reactions (green) and all RO_2 + NO_3 reactions (red).

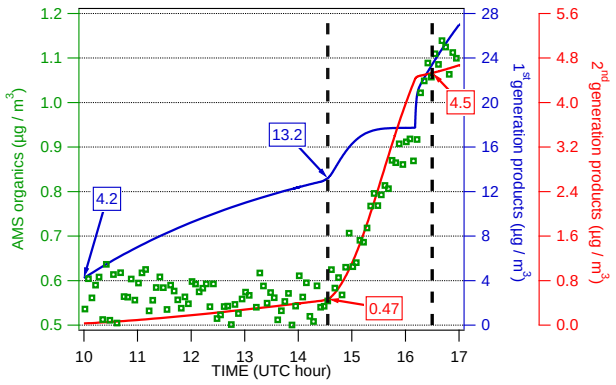

Figure 3.7: Wall loss corrected AMS organics (green line, left axis), the modeled first generation oxidation products (blue line) and second generation oxidation products (red). Modeled first and second generation products are both expressed in units of $\mu g/m^3$ of the initial isoprene reacted, calculated as moles / m^3 of product $\times$ the molecular weight of isoprene, allowing the mass yield ($\Delta VOC / \Delta SOA$) from each step to be calculated by comparing the product mass to measured organic aerosol mass. Different time periods used to calculate the yield of SOA from first generation oxidation (10 - 14:30) and second generation oxidation (14:30 - 16:30) are separated by vertical dashed lines. The indicated data points are used for calculating the yields.

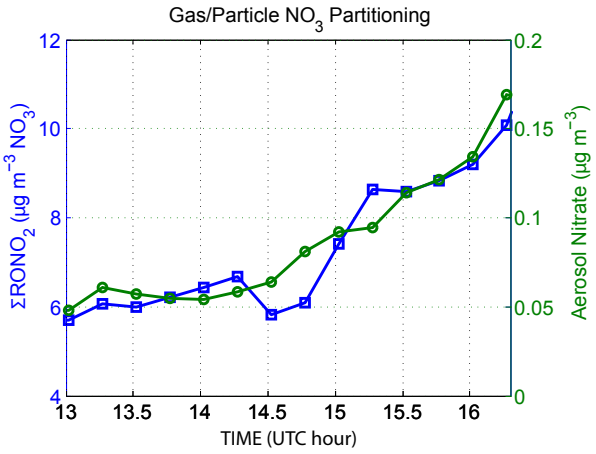

Figure 3.8: Increases in TDLIF gas + aerosol $RONO_2$ (blue) and AMS nitrate (green) during the second oxidation step in the chamber. AMS and TDLIF data are mapped to the same time resolution using 15 min means.

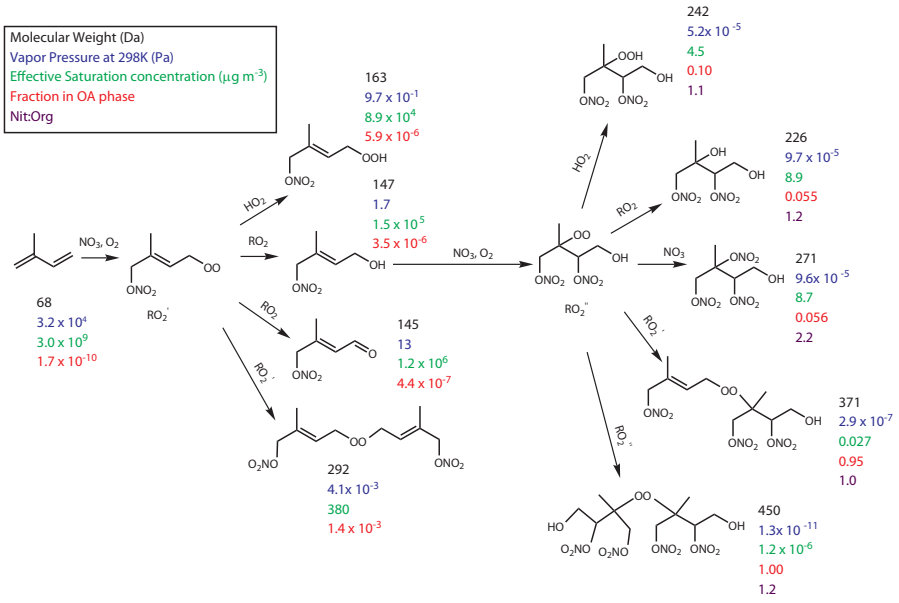

Figure 3.9: The molecular weight (Da, black), vapor pressure (Torr, blue), effective saturation at $MW_{\mathrm{om}} = 226$ g/mol (μg/m^3, green) equilibrium partitioning in OA phase at 0.52 μg/m^3, and nitrate:organic ratio of the expected products of two stages of isoprene oxidation by NO_3.

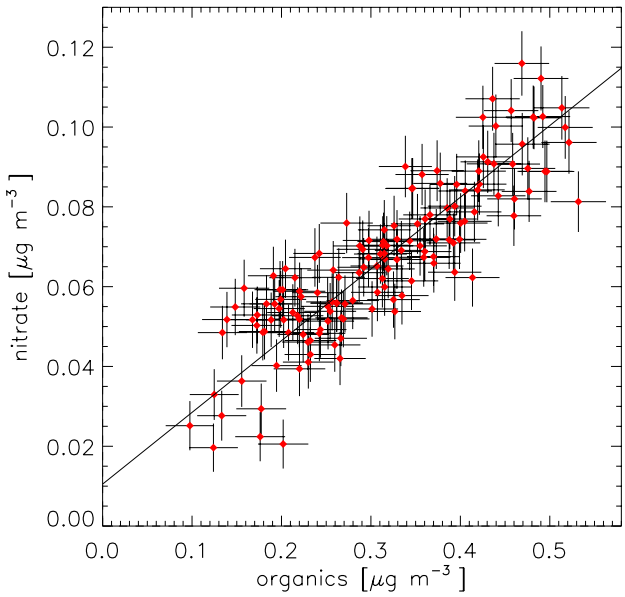

Figure 3.10: AMS organic aerosol vs AMS nitrate aerosol following 14:15 UTC. A linear fit to the data yields a slope of 0.180 ± 0.007, $R^2 = 0.76$, $\chi^2/N = 1.19$.

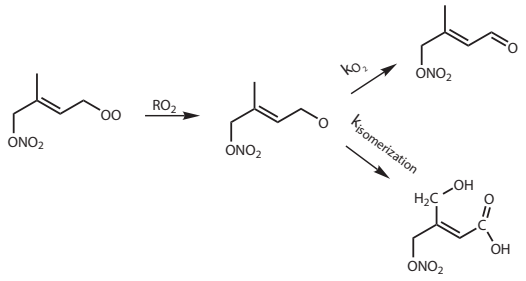

Figure 3.11: Isomerization vs decomposition of the nitrate oxy radical. Multiple steps in the isomerization channel are left out of diagram for simplicity. Only final stable products are shown.

Table 3.1: Gas phase reactions and rates included in reduced isoprene chemistry model.

rxn #	reaction	rate at 298K (molecule $^{-1}$ cm^3 s^{-1} unless noted)	reference
1	C5H8 + NO_3 → NISOPO2	6.78×10^{-13}	MCM V3.1
2	NISOPO2 + NO_3 → 0.70NIT1 + 0.035 MVK + 0.035 MACR + 1.25 NO_2 + 0.80 HO_2	2.5×10^{-12}	MCM V3.1
3	NISOPO2 + HO_2 → 0.70NIT1 + 0.035 MVK + 0.035 MACR + 0.25 NO_2 + 0.80 HO_2	2.3×10^{-11}	MCM V3.1
4	NISOPO2 + RO_2 → 0.70NIT1 + 0.035 MVK + 0.035 MACR + 0.25 NO_2 + 0.80 HO_2	1.30×10^{-12}	MCM V3.1
5	NIT1 + NO_3 → NIT1NO3OO	7×10^{-14}	fit
6	NIT1NO3OO + NO_3 → 0.6 NIT2 + 0.4 NIT3 + NO_2 + 0.8 HO_2	2.5×10^{-12}	MCM V3.1
7	NIT1NO3OO + HO_2 → 0.6 NIT2 + 0.4 NIT3 + 0.8 HO_2	2.3×10^{-11}	MCM V3.1
8	NIT1NO3OO + RO_2 → 0.6 NIT2 + 0.4 NIT3 + 0.8 HO_2	1.30×10^{-12}	MCM V3.1
9	NIT1 + O_3 → NIT4	3×10^{-18}	fit (assumed $4.3 \times 10^{-5} \times k_5$)
10	NO_3 → walls	1.0×10^{-3} s^{-1}	fit
11	N_2O_5 → walls	1.1×10^{-4} s^{-1}	fit
12	$RONO_2$ → walls	2.2×10^{-5} s^{-1}	fit

Table 3.2: Summary of studies reporting quantified yields of total organic nitrates from isoprene + NO_3 reaction.

description	detection	results	source
$\approx 10 - 24 \times 10^{13}$ molecules cm^{-3} N_2O_5 added to $\approx 5 \times 10^{14}$ molecules cm^{-3} isoprene in a 420 L glass reaction chamber at 298±2K	In situ FT-IR of $RONO_2$.	$\approx$ 80% yield of $RONO_2$	*Skov et al.* [1992]
134 ppb isoprene added to 82 - 90 ppb N_2O_5 in 5500L teflon chamber	TD-LIF detection of $\Sigma RONO_2$ and PTR-MS detection of specific oxidation products.	65±10% $RONO_2$ yield	*Perring et al.* [2009]
9.6 ppb isoprene, 16 ppb NO_2 and 37 ppb O_3 added to 270 m^3 chamber	TD-LIF detection of $RONO_2$, PTR-MS detection of isoprene.	70±8% yield of $RONO_2$	This study

Chapter 4

Elemental analysis of aerosol organic nitrates with electron ionization high-resolution mass spectrometry

4.1 introduction

Aerosol mass spectrometry is a widely used method for measuring atmospheric aerosol composition. The most common implementation of this class of instruments is the Aerodyne Aerosol Mass Spectrometer (AMS) of which more than 80 instruments are currently in operation worldwide. Due to its ubiquitous use in laboratory and field experiments, much of what is known about ambient atmospheric and laboratory aerosol composition relies on the accurate interpretation of AMS data. One of the main advantages of the AMS is it's combination of flash volatilization with electron impact (EI) ionization which results in a relatively uniform sensitivity to all non-refractory (NR) components of aerosols, allowing for a measurement of total particle mass with high time resolution and without requiring detailed prior knowledge of the aerosol chemical composition [*Jimenez et al.*, 2003].

AMS spectra of ambient aerosol consists of a complex set of fragments with the majority of the mass typically detected as fragments with mass/charge ratios (m/z) less than 100 due to the high degree of fragmentation induced by flash volatilization and electron impact. The increased internal energy of the vapors due to the flash volatilization is known to increase the degree of fragmentation relative to molecules at standard temperature [*Alfarra*, 2004; *Dzepina et al.*, 2007] and thermally unstable molecules such as ammonium nitrate are known to decompose prior to ionization. Due to the molecular fragmentation of the sampled particles, chemical speciation is typically limited to the identification of compounds with signature m/z (i.e. sulfate, nitrate, ammonium, chloride) and an assumption that the majority of the unidentified mass is organic [*Allan et al.*, 2004]. Positive matrix factorization has been applied to the resulting organic spectra [*Zhang et al.*, 2005; *Lanz et al.*, 2007, 2008] revealing

unique components of the spectra which are indicative of e.g. more or less oxidized molecules. Generally, oxygen content of the aerosol is observed to increase with the photochemical age of a plume and this trend has been shown to be consistent with other measures of organic mass:organic carbon.

Organic nitrates (R-O-NO_2) are ubiquitous in the atmosphere and are generated both from photochemical oxidation of VOC's in the presence of NO, as well as through oxidation of alkenes by nitrate radicals (NO_3). In particular, hydroxy nitrates (β and δ isomers) are the dominant organic nitrate oxidation product of alkenes including isoprene and monoterpenes (e.g. *Noziére et al.*, 1999, *Paulot et al.*, 2009). The addition of nitrate and alcohol groups have similar effects on the vapor pressure, and hence condensibility of an organic compound [*Pankow and Asher*, 2008; *Kroll and Seinfeld*, 2008]. As a result, oxidation of biogenic VOC's (BVOC) by NO_3 has been observed to produce aerosol with significant yields in chamber studies [e.g. *Hoffmann et al.*, 1997; *Ng et al.*, 2008; *Fry et al.*, 2009; *Rollins et al.*, 2009]. Organic nitrates might be expected to play an important role in production of Secondary Organic Aerosols (SOA) because of the correlation between NO_x and anthropogenic VOC emissions, because NO_3 is an effective means for oxidizing BVOC, and because $RONO_2$ are produced in high ($\approx$25%) yield in the RO_2+NO reaction for R>C_8 [*Arey et al.*, 2001]. However, identification of organic nitrates in ambient aerosol is difficult because it is expected to occur in coincidence with a large amount of inorganic nitrate. In AMS instruments the NO_3^- results in a large background signal at the main nitrate peaks (NO^+ and NO_2^+). Organic nitrates could in principle be determined by subtraction of the inorganic contribution at these peaks which is calculated assuming an ion balance between ammonium, sulfate and nitrate, and other minor inorganic components if present in the aerosol. This is difficult and a direct organic signature would be desirable.

Recently, the high resolution version of the AMS (HR-ToF-MS) has been used to determine elemental composition of organic aerosol [*Aiken et al.*, 2007, 2008]. While the AMS is to first order equally sensitive to all NR aerosol [*Jimenez et al.*, 2003], it is known to detect oxygen and nitrogen with somewhat reduced efficiency relative to carbon and hydrogen. *Aiken et al.* [2008] used a series of organic standards to determine calibrations for the calculation of O/C, H/C and N/C ratios from AMS data. This is possible with the HR-ToF-AMS because of its ability to distinguish different fragments with the same nominal mass, and compare the measured composition to the composition of the standards. These experiments did not include any organic nitrates because semi-volatile organic nitrates were not commercially available. Other nitrogen containing organic compounds were tested including amine, amide nitro and pyradine compounds. In contrast to these species organic nitrates are relatively thermally unstable and are known to decompose at 300–400 in 10's of ms the gas phase at atmospheric pressure [*Day et al.*, 2002]. Thus their detection could be more significantly affected by the combination of flash volatilization/EI than these other nitrogen containing organics.

We have synthesized 4 organic nitrates (C_4–C_{15}) and investigated the response of the AMS to these compounds. The molecules used here were all hydroxynitrates and were chosen for

their similarity to known oxidation products of atmospheric VOC's. Hydroxynitrates with e.g. isoprene and monoterpene carbon backbones have been observed in ambient aerosols [*Surratt et al.*, 2006; *Gómez-González et al.*, 2008b] making the molecules used in this study representative of organic nitrates believed to be in ambient aerosols. High resolution spectra were used to determine calibrations for elemental analysis based on these compounds. The differences between elemental analysis calibrations for organic nitrates and for the suite of compounds and ambient sample investigated by *Aiken et al.* [2008] and differences between AMS spectra of inorganic and organic nitrates are discussed.

4.2 Experimental

Four hydroxynitrate compounds including 2-hydroxy-limonene-1-nitrate, 1-hydroxy-butane-2-nitrate, 3-hydroxy-pinene-2-nitrate, and 3-hydroxy-caryophyllene-4-nitrate (and regioisomers) were synthesized by reacting an epoxide with fuming nitric acid (90%). Previous studies describing hydroxynitrate synthesis and characterization using this and other synthetic methods include *Nichols et al.* [1953], *Muthuramu et al.* [1993], *Treves et al.* [2000], *Spittler* [2001] and *Treves and Rudich* [2003]. The synthesis generated a mixture of regioisomers, and in Fig. 4.1 we show one isomer of each standard. In the following we describe the synthesis of the limonene hydroxynitrate. The other three compounds were prepared analogously.

4.2.1 Synthesis

To a flame dried 25 mL round bottom flask equipped with a stir bar was added 6.52 mmols (1.07 mL) of limonene-1,2-oxide (mixture of cis and trans, 97%, sigma-aldrich) and dissolved in 8 mL of dry diethyl ether (starting materials for the other standards were α-Pinene oxide (97%), 1,2-Epoxybutane (99%) and Caryophyllene oxide (>95%) all of which were obtained from Sigma-Aldrich). To another flame dried 25 mL round bottom flask equipped with a stir bar was added 3 mL of dry diethyl ether and 7.39 mmols (0.3 mL) of fuming nitric acid. These flasks were placed, under nitrogen, in a dewar and cooled to -90 via a methanol/acetone bath in a CryoCool immersion cooler. After cannulating the acid into the epoxide, the solution was kept at -90 for an additional hour. The reaction flask was then allowed to warm to room temperature over 12 h. The solution was washed several times with sodium bicarbonate to remove excess HNO_3 and then dried over magnesium sulfate. The ether layer was removed with a rotatory evaporator. The product was purified on a silica gel column with a 60/40 mixture of hexanes/ethyl acetate. A diffusion pump was finally used to remove any moderately volatile products from the standards by applying vacuum to $\sim$5 mTorr for one hour.

4.2.2 Characterization of standards

A 400 MHz NMR spectrometer was used to obtain ^{1}H NMR and ^{13}C NMR spectra. The observed chemical shifts for the limonene hydroxynitrate dissolved in $CDCl_3$ are as follows:

- ^{1}HNMR: 1.45 (2, m); 1.6 (3, s); 1.7 (3, s); 1.80 (2, m); 2.18 (2, m); 2.35 (1, m); 4.09 (1, m); 4.73 (2, m),
- ^{13}CNMR: 20.78; 20.83; 26.05; 29.88; 33.80; 36.78; 69.1; 91.45; 109.35; 148.43.

Our NMR observations are in agreement with those of *Spittler* [2001].

Thermal dissociation-laser induced fluorescence [*Day et al.*, 2002] measurements of the vapors in the headspace in each sample vial unambiguously identified the standards as being composed of alkyl nitrates. HNO_3, NO_2 and RO_2NO_2 compounds were not detected in the vapors.

Samples were analyzed for elemental composition using a standard combustion method (Perkin Elmer 2400 Series II). With this method, carbon, hydrogen and nitrogen content were measured on a mass basis with a stated accuracy of ±0.3%. Oxygen was assumed to be the remaining mass such that C+H+O+N=100%. Results of the combustion analysis are listed in Table 4.1.

4.2.3 HR-ToF-AMS analysis

The AMS has been extensively described in the literature [*Canagartna et al.*, 2007; *DeCarlo et al.*, 2006] and is only briefly described here. The AMS exists in three basic implementations. These instruments all sample gas and particles through an aerodynamic inlet which reduces the sampled gas relative to the particles by a factor of $\approx 10^7$. The resulting focused beam of particles with aerodynamic diameters ≈30–1000 nm is impacted on a heated surface (≈600 °C) where the non-refractory component of the aerosol is vaporized. The resulting vapors are ionized with 70 eV electron impact and measured with mass spectrometry. The three versions of the AMS differ primarily in the mass spectrometer used, which has evolved from quadrupole (Q-AMS) to time of flight (ToF-AMS) to high resolution time of flight (HR-ToF-AMS). The ToF-AMS has much higher precision than the Q-AMS because it is not a scanning instrument and therefore can in principle collect all of the m/z fragments from a single particle. HR-ToF-AMS has improved mass resolution, allowing for the distinction between different fragments with the same nominal mass (e.g. CH_2O^+ vs. NO^+).

For these experiments the higher resolution W mode of a HR-ToF-MS was used. Data was collected from m/z =10 to m/z =500. The data was analyzed using Igor Pro 6.04 (Wavemetrics, Lake Oswego, OR) which runs the standard HR-ToF-AMS software packages Squirrel 1.43 (ToF-AMS), Pika 1.03 (HR-ToF-AMS module) and Apes 1.00 (organic aerosol elemental analysis module).

Performing EA using the HR-ToF-AMS has been described in the literature [*Aiken et al.*, 2007, 2008] and is briefly described in this paper. This analysis relies on the principle that a given magnitude of signal (Hz) at any m/z corresponds roughly to the same original mass in the EI region of the instrument. For example, 1 μg/m^3 He and 1 μg/m^3 Ar would produce approximately equal signal count rates at m/z=4 (He^+) and 40 (Ar^+), even though the number of Ar atoms relative to He is 1/10. Furthermore, for molecules which fragment upon ionization, the size and identity of the fragment which retains the charge and is detected has no bearing on the size of the signal. This is because the detection efficiency is proportional to the probability of a molecule becoming ionized, which is to first order linear in the number of electrons and therefore the mass of the molecule [*Jimenez et al.*, 2003]. Regardless of the size of the fragment that leaves as charged, the resulting signal from one ionizing event

is 1 count (scaled by the detection efficiency of the instrument). Since the HR-ToF-AMS can determine the elemental composition of individual fragments by distinguishing between different fragments with the same nominal mass [*DeCarlo et al.*, 2006], an average elemental composition and atomic ratios can be calculated for the entire HR-ToF-AMS spectrum. Calculating the average elemental composition of just the organic part of the aerosol requires determining which fragments and also how much of the total signal at each fragment comes from the organic part of the aerosol. For ambient aerosol this can be difficult since inorganic aerosol and air may overlap at important *m/z* for particular types of compounds. As a pair of examples, H_2O^+ may come from both water vapor and the alcohol functional group, while NO^+ may appear due to either ammonium nitrate or organic nitrate molecules.

As discussed by *Aiken et al.* [2007, 2008] the contribution to the organic spectrum from the CO^+, O^+, OH^+ and H_2O^+ fragments cannot typically be measured directly by the AMS when sampling particles in air due to inorganic gas phase and particle phase interferences. The signal from the gas phase interferences is measured by intermittently blocking the particle beam, resulting in a gas only signal which is then subtracted from the gas+particle signal measured with the beam not blocked. The result will be precise however only if the gas is a small fraction of the total signal. CO_2 is one gas for example for which this could be expected to be an issue. 380 ppm CO_2 at standard conditions is $\approx 7\times10^5\, mu g/m^3$. Applying the nominal particle:gas enhancement factor of 10^7 to this results in a signal of $\approx 0.07\,\mu g/m^3$ from gas phase CO_2 which is a background signal over which the particle signal must be measured. For ambient organic aerosols on the order of $10\,\mu g/m^3$ where the CO_2 is typically on the order of 10–20% of the total organic aerosol signal [*Zhang et al.*, 2005; *Aiken et al.*, 2008] gas phase CO_2 is a minor interference. However, for less oxidized aerosols such as standards and chamber SOA, it can be significant because these aerosols produce very little CO_2^+ signal. We found for example with our pinene hydroxynitrate standard that with $150\,\mu g/m^3$ organic aerosol concentration, the gas and particle signals at CO_2^+ were ≈4:5, particle:gas. However, the reduction in the precision of the CO_2^+ fragment measurement for less oxidized aerosols has a small impact on the precision of the calculated O/C because as the noise in the particle CO_2^+ signal increases, the fraction of total particle mass from this fragment decreases. A similar analysis on water vapor at 50% RH and standard conditions results in a gas phase signal of $1.2\,\mu g/m^3$ H_2O, which is always a significant interference, even if gas phase water is reduced with a diffusion dryer. In our measured spectra of the butane hydroxynitrate we found that the expected H_2O^+ organic aerosol signal one calculates from the measured CO_2^+ and the fragmentation suggested by *Aiken et al.* [2008] is 0.04% of the total measured H_2O^+ signal, making a determination of H_xO^+ fragments from difference spectra impossible. The large N_2^+ peak from air in these experiments was typically ≈100 times larger than the adjacent CO^+ fragment which itself is due both to gas phase CO_2 as well as CO^+ fragments from organic particles. For all of these reasons we observed that the precision in the measured particle signals from CO^+, O^+, OH^+ and H_2O^+, were all much lower than precision in all other significant components of the spectra, including CO_2^+. For this reason we calculated the particle phase signals at these fragments based on the measured

particle CO_2^+ fragment, and the fragmentation table suggested by *Aiken et al.* [2008]. Because of the relatively low signals at these fragments these choices had a minor effect on the calculated atomic ratios. For all of the standards except for the butane hydroxynitrate the O/C based on measured vs. calculated values of these fragments were within 5%. For the butane hydroxynitrate standard the difference was larger, but only because the total aerosol concentration was much lower, and gas phase water therefore introduced much more noise into the measurement of H_xO^+ fragments. Using the calculated fragments resulted in O/C from the three measured spectra of this standard with precision ±3%. The AMS elemental ratios we report are those calculated before applying any corrections for reduced detection efficiency of H, N, or O relative to C.

4.2.4 Organic nitrate standards

Polydisperse aerosols of each standard were generated by nebulizing a methanol solution of each standard with zero air using a Meinhard nebulizer (Meinhard Glass Products, Golden, CO). The resulting aerosol was passed through a silica gel diffusion dryer and multiple charcoal denuders to remove the solvent and excess gas phase organics before sampling into the HR-ToF-AMS. Pure samples of the methanol solvent sampled into the AMS in the same way resulted in zero signal. Zero air produced from a zero air generator was chosen as opposed to e.g. argon gas to give a realistic AMS signal with the same interferences encountered in field measurements. 3–5 replicate spectra were recorded for each of the standards. Each spectrum was collected from 1 min of data and particle loadings were from 83–340 $\mu g\,m^{-3}$. The precision for individual standards was high, with the precision of the resulting atomic ratios being ±4%. We report the averages of the spectra and atomic ratios.

4.3 AMS organic nitrate spectrum

Figure 4.2 (top panel) shows the average of the AMS spectra from the four standards. HR analysis was used to identify the peaks containing nitrogen (blue), and then the spectrum was summed to unit mass resolution. To focus on the organic nitrate functionality and compare the four compounds which had quite different carbon backbones, a subset of the spectrum of each standard was used where only the HR peaks containing nitrogen were identified and then scaled by the nitrogen content of each fragment (i.e. each fragment with one N atom was multiplied by $\frac{14}{m/z}$), and then the spectra were summed to unit mass resolution. Figure 4.2 (bottom) shows the average nitrogen specta of the four standards obtained this way.

In comparison to ammonium nitrate where typically >98% of the nitrate signal appears at the NO^+ and NO_2^+ peaks, we observed only 30% of the nitrogen at the sum of these two peaks. We observed 5% at various $C_xH_yO_zN^+$ fragments, 12% in the NH_x^+ fragments (mainly the butane standard) and 53% at various $C_xH_yN^+$ fragments. The NH_x^+ fragments were almost exclusively observed in the butane hydroxynitrate standard. We have no evidence that this

is not unusual ion chemistry but acknowledge that these peaks may indicate an undetected impurity in the sample. The ubiquity of the CHN^+ fragments across the 4 standards was surprising and suggests a high degree of molecular rearrangement, not simple fragmentation, occurs prior to detection.

An attempt was made to identify a unique and consistent feature of the spectra which could be used to quantify the organic nitrate content of ambient OA using either a Unit Mass Resolution (UMR) – or High Resolution (HR) – AMS. Although qualitative similarities between the spectra of the four standards are obvious, no single peak was an unambiguous marker that could be used to quantify organic nitrates. Table 4.2 shows the observed NO^+:NO_2^+ ratios observed for the four compounds. This ratio has been shown previously [*Alfarra et al.*; *Cottrell et al.*, 2008; *Fry et al.*, 2009] to differ significantly between inorganic and organic nitrates. The NO^+:NO_2^+ ratio has been shown to also vary between different instruments, and to change between tunings of a single instrument. Reported ranges for ammonium nitrate are typically 1.5–2.5 NO^+:NO_2^+, with larger ratios observed for other compounds, ranging as high as 29 NO^+:NO_2^+ for sodium nitrate. We observed ratios ranging from 0.99 to 5.30 for the organic nitrate standards. The average spectrum shown in Fig. 4.2 (bottom panel) has an *m/z* 30:46 ratio of 2.94. This scatter in the NO:NO_2 ratios was unexpected as we anticipated that based on the gas phase decomposition of alkyl nitrates [*Day et al.*, 2002] the majority of these compounds would thermally decompose to RO+NO_2 on the AMS filament, yielding essentially a mass spectrum of NO_2. For example, at 600 and 1 atm the lifetime of n-propyl nitrate in the gas phase to this thermal decomposition channel is 300 ns.

None of the other major peaks were observed to bear a consistent relationship to the total N mass, or to either of the peaks at *m/z* 30 or 46. One obvious feature in the spectrum is the clusters of mass around the groups $C_xH_yN^+$, with the highest peak in each group occurring at y=2x (28, 42, 56, 70). While this may be a unique signature of organic nitrates, the individual peaks are all small compared to the typical size of peaks at the same UMR *m/z* in an ambient spectrum.

Assuming that the average of the four standards is representative of how particulate organic nitrates would appear in an AMS spectrum, we calculate that 58% of the nitrogen is measured at peaks other than the NO_x^+ and NH_x^+. Using a HR-AMS to identify nitrogen containing fragments, if M is the total amount of organic nitrogen measured at these non NO_x^+ and NH_x^+ peaks, then the total amount of organic nitrogen in all fragments would be $M/0.58$=1.7×M, and the amount of organic nitrogen detected at the NO_x^+ peaks would be 1.7×0.30×M=0.51×M.

4.4 AMS/combustion comparison

To evaluate the AMS's relative detection efficiency of C, H, N, and O we compare the elemental ratios of the standards determined with the AMS to those measured with combustion

analysis. The data are listed in Table 4.1 and plotted in Fig. 4.3. In Table 4.1 we also list the atomic ratios expected for pure samples of the standards. Assuming that the combustion analysis is the best measure of the composition of the compounds, this analysis indicates that the N/C and O/C of the synthetic standards are lower than expected. Though the standards were purified via flash chromatography, this suggests there was a carbon impurity in the standards, presumably from unreacted starting material or minor product(s) of the synthesis. The direct comparison of the two EA measurements may help to eliminate the need to assume a pure sample of the standard, though we expect that an impurity of lower vapor pressure than the standard would lead to more relative signal in the AMS than in the combustion method.

Correlation between AMS and thermal EA measurements is high for all three ratios (R^2=0.988, 0.966, 1.000 for H/C, N/C, O/C). For H/C and N/C a negligible improvement in the linear regression was achieved by allowing the y-intercept to vary (R^2=0.995 vs. 0.988 for H/C and 0.978 vs. 0.966 for N/C). However for the O/C a reasonably significant improvement is observed (0.894 vs. 1.000) by allowing the y-intercept to be non-zero. The positive y-intercept might indicate a positive bias in the AMS measurement of oxygen, possibly from a constant in the gas phase background. This would presumably appear as a large fraction of the total measured oxygen appearing at a nominally "air" m/z, such as O^+, O_2^+, CO^+ or CO_2^+. However, O_2^+ is filtered out in the analysis, and O^+ and CO^+ are calculated from the observed CO_2^+ signal which was overall a small fraction of the total measured oxygen. The deviation of the intercept from zero could also be explained by a negative bias in the detection of carbon. Because the AMS elemental analysis only considers fragments up to m/z =100, if a larger fraction of the total carbon relative to oxygen is contained in the excluded fragments greater than, m/z =100, then the AMS O/C would be systematically high. To consider the potential magnitude of this effect we calculated the mass weighted average m/z for the observed C, H, N, and O and results are listed in Table 4.3. Also listed in Table 4.3 is the fraction of total organic mass (calculated with unit mass resolution) located at $m/z \leq$100. In general O and N are found at lower m/z than are C and H, and the fraction of total mass located at $m/z >$100 and therefore excluded from the elemental analysis increases monotonically with compound mass. These results suggest that in general if the majority of oxygen is always located at $m/z \leq$100, larger compounds with more C excluded from the analysis will have an overestimated O/C which increases with the size of the compound. To test the effect that this could have on our results we re-fit the AMS/thermal O/C comparison, making the assumption that all oxygen is detected below m/z 100, and that the fraction of total carbon detected below m/z 100 is equal to the fraction of OM observed below m/z 100 in the UMR analysis. Doing so brings the y-intercept of the O/C panel in Fig. 4.3 from 0.059 to 0.029, with the slope of the line only increasing slightly from 0.234 to 0.237. Adjusting the carbon in this way also reduces the difference between the quality of fit found from allowing the y-intercept to vary (R^2=0.999) and with y-intercept fixed at zero (R^2=0.962). A similar analysis was performed on the N/C because Table 4.3 shows that nitrogen is found on average at even lower m/z than is oxygen and yet no significant offset was found in the

AMS/thermal N/C comparison. The correction due to excluded carbon above m/z 100 has a much less notable impact on the N/C, with the difference between fitting the y-intercept (R^2=0.977) and fixing at zero (R^2=0.946). This less significant effect is observed because the N/C for the largest compound is already very small, and shifting it slightly has a minor effect on the fit line.

H/C measured for hydroxynitrates (0.94±0.01) and by *Aiken et al.* [2008] for a range of other compounds (0.91±0.02) are equivalent within the combined uncertainty. N/C for hydroxynitrates was biased high (1.4±0.1) as compared to the small negative bias previously observed for nitrogen containing organics (0.96±0.05). Our observed O/C ratio (0.23±0.01) is significantly lower than that of Aiken et al. (2008) (0.75±0.05). This pair of findings would seem to be reasonable considering that the nitrogen in these molecules was bonded to oxygen. Because oxygen is strongly electronegative and upon EI leaves preferentially as a neutral, the nitrogen is forced to preferentially leave as an ion.

The origin of the nonzero y-intercept in the comparison of AMS and combustion measurements of O/C is not entirely clear, and as discussed is likely related to the size of the carbon backbone of the parent molecule. Thus, to make an estimate of how the O/C of organic nitrates may appear for ambient aerosol we take the average of the AMS O/C / combustion O/C for the four compounds. The average of this value for the four compounds (Table 4.1, bottom line) is 0.50, which is close to the individual values observed for the two monoterpene derived compounds (0.46 and 0.46). The four compounds tested in this study were nominally composed of one alcohol group (R-O-H) and one alkyl nitrate group (R-O-NO_2) with a total of 4 oxygen atoms per molecule. We estimate the reduced detection efficiency of oxygen in the organic nitrate groups alone by assuming that the oxygen in the alcohol groups were detected with 75% efficiency [*Aiken et al.*, 2008], and the reduced detection efficiency of O in nitrates lead to the overall observed value of 0.50. Under these assumptions, the detection efficiency for oxygen in a nitrate group is 42%.

4.5 Impact on ambient OA observations

In this section we estimate how the reduced efficiency of oxygen detection in organic nitrates might affect observations of O/C using the HR-ToF-AMS EA technique in the extreme case that all detected nitrogen is from organic nitrates. Under this assumption, we use our results from Sects. 4.3 and 4.4 to calculate that the O/C and N/C ratios reported using standard assumptions about AMS spectra and the calibration factors determined in *Aiken et al.* [2008] is related to the true O/C ratio by:

$$\left(\frac{\mathrm{O}}{\mathrm{C}}\right)_{\mathrm{true}} = \left(\frac{\mathrm{O}}{\mathrm{C}}\right)_{\mathrm{rep}} + 1.5\left(\frac{\mathrm{N}}{\mathrm{C}}\right)_{\mathrm{rep}} \tag{4.1}$$

such that the fractional adjustment to the reported O/C ratio would be $150\frac{\mathrm{N/C}}{\mathrm{O/C}}\%$. Here, "true" refers to atomic ratios existing in atmospheric aerosols, "observed" (obs) ratios are

those one measures with the raw AMS data without any corrections for relative biases between atoms, and "reported" (rep) ratios are those one finds in the literature (e.g. *Aiken et al.* [2008]) using previously determined correction factors.

In the following we derive Eq. 4.1 using the various relationships between measured and true O/C and N/C ratios reported in this study, and that of *Aiken et al.* [2008]. These values are summarized in Table 4.4. First we consider the differences in O/C between the two studies. We assume that the oxygen in organic nitrate groups is detected with 42% efficiency, and all other organic oxygen at 75% efficiency. Since each nitrate group has 3 oxygen atoms, the contribution to the observed O/C from nitrates is $0.42 \times 3 \left(\frac{\mathrm{N}}{\mathrm{C}}\right)_{\mathrm{true}}$ and the contribution from the other (non-nitrate) oxygen containing organics is $0.75 \times \left[\left(\frac{\mathrm{O}}{\mathrm{C}}\right)_{\mathrm{true}} - 3\left(\frac{\mathrm{N}}{\mathrm{C}}\right)_{\mathrm{true}}\right]$. Thus the true O/C is related to the observed O/C by the sum of the these two contributions, which can be rearranged to yield the following expression:

$$\left(\frac{\mathrm{O}}{\mathrm{C}}\right)_{\mathrm{true}} = \frac{\left(\frac{\mathrm{O}}{\mathrm{C}}\right)_{\mathrm{obs}} + 0.99\left(\frac{\mathrm{N}}{\mathrm{C}}\right)_{\mathrm{true}}}{0.75} = \frac{\left(\frac{\mathrm{O}}{\mathrm{C}}\right)_{\mathrm{obs}}}{0.75} - 1.3\left(\frac{\mathrm{N}}{\mathrm{C}}\right)_{\mathrm{true}} \quad (4.2)$$

Since the factor 0.75 has been used in the literature to report O/C values, we have:

$$\left(\frac{\mathrm{O}}{\mathrm{C}}\right)_{\mathrm{reported}} = \frac{\left(\frac{\mathrm{O}}{\mathrm{C}}\right)_{\mathrm{obs}}}{0.75} \quad (4.3)$$

We assume that the reported and observed N/C ratios are related by $\left(\frac{\mathrm{N}}{\mathrm{C}}\right)_{\mathrm{rep}} \times 0.96 = \left(\frac{\mathrm{N}}{\mathrm{C}}\right)_{\mathrm{obs}}$ and as we have seen, for organic nitrates $\left(\frac{\mathrm{N}}{\mathrm{C}}\right)_{\mathrm{true}} = \left(\frac{\mathrm{N}}{\mathrm{C}}\right)_{\mathrm{obs}} / 1.4$. Typically however, elemental analysis is applied to the "organic" part of the AMS spectrum which is determined as such through standard assumptions about the spectrum [*Allan et al.*, 2004] followed by the application of a multivariate linear regression technique such as positive matrix factorization which essentially removes all signal at the $\mathrm{NO}_{\mathrm{x}}^{+}$ and $\mathrm{NH}_{\mathrm{x}}^{+}$ peaks [*Zhang et al.*, 2005; *Lanz et al.*, 2007, 2008]. To account for organic N in these peaks the reported N/C should be scaled up by a factor of 1.7 as discussed in Section 4.3, resulting in the relationship

$$\left(\frac{\mathrm{N}}{\mathrm{C}}\right)_{\mathrm{true}} = \frac{\left(\frac{\mathrm{N}}{\mathrm{C}}\right)_{\mathrm{rep}} \times 0.96}{1.4} \times 1.7 \quad (4.4)$$

Combining Eqs. (4.3) and (4.4) with Eq. (4.2) we arrive at Eq. (4.1).

Applying Eq. (4.1) to the diurnal average N/C and O/C ratios observed by *Aiken et al.* [2008] in Mexico City (MILAGRO campaign) we obtain an average increase in the O/C ratio of 8.6%. Ambient N/C and O/C ratios however are anticorrelated. Thus, the while the O/C ratio observed by Aiken et al. (2008) ranges from 0.31–0.55, the N/C ratio ranges from 0.024–0.009 (approx, read from charts). This suggests that the organic nitrate correction to OA oxygen content for this study would vary from 2–12%, being the most important just before sunrise, and least important late in the day.

The results of the above analysis rely on the critical assumption that all observed N in the organic spectrum is from organic nitrates. This is however unlikely to be the case, meaning that the 2–12% correction we calculate to the O/C is an upper limit. For example, *Moffet et al.* [2008] report single particle mass spectrometric measurements during the Mexico City Metropolitan Area-2006 campaign (MCMA-2006) and find a significant class of nitrogen containing organic particles which they hypothesize to be due to industrial emissions of amines. *Aiken et al.* [2009] report PMF analysis of HR-AMS data from this same campaign, and find a component high in organic nitrogen (called LOA in that study) which they suggest is likely of similar origin. It is worth noting though that in the study of *Aiken et al.* [2009] only 33% of the organic nitrogen was found in the LOA component, with the OOA, HOA and BBOA having 29%, 25% and 13% each, respectively. As well, one of the pieces of reasoning used to conclude that the nitrogen is from amines is that it is detected in $C_xH_yN^+$ fragments, such as *m/z* 58 [*Moffet et al.*, 2008] and *m/z* 86 [*Huffman et al.*, 2009] which are observed in mass spectroscopic studies of amines. Our observations of significant quantities of $C_xH_yN^+$ fragments from organic nitrates including in particular *m/z* 58 and 86 suggests that these fragments may not be perfect tracers for amines. Finally, we note that the range of possible corrections calculated in this paper are well within the stated 31% accuracy [*Aiken et al.*, 2008] of the AMS EA technique.

4.6 conclusions

We have tested the response of the Aerodyne HR-TOF-AMS to aerosols formed from C_4–C_{15} hydroxynitrates. We found on average that 42% of the nitrogen mass was detected at the NO_x^+ and NH_x^+ peaks, which are typically assumed to be inorganic nitrogen. We find that the oxygen in these molecules was detected with significantly reduced efficiency (50% on average) as compared to a previously reported series of organics (75%). This could result in as much as an 12% increase in the O/C ratio previously reported for Mexico City where the observed N/C was high. Analysis of the mass spectrum did not yield any patterns which could be used universally to quantify the organic nitrate content of aerosol, but suggests that 58% of the N is detected at CHN^+ and $CHNO^+$ fragments.

Table 4.1: H/C, N/C and O/C data from combustion elemental analysis and AMS elemental analysis.

Compound name	Butane	Pinene	Limonene	Caryophyllene
Compound formula	$C_4H_9O_4N$	$C_{10}H_{17}O_4N$	$C_{10}H_{17}O_4N$	$C_{15}H_{25}O_4N$
Atomic H:C	2.25	1.70	1.70	1.67
Atomic N:C	0.25	0.10	0.10	0.067
Atomic O:C	1	0.4	0.4	0.27
Combustion H:C	2.32	1.54	1.79	1.69
Combustion N:C	0.22	0.057	0.071	0.013
Combustion O:C	0.97	0.25	0.26	0.11
AMS H:C	2.2	1.5	1.7	1.6
AMS N:C	0.33	0.041	0.099	0.022
AMS O:C	0.29	0.12	0.12	0.086
AMS O:C/combustion O:C	0.20	0.46	0.46	0.79

Table 4.2: Contributions (%) to the HR-AMS mass spectra of each of the standards (columns 1–4), and ratios of these peak heights (columns 5, 6). 30 and 46 are all of the signal at these UMR peaks. NO^+ and NO_2^+ are determined in the HR analysis. Stated AMS atomic ratios are without using correction factors for non-uniform detection of C, H, N, and O.

Compound	30	46	NO^+	NO_2^+	30:46	NO^+:NO_2^+
Butane	14.35	4.47	7.64	4.18	3.21	1.83
Limonene	3.37	2.23	2.07	2.09	1.51	0.99
α-Pinene	2.96	0.58	2.65	0.50	5.10	5.30
Caryophyllene	2.01	0.45	1.79	0.40	4.47	4.48

Table 4.3: Mass weighted average location of C, H, N, and O calculated by high resolution AMS analysis of $m/z \leq 100$ (first four columns) and the percent of organic mass located$\leq m/z$ 100 evaluated by unit mass resolution up to $m/z = 500$. Correction factors for non-uniform detection of C, H, N, and O have not been applied to the data.

Compound	C	H	N	O	%
Butane	51.1	47.2	36.0	40.1	91
Pinene	62.3	59.4	40.1	49.0	74
Limonene	60.4	58.0	44.5	50.0	74
Caryophyllene	64.7	62.1	42.5	51.4	69

Table 4.4: A summary of the conversion factors used in deriving Eq. (4.1)

.

Value	Description of value	Reference
0.42	observed O:C / true O:C for organic nitrates	this study, Sect. 4.4
0.75	observed O:C / true O:C for all organics	*Aiken et al.* [2008]
1.4	observed N:C / true N:C for organic nitrates	this study, Sect. 4.4
0.96	observed N:C / true N:C for all organics	*Aiken et al.* [2008]
1.7	organic N in all fragments / organic N in "organic" fragments	this study, Sect. 4.3

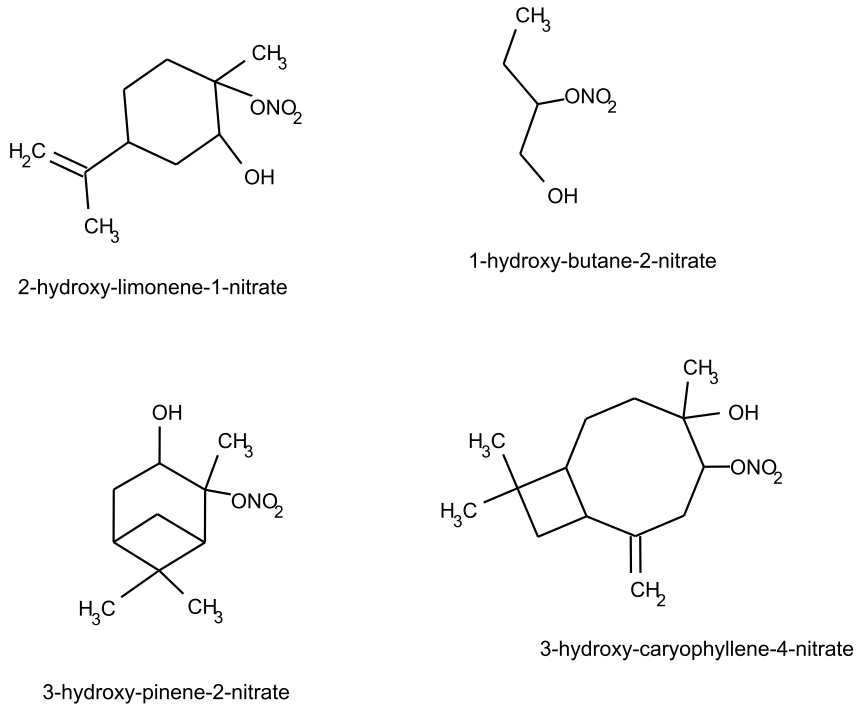

Figure 4.1: One isomer of each each standard synthesized for this study.

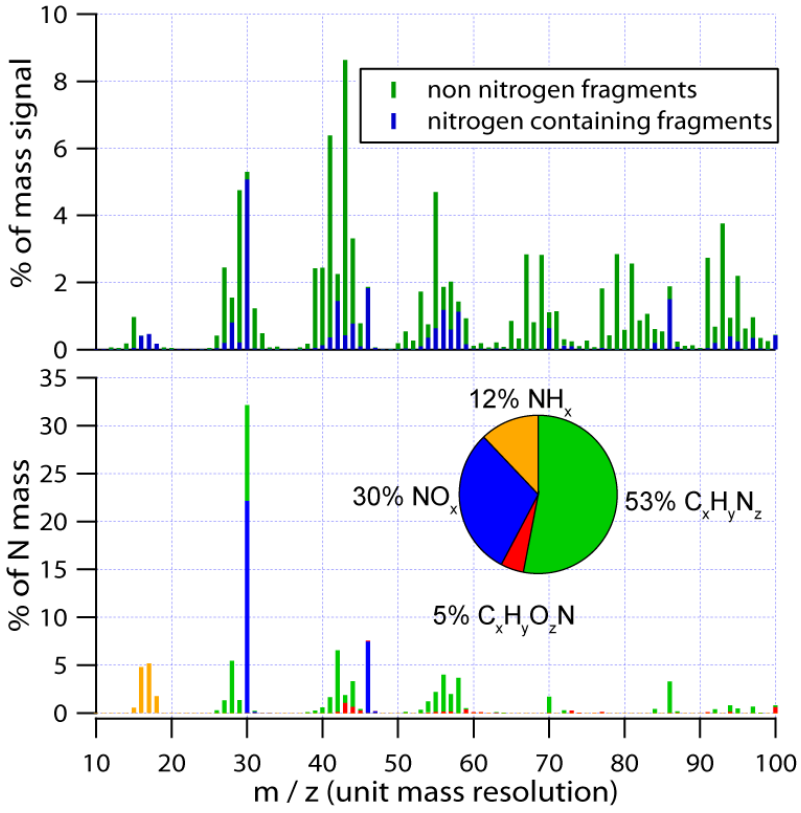

Figure 4.2: Top: the average of the AMS spectra of the four standards, with nitrogen and non-nitrogen fragments identified. Numbers identify the m/z of some of the major peaks. Bottom: the average for the standards of the nitrogen containing peaks, weighted by the fraction of each peak which is nitrogen by mass. Each peak containing one nitrogen atom is scaled by $\frac{14}{m/z}$.

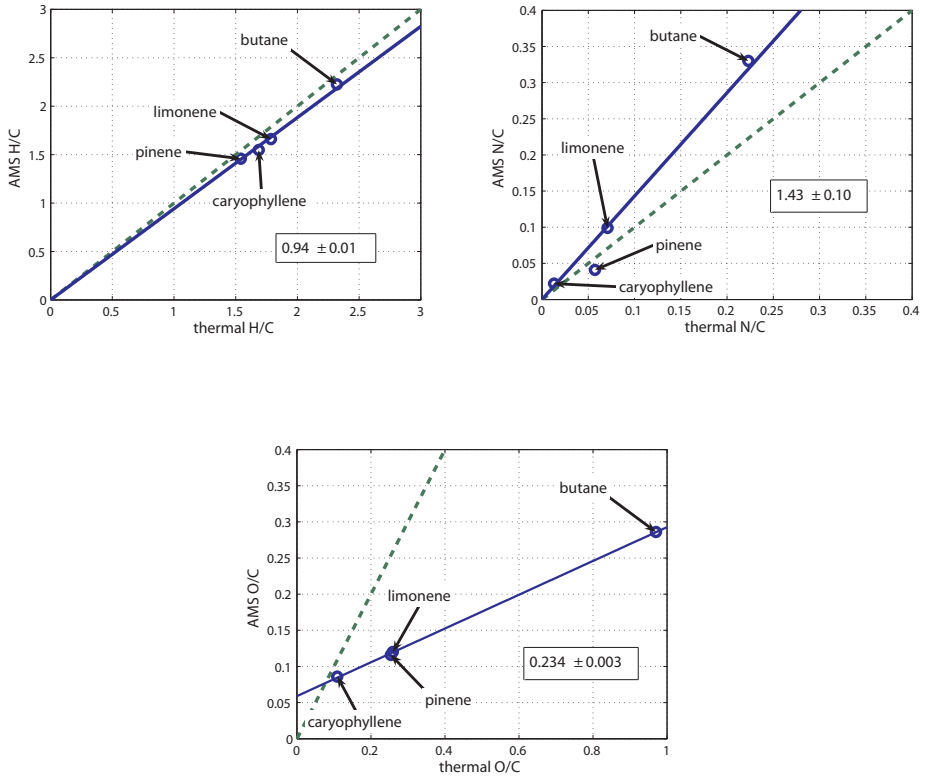

Figure 4.3: Comparison of atomic ratios measured with the AMS, to atomic ratios measured by combustion elemental analysis. Here we plot the elemental ratios calculated assuming equal response to CHN and O (corrections to elemental analysis recommended by *Aiken et al.* [2008] have not been applied to the data). Green dashed line is a 1:1, and solid blue is a linear fit to the data with y-intercept forced to zero.

Chapter 5

Real time in situ detection of organic nitrates in atmospheric aerosols

5.1 Introduction

Organic nitrates ($RONO_2$) are formed in the atmosphere as a minor product of reactions between organic peroxy radicals and nitric oxide (NO), as well as a major product from reactions of alkenes with the nitrate radical (NO_3). As a result, $RONO_2$ molecules are chemically produced during the day and the night and are a significant fraction of the total oxidized nitrogen (NO_y) anywhere that non-methane organic compounds are available (e.g. [*Day et al.*, 2003]). Specific individual gas phase $RONO_2$ molecules have been observed using gas chromatography (e.g. [*Atlas*, 1988; flo, 1991; *Shepson et al.*, 1993; *Luxenhofer et al.*, 1996; *Schneider et al.*, 1998]) and chemical ionization mass spectrometry [*D'Anna et al.*, 2005; *Paulot et al.*, 2009; *Perring et al.*, 2009], and the total of gas and aerosol $RONO_2$ has been observed by Thermal Dissociation Laser Induced Fluorescence (TD-LIF) [*Day et al.*, 2002, 2003; *Rosen et al.*, 2004; *Cleary et al.*, 2005]. Recently there has been growing interest in understanding the partitioning of $RONO_2$ to atmospheric particles [*Lim and Ziemann*, 2005; *Ng et al.*, 2008; *Rollins et al.*, 2009; *Bruns et al.*, 2010; *Farmer et al.*, 2010; *Rollins et al.*, 2010]. $RONO_2$ molecules with 2 - 4 functional groups and a carbon backbone of $\geq C_4$ have low enough vapor pressures to condense under ambient conditions and mechanistic studies show that $RONO_2$ can be among the most important molecules to SOA formation (e.g. [*Lim and Ziemann*, 2005; *Jordan et al.*, 2008]).

Despite the theoretical and laboratory evidence that $RONO_2$ should be important to the composition of atmospheric organic aerosols, there remains little evidence that $RONO_2$ are widespread components of ambient SOA. The most compelling evidence derives from direct FTIR analysis of particles impacted on ZnSe plates. This technique has been used to identify organic nitrates as ubiquitous components of submicron particles sampled in the Los Angeles basin [*Mylonas et al.*, 1991; *Allen et al.*, 1994] and in Houston [*Garnes*

and Allen, 2002]. FTIR analysis provides quantitative measurements of positively identified organic functionalities, with time resolution limited to the rate at which filters are changed (typically hours - days). Interferences due to evaporative loss from the filters or heterogeneous reactions on the filters during sampling are known issues and difficult to quantify. Individual large multifunctional nitrates have been observed in ambient aerosol samples collected on filters using electrospray ionization mass spectrometry [*Gómez-González et al.*, 2008b; *Surratt et al.*, 2008]. However the most widely used methods for aerosol chemical characterization including Aerosol Mass Spectrometry (AMS) have had limited success. The difficulty of distinguishing inorganic and organic nitrates using AMS has been recently discussed in the literature [*Bruns et al.*, 2010; *Rollins et al.*, 2010; *Farmer et al.*, 2010]. Nitrates have not yet been reported by Thermal Desorption Aerosol Gas-Chromatography (TAG) [*Williams et al.*, 2006] or other methods of detailed realtime aerosol characterization.

In this paper a new technique for the detection of aerosol organic nitrate is described. The new method quantifies particulate organic nitrate with high time resolution, low background signal, and no interference from inorganic nitrate ion (NO_3^-). Here we apply the method to measure the organic nitrate content of SOA produced in the laboratory from high NO_X photooxidation of one alkane and three alkenes. In these experiments, we show that the fraction of the total organic mass which is organic nitrate is consistent with the expected organic nitrate yields from high NO_X photooxidation.

5.2 Instrument Design and Evaluation

The selective measurement of particle phase nitrates is achieved by removing gas phase NO_2 and nitrates (both RO_2NO_2 and $RONO_2$) from the sample stream with an activated carbon denuder. The aerosol flow is then heated so that particles are vaporized to their gas phase precursors and detected using TD-LIF by which $RONO_2$ is thermally converted to RO + NO_2 and NO_2 is detected by LIF [*Day et al.*, 2002]. A schematic of the instrument inlet system used in this study is shown in 5.1.

5.2.1 Thermal Dissociation Laser Induced Fluorescence

The core measurement used in TD-LIF is the laser induced fluorescence detection of NO_2 [*Thornton et al.*, 2000]. Details of the specific LIF instrument used for this study are described in *Wooldridge et al.* [*Wooldridge et al.*, 2009]. Briefly, gas is sampled through a critical orifice into a 38 pass White cell held at $\approx$2 torr. In the cell, NO_2 is electronically excited with a 30 mW diode laser centered at 408 nm (Power Technologies Inc.). Red shifted NO_2 fluorescence passes through a 650 nm long pass dielectric filter and a red glass filter which block scatter and is detected with a photomultiplier tube (Hamamatsu H7421-50). In the pressure regime used here the fluorescent signal is directly proportional to the mixing ratio of NO_2 in the cell. The NO_2 instrument is calibrated periodically using dynamic dilutions of

NO_2 from a calibrated NIST traceable standard, typically $\approx$5 ppm diluted by a factor of 100 - 1000. The method has been compared to independent approaches to detection of *Thornton et al.* [2003] NO_2 [*Fuchs et al.*, 2010], ΣPNs [*Wooldridge et al.*, 2009] and ΣANs [*Perring et al.*, 2009]. Alkyl nitrates and nitric acid (HNO_3) are quantified by sampling through a heated inlet which thermally dissociates these molecules to NO_2 and a corresponding radical (RO in the case of organic nitrates, HO in the case of HNO_3). $RONO_2$ and HNO_3 are easily distinguished by the threshold temperature required for thermal dissociation. In this work we used an inlet which consisted of a 4 mm i.d. quartz tube wrapped in nichrome wire providing a heated length of 20 cm. Using a flow rate of 125 sccm the residence time in the heated region was 1.2 s. The temperature was measured with a type K thermocouple which was in contact with a second piece of quartz tubing fitting tightly around the nichrome wire wrapped tube. The setpoint used to thermally dissociate all organic nitrates, while rejecting HNO_3 was determined by scanning the inlet temperature while sampling a mixture of ethyl nitrate and HNO_3 (5.2).

TD-LIF has previously been used to quantify various classes of gas + particle NO_y by taking the difference in LIF signals measured with two inlets at two different temperatures [*Day et al.*, 2002]. For example, without using a gas / particle separation technique, the sum of all gas and particle organic nitrates are quantified by measuring the NO_2 signal with the inlet at $\approx$300°C (which would be the sum of organic nitrates + NO_2) and subtracting from this the NO_2 measured in an unheated inlet. However for the application described in this work, gas phase species including NO_2 are separated from particles before entering the heated portion of the inlet, and thus no subtraction is required.

5.2.2 Gas/Particle Separation

Gas phase NO_y is removed using a single channel cylindrical denuder, 25 cm in length, and 1.0 cm i.d., which provided 9.3 s residence time at a flow rate of 125 sccm. We tested the effectiveness of the denuder for removing NO_2 and organic nitrates by using an injector inside the denuder in a concentric flow tube configuration. We measured the penetration of NO_2 and n-propyl nitrate (NPN) as a function of length of denuder exposed and gas flow rate. The data were compared to the predicted penetration as calculated by the expression obtained by *Ingham et al.*[*Ingham*, 1975] (equations 23 and 24 in that paper). The experiments showed that uptake of NO_2 and NPN by the denuder walls could be accurately predicted assuming removal is limited only by gas phase diffusion. In 5.3 we show observations and model predictions of gas penetration from experiments using NO_2 and NPN. The diffusivity of NO_2 in air is 0.154 $cm^2\ s^{-1}$ [*Glasius et al.*, 1999] and that of NPN was estimated using a hard sphere model and the method of Chapman and Cowling [*Chapman and Cowling*, 1970] to be 0.070 $cm^2\ s^{-1}$. The largest deviations between the model and data occur at the higher flow rates and short denuder lengths and are likely due to the entrance length required to establish laminar flow, which was not accounted for here but is estimated to be less than 1 cm at 125 sccm. At the lowest flow rates of 255-260 sccm used in the experiments the

model and measurements are in excellent agreement. We use the diffusion limited model to calculate the removal efficiency as a function of diffusivity at 125 sccm. The bottom panel of 5.3 shows that at this flow rate even large gas phase molecules are predicted to be removed efficiently.

Once particles leave the denuder they enter the heated quartz tube at 325°C where they evaporate. The approximate time required to completely evaporate the particles was calculated using a model which integrates the Hertz-Knudsen equation (5.1) assuming evaporation and condensation onto spherical particles.

$$J = \frac{\gamma p}{\sqrt{2\pi m k_B T}} \tag{5.1}$$

Here, J is the molecular flux across the particle surface (molecules cm^{-2} s^{-1}), γ is the evaporation coefficient, p is the vapor pressure of the compound (saturation vapor pressure for evaporation (p_{sat}) and actual partial pressure in the vapor phase for condensation), m is the molecular mass (g), k_B is the Boltzmann constant, and T is the temperature. Application of the Hertz-Knudsen equation requires knowledge of the saturation vapor pressure, which is related to the saturation concentration C^* by

$$C^* = \frac{\zeta MW_{om} p_{sat}}{RT} \tag{5.2}$$

Here, ζ is the activity coefficient, MW_{om} is the molecular weight, and R is the gas constant. 5.4 shows the calculated evaporation time at 325°C as a function of the saturation concentration of the organic aerosol (C^* at 300K). In this calculation we assumed that the evaporation coefficient, γ, is 1, MW_{om} is 150 g mol^{-1}, organic aerosol density is 1.2 g cm^{-3} and total OA concentration is 1000 μg m^{-3}. The vapor pressure at 325°C is calculated from the room temperature vapor pressure using a typical adjustment based on the Clausius-Clapeyron equation and we have ignored any temperature dependence of ΔH^{vap}. The C^* and T dependencies of ΔH^{vap} for SOA have recently been discussed in detail by *Epstein et al.* [*Epstein et al.*, 2009]. Here we apply their result (equation 12 in that paper) where ΔH^{vap} is a function of C^* only. In this formulation, $\Delta H^{vap} = -11 \log_{10} C^*_{300} + 129$ where ΔH^{vap} is in kJ mol^{-1} and C^* is in μg m^{-3}. The earlier formulation by *Donahue et al.* [*Donahue et al.*, 2006] where $\Delta H^{vap} = -6 \log_{10} C^*_{300} + 100$ was also used to calculate evaporation time, and in 5.4 we plot both. Significant differences in evaporation time are calculated using the different ΔH^{vap}, but both models indicate that OA with $C^* > 10^{-5}\,\mu$g m^{-3} is evaporated in less than 10 ms which is much less than the 1.2 s residence time in the heated section of our inlet. Because the evaporation time is inversely proportional to the evaporation coefficient a decrease in γ increases the calculated evaporation time. For example, $\gamma = 0.1$ increases the time by a factor of 10. Few measurements of γ for organic compounds are in the literature, but those reported are all in the range of 0.01 to 1 [*Saleh et al.*, 2009; *Riipinen et al.*, 2010]. At 325°C, the evaporation time that we calculated was insensitive to total OA concentration. Complete evaporation in the 1.2 s inlet was verified in one experiment by using an additional

heating section at 150°C and with a 2 minute residence time which is calculated to evaporate particles with $\log_{10} C^*$ greater than approximately -7.5. In this experiment no differences in signal were observed between having this additional section held at room temperature or at 150°C, indicating that particles are completely evaporated in the shorter 325°C inlet.

5.2.3 Particle Transmission Efficiency

Because semivolatile particles exist in equilibrium with their gas phase precursors, removal of the gas in the denuder might lead to evaporative loss of particles in the system [*Cappa*, 2009]. To estimate the importance of this process we used the same model as described here for calculating the evaporation of particles in the heated part of the inlet, this time setting the condensation rate of vapors onto the particles to zero. 5.5 shows the calculated fraction of particle mass remaining as a function of C^* assuming 9.3 s at 300 K for 4 initial particle sizes. For this calculation we set the evaporation coefficient to 1, which is the upper limit of evaporative loss. For C^* ¡1 all particle mass is calculated to be transmitted with ¿97% efficiency. At $C^* = 10$, 25% of the mass of the smallest particles is lost, but for particles larger than 100 nm, more than 88% of mass is transmitted. Significant particle loss may occur for more volatile particles of C* ¿100. However, these more volatile particles are not expected to be an appreciable fraction of the mass in ambient aerosols [*Hallquist et al.*, 2009; *Jimenez et al.*, 2009], and while the smaller particles ¡100 nm may be important by number, in a mass weighted distribution they are also of little importance.

Loss of particles due to diffusion or thermophoresis in the heated part of the inlet are expected to be non-negligible. To determine an upper limit to the loss of particles due to these combined effects we measured the transmission of non-volatile NaCl particles through the denuder and thermal-dissociation heater sections of the instrument. For this experiment a dry polydisperse aerosol was generated by atomizing an aqueous solution of NaCl (TSI 3076 atomizer) and passing aqueous particles through a homemade silica gel diffusion drier. The particles were size selected with a differential mobility analyzer (TSI 3081) and two condensation particle counters (TSI 3772) were used to simultaneously measure the particle number concentration before and after the sample stream passed through the inlet system. The heated part of the inlet was held at 325°C and the flow rate was 125 sccm. The observed transmission is shown in 5.6, with an empirical fit to the data. Significant losses were observed for the smallest particles; particles with diameters greater than 100 nm were transmitted with ¿85%. The transmission efficiency observed with NaCl is expected to represent a lower limit to the transmission and detection efficiency for semivolatile particles, as semivolatile particles are expected to evaporate and dissociate to NO_2 rapidly rather than deposit on the walls of the tube in regions of strong thermal gradients.

The effects of thermophoretic and evaporative loss were combined to evaluate the total penetration of particle mass through the inlet. The results show that the evaporative losses are negligible compared to deposition of particles in the inlet for C^* ¡ 1. At $C^* = 10$, the difference between deposition only and deposition combined with evaporation is largest for

particles with diameters between 100 and 200 nm, with a difference of about 10% of the mass for a 100 nm particle and about 5% for a 200 nm particle. Generally, the depositional losses we observed dominate the total mass loss in all conditions, though as discussed the detection efficiency of semivolatile particles is likely higher than NaCl particles.

5.2.4 Detection Limit

The lower limit of detection of the instrument is determined by the ratio of the NO_2 LIF signal relative to the to noise produced from scatter and single photon counting statistics. Using c as the NO_2 mixing ratio (ppb), A as the calibration constant (counts s^{-1} ppb^{-1}) and B as the background count rate (counts s^{-1}) the signal to noise ratio for some integration time t (s) is given by

$$\frac{Signal}{Noise} = \frac{Act}{\sqrt{Bt + Act}} \tag{5.3}$$

We define the detection limit as the minimum NO_2 concentration required for a signal:noise ratio of more than 2. The instrument used in this study had a typical background signal of 675 counts s^{-1} and a typical calibration constant of 150 counts s^{-1} ppb^{-1}. These values result in a detection limit of 110 ppt for 10 seconds of averaging, or 45 ppt for one minute. Higher sensitivity NO_2 instruments are available and have been employed in other studies [*Thornton et al.*, 2000; *Wooldridge et al.*, 2009; *Fuchs et al.*, 2010]. At standard conditions (1013 hPa, 300 K) the detection limit for this instrument converts to 0.11 μg NO_3 m^{-3} min^{-1}. It is worth noting that since the instrument is sensitive to the mixing ratio of NO_2 produced by the evaporation and thermal dissociation of particles as opposed to the volumetric density, the sensitivity in μg m^{-3} improves at increased altitude. For example, at 300 hPa the detection limit would be 0.033 μg NO_3 m^{-3} min^{-1}. The total inlet residence time is calculated to be $\approx$10 sec and experiments demonstrated that the instrumental response time to ambient changes was changes was in good agreement with this value. No extended residual signal was observed upon sudden changes such as overflowing the inlet with zero air. 5.7 shows sample observations with 10 seconds of signal averaging.

5.3 SOA Experiments

A series of secondary organic aerosol experiments was performed to measure the contribution of organic nitrates to SOA formed under high-NO_x conditions. Experiments were carried out by generating SOA in a quartz flow tube reactor with an inner diameter of 65 mm. The tube was surrounded by 4, T10 Hg vapor lamps, 130 cm long (UHP, LLC) providing $\approx$12 mW cm^{-2} of 254 nm light. OH was generated through the photolysis of H_2O_2 which was produced by flowing 100 sccm N_2 through a mixture of urea hydrogen peroxide (Sigma) and sand which was warmed slightly (30-40°C). Continuous streams of limonene, α-pinene, Δ-3-carene, or tridecane vapors were produced by flowing 1000 sccm N_2 over the

output of a syringe pump loaded with the respective liquids. The concentrations of the organic compounds added to the flow tube were controlled by varying the pumping rate of the syringe pump, and/or the fraction of the 1000 sccm N_2/organic mixture which was exhausted rather than sent to the flow tube. 10 ppm NO was added at 100 sccm along with N_2 and O_2 to balance the total flow in the reactor at 2000 sccm and achieve an O_2 concentration of 20% and an NO concentration of 500 ppb. Though the concentrations of the organics were typically ¡100 ppb, the 500 ppb NO concentrations were used to be assured the experiments were high-NO_X. Average OH concentrations were $\approx 10^9$ molecules cm^{-3} as was verified by measuring the loss rate of hexane. The steady state HO_2 produced by H_2O_2 photolysis converts a large fraction of the NO to NO_2. The Master Chemical Mechanism (MCM) [*Saunders et al.*, 2003] was used with modified photolysis rates for 254 nm to calculate that ¿90% of the organic peroxy radicals reacted with NO in the experiments. The MCM simulations were run for α-pinene and n-dodecane ($C_{12}H_{26}$). Detailed reaction mechanisms are not currently available in the MCM for tridecane, limonene or Δ-3-carene. However the tridecane and dodecane mechanisms are expected to be almost identical, and α-pinene, limonene and Δ-3-carene have very similar photochemistry [*Calbert et al.*, 2000; *Atkinson and Arey*, 2003]. Thus, the conditions used here were expected to be sufficient such that RO_2 + NO was the dominant peroxy radical fate in all cases.

A scanning mobility particle sizer (SMPS) system (TSI) was used to measure particle size distributions. Total particle mass was calculated from the SMPS data assuming a particle density of 1.2 g cm^{-3} which is similar to that reported in a number of studies for high-NO_X SOA of terpenes [*Bahreini et al.*, 2005; *Alfarra et al.*; *Ng et al.*, 2007b; *Offenberg et al.*, 2007; *Yu et al.*, 2008; *Zelenyuk et al.*, 2008]. Particle number distributions were typically centered at 100 - 150 nm. 5.7 shows a sample time series of NO_2, particle -ONO_2 and total aerosol mass from the Δ-3-carene experiment. In this experiment, the organics, H_2O_2 and air were initially flowing into the flow tube reactor. Just after 9:45 the NO flow was also added and due to a slight NO_2 impurity 12 ppb NO_2 was observed. The bottom panel of 5.7 shows a magnified view of the first 15 minutes of this experiment confirming that NO_2 is not an interference for the particle -ONO_2 measurement. At 9:51 the lights were turned on, generating OH and HO_2, which produced SOA and NO_2. After 10:00 the concentration of aerosol produced was varied by adding additional the amount of organic precursor to the flow tube at 10:15, 10:25 and 10:37.

5.8 shows regression plots of the measured particle -ONO_2 vs. total particle mass from the four different organic experiments. In all four experiments the particle -ONO_2 and total particle mass were well correlated (R^2 ¿ 0.94). The slopes of the linear fits (y-intercepts were held at zero) are the fraction of aerosol mass which is the -ONO_2 functional group. The observed -ONO_2 content was 6.2% for α-pinene, 8.5% for Δ-3-carene, 12% for limonene and 15% for tridecane. The assumed SOA density used to calculate the total mass from the SMPS data has a direct impact on these calculations. Based on the range of reported values for α-pinene SOA [*Bahreini et al.*, 2005; *Alfarra et al.*; *Ng et al.*, 2007b; *Offenberg et al.*, 2007; *Yu et al.*, 2008; *Zelenyuk et al.*, 2008], 1.2 $\pm$ 0.2 g cm^{-3} is the maximum expected

range of particle density produced here, resulting in a ±17% accuracy in the total calculated OA mass and fractional -ONO_2 content.

To estimate the fraction of SOA molecules which are organic nitrates, we make some simple assumptions about the presumed oxidation products of the reactions. The monoterpenes are expected to react with OH and then O_2 to produce hydroxy alkyl peroxy radicals. Under high NO_X conditions the dominant pathway is for the peroxy radicals to react with NO to form either a hydroxy-nitrate with a molecular weight of 215, or a hydroxy-alkoxy radical which reacts with O_2 to form a hydroxy-carbonyl compound (MW = 168) [*Atkinson and Arey*, 2003]. Analogous assumptions for the tridecane + OH reaction which is initiated by hydrogen abstraction results in an alkyl nitrate (MW = 245) and a hydroxy-carbonyl (MW = 215) [*Atkinson et al.*, 2008]. If we assume that the observed -ONO_2 content of the aerosol is due to a linear combination of these two types of molecules, we can calculate the fraction of SOA molecules which are hydroxy-nitrates. Under these assumptions we calculate 18% of the molecules are organic nitrates for α-pinene SOA, 25% for Δ-3-carene, 36% for limonene and 56% for tridecane. No doubt the product distribution which contributed to the observed SOA was more complicated than described here, but our analysis relies only on the approximate molecular weights. If for example we assume that all SOA (nitrate and non-nitrate) from the α-pinene reaction had a molecular weight of 150, we calculate 15% instead of the 18% for condensed organic nitrates. These values are in good agreement with reported yields of total organic nitrates from high-NO_X oxidation. *Noziére et al.* [*Noziére et al.*, 1999] report a measured total organic nitrate yield of 18 ± 9% from high-NO_X photooxidation of α-pinene. To our knowledge, the organic nitrate yields from limonene and Δ-3-carene have not been reported. Total alkyl nitrate yield for the first generation products of tridecane are expected to be ≈35% (*10*). *Lim et al.* [*Lim and Ziemann*, 2005] have studied the SOA formed from high-NO_X photooxidation of a series of n-alkanes in a chamber and concluded that all observed SOA was organic nitrate. The good correspondence between the previously observed and calculated total alkyl nitrate yields, and our calculated contribution of alkyl nitrates to SOA (i.e. 18% total $RONO_2$ [*Noziére et al.*, 1999] and 18% of SOA is $RONO_2$), suggests that the organic nitrate products of high-NO_X photooxidation are roughly as condensable as the non-nitrate products.

In summary, we have described and evaluated a new technique which quantifies the total organic nitrate component of aerosols with high time resolution. The technique is sensitive, accurate and specific to organic nitrates. Near unit efficiency was observed for the detection of particles larger than 100 nm. The measurement was used to show that organic nitrates can be a significant contributor to high NO_X SOA, with the nitrate group itself being an important contribution to the total aerosol mass. These experiments suggest that in general, the organic nitrate fraction of SOA molecules produced in photooxidation, may be similar to the total yield of $RONO_2$ from the RO_2 + NO reaction, at least for molecules that are C_{10} or larger. These yields have not been studied extensively for terpenes or aromatic compounds, but are known to generally increase with the size of the R group, from 8% for isoprene, [*Paulot et al.*, 2009] to ≈35% for large alkanes ([*Arey et al.*, 2001]).

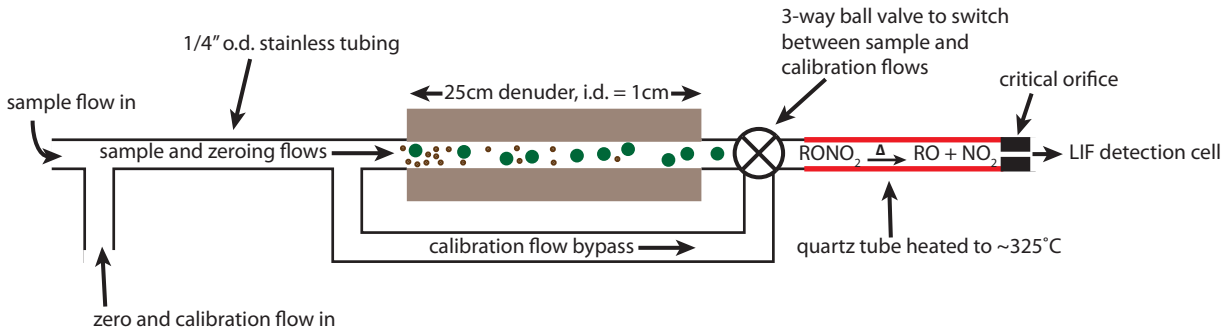

Figure 5.1: Schematic of particle organic nitrate inlet system. Gas and particles are sampled through ≈10 cm of 0.25" o.d. stainless tube. The flow enters the denuder where particles (green dots) pass while gas phase NO_y (brown dots) is removed by uptake on the denuder walls. Organic nitrate particles are converted to NO_2 in a heated quartz tube. A critical orifice reduces the pressure to ≈2 torr for measurement by LIF.

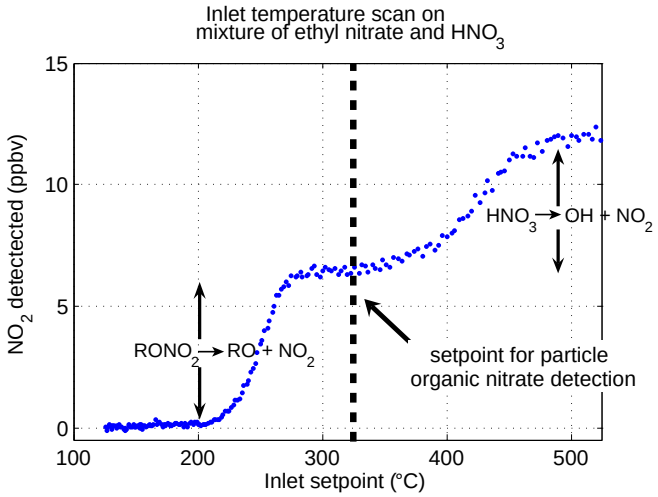

Figure 5.2: Inlet temperature scan on a mixture of gas phase n-propyl nitrate and nitric acid.

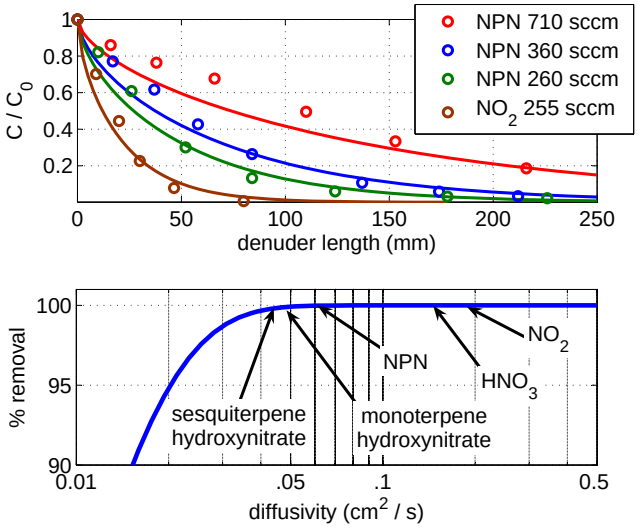

Figure 5.3: Top: Measured penetration of gas phase NO_2 and NPN in the denuder. Bottom: Calculated removal of gas phase nitrates at a flow rate of 125 sccm as a function of diffusivity. NO_y compounds are noted by their measured (NO_2, HNO_3) and approximated (others) diffusivities in air.

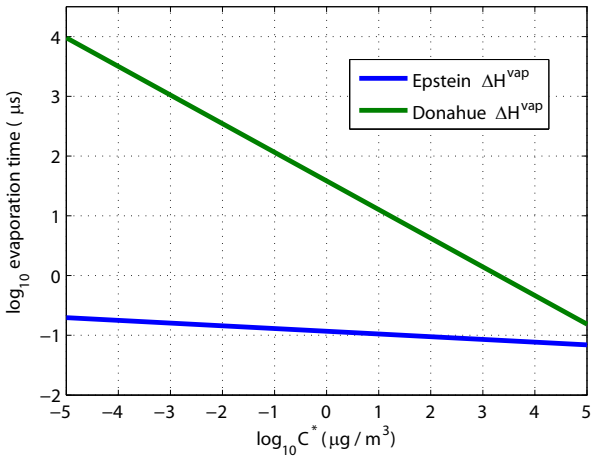

Figure 5.4: Calculated evaporation times for 500 nm particles.

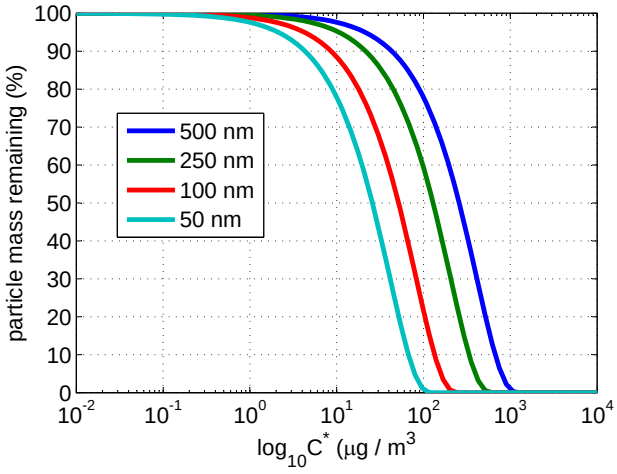

Figure 5.5: Modeling of evaporative particle loss in the denuder. We assume the fastest possible evaporation (activity and evap. coefficient = 1) to calculate the upper limit to particle loss. Stated sizes are the initial particle diameters.

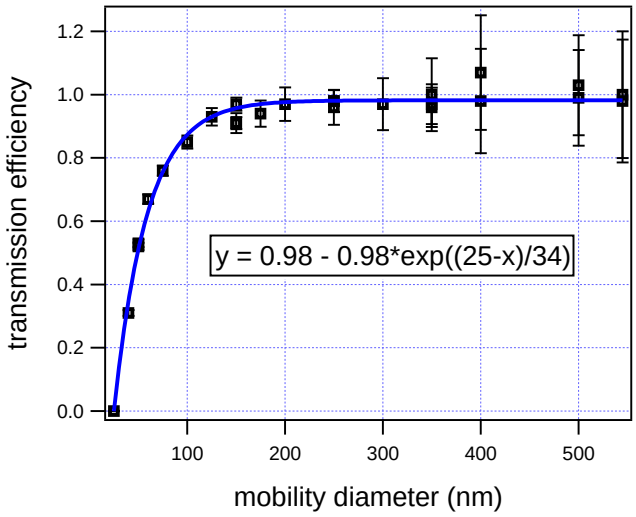

Figure 5.6: Measured inlet transmission efficiency of NaCl particles with heater at 325°C

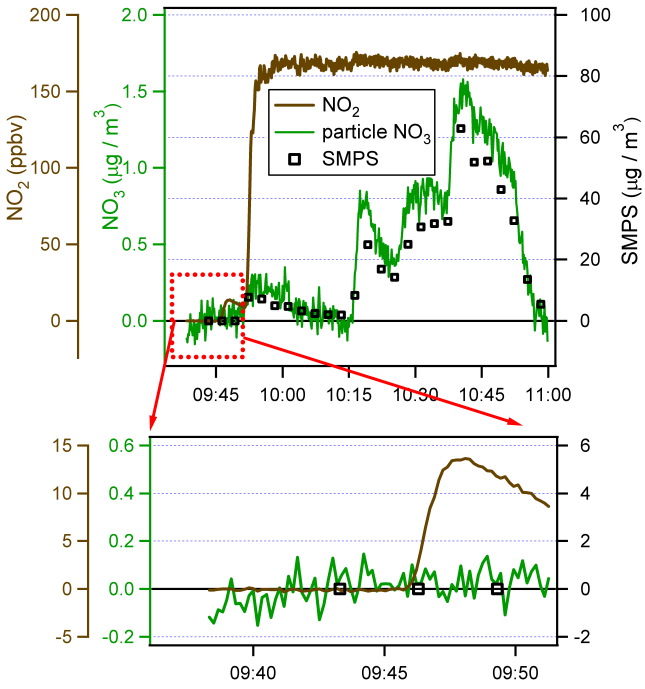

Figure 5.7: Sample time series from Δ-3-carene experiment. The time series begins sampling air from the irradiated H_2O_2 / air mixture. NO is added just after 9:45, and then at 9:50 more NO is added along with carene. The different aerosol concentrations were achieved by varying the syringe pump flow rate used to deliver the liquid organic material to the air flow stream, and by flowing various amounts of the organic vapor / air mixture into the flow tube vs. to the exhaust.

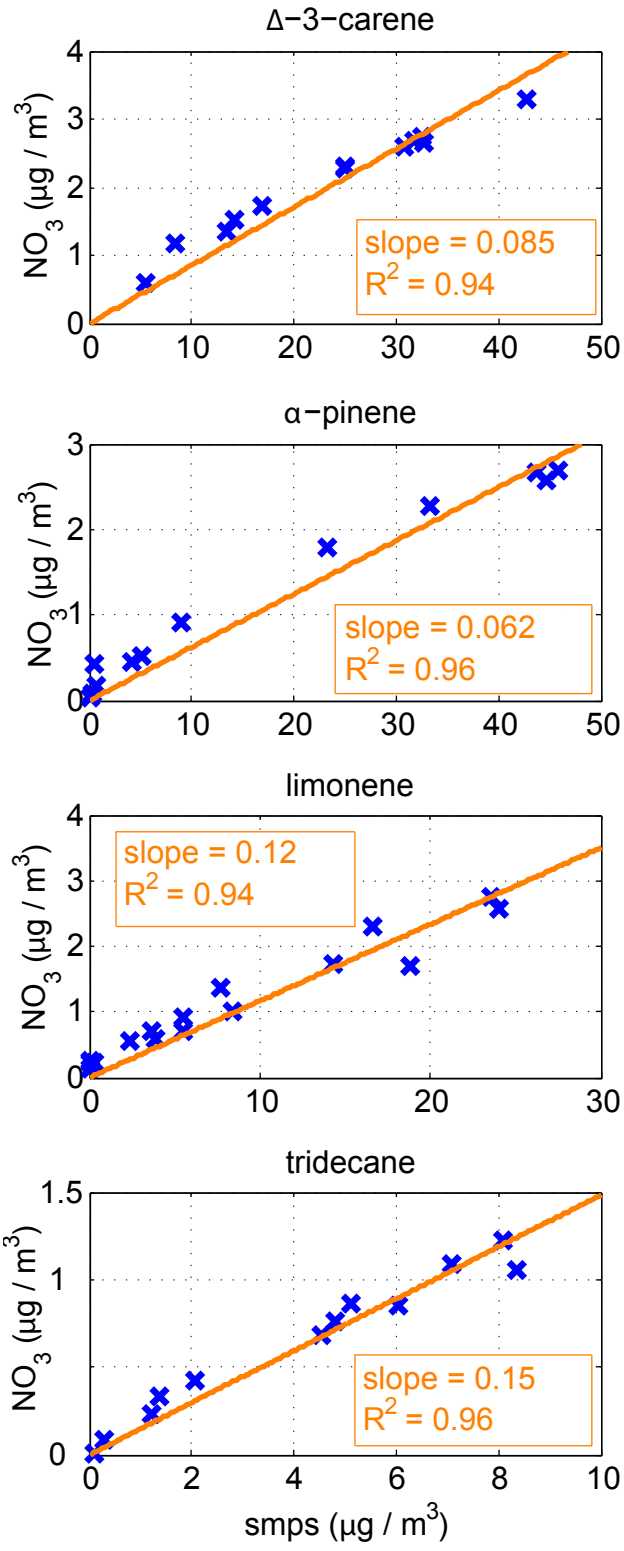

Figure 5.8: Regressions of particle NO_3 and total aerosol mass measurements from the high-NO_x photooxidation experiments.

Bibliography

Measurements of alkyl nitrates in rural and polluted air masses, *Atmospheric Environment. Part A. General Topics*, *25*(9), 1951 – 1960, 1991.

Aiken, A., P. DeCarlo, and J. Jimenez, Elemental analysis of organic species with electron ionization high-resolution mass spectrometry, *Anal. Chem.*, *79*, 8350–8358, 2007.

Aiken, A. C., et al., O/c and om/oc ratios of primary, secondary, and ambient organic aerosols with high-rresolution time-of-flight aerosol mass spectrometry, *Environ. Sci. Technol.*, *42*, 4478 – 4485, 2008.

Aiken, A. C., et al., Mexico city aerosol analysis during milagro using high resolution aerosol mass spectrometry at the urban supersite (t0) part 1: Fine particle composition and organic source apportionment, *Atmospheric Chemistry and Physics Discussions*, *9*(2), 8377–8427, 2009.

Albrecht, B. A., Aerosols, cloud microphysics, and fractional cloudiness, *Science*, *245*, 1227–1230, 1989.

Alfarra, M., D. Paulsen, M. Gysel, A. Garforth, J. Dommen, A. Prevot, D. Worsnop, U. Baltensperger, and H. Coe, A mass spectrometric study of secondary organic aerosols formed from the photooxidation of anthropogenic and biogenic precursors in a reaction chamber, *Atmos. Chem. Phys.*

Alfarra, M. R., Insights into atmospheric organic aerosols using an aerosol mass spectrometer, Ph.D. thesis, University of Manchester, 2004.

Allan, J., et al., A generalised method for the extraction of chemically resolved mass spectra from aerodyne aerosol mass spectrometer data, *J. of Aerosol Sci.*, *35*, 909–922, 2004.

Allen, D. T., E. J. Palen, M. I. Haimov, S. V. Hering, and J. R. Young, Fourier transform infrared spectroscopy of aerosol collected in a low pressure impactor (lpi/ftir): Method development and field calibration, *Aero. Sci. Tech.*, *21*, 325 – 342, 1994.

Apodaca, R. L., et al., Intercomparison of n_2o_5 sensors using saphir reaction chamber, in preparation, 2009.

Arey, J., S. M. Aschmann, E. S. C. Kwok, and R. Atkinson, Alkyl nitrate, hydroxyalkyl nitrate and hydroxycarbonyl formation from the no_x-air photooxidations of c_5 - c_8 n-alkanes, *J. Phys. Chem. A*, *105*, 1020 – 1027, 2001.

Atkinson, R., Rate constants for the atmospheric reactions of alkoxy radicals: An updated estimation method, *Atmos. Environ.*, *41*, 8468–8485, 2007.

Atkinson, R., and J. Arey, Gas-phase tropospheric chemistry of biogenic volatile organic compounds: a review, *Atmospheric Environment*, *37*(Supplement 2), 197 – 219, doi:DOI:10.1016/S1352-2310(03)00391-1, the 1997 Southern California Ozone Study (SCOS97-NARSTO). Dedicated to the Memory of Dr. Glen Cass (1947-2001), 2003.

Atkinson, R., S. M. Aschmann, A. M. Winer, and J. N. J. Pitts, Kinetics of the gas-phase reactions of no_3 radicals with a series of dialkenes, cycloalkenes, and monoterpenes at 295 ± 1k, *Environ. Sci. Technol.*, *18*, 370–375, 1984.

Atkinson, R., D. L. Baulch, R. A. Cox, J. N. Crowley, R. F. Hampson, R. G. Hynes, M. E. Jenkin, M. J. Rossi, and J. Trow, Evaluated kinetic and photochemical data for atmospheric chemistry: Volume ii - gas phase reactions of organic species, *Atmos. Chem. Phys.*, *6*, 3625 – 4055, 2007.

Atkinson, R., J. Arey, and S. M. Aschmann, Atmospheric chemistry of alkanes: Review and recent developments, *Atmospheric Environment*, *42*(23), 5859 – 5871, doi:DOI:10.1016/j.atmosenv.2007.08.040, selected Papers from the First International Conference on Atmospheric Chemical Mechanisms, 2008.

Atlas, E., Evidence for $\geq c_3$ alkyl nitrates in rural and remote atmospheres, *Nature*, *331*, 426 – 428, 1988.

Bahreini, R., M. Keywood, N. Ng, V. Varutbangkul, S. Gao, R. Flagan, J. Seinfeld, D. Worsnop, and J. Jimenez, Measurements of secondary organic aerosol from the oxidation of cycloalkenes, terpenes and m-xylene using an aerodyne mass spectrometer, *Environ. Sci. Technol.*, *39*, 5674 – 5688, 2005.

Baltensperger, U., et al., Combined determination of the chemical composition and of health effects of secondary organic aerosols: The polysoa project, *Journal of Aerosol Medicine and Pulmonary Drug Delivery*, *21*(1), 145–154, 2008.

Barnes, I., V. Bastian, K. H. Becker, and Z. Tong, Kinetics and products of the reactions of no_3 with monoalkenes, dialkenes, and monoterpenes, *J. Phys. Chem.*, *94*, 2413–2419, 1990.

Benter, T., and R. N. Schindler, Absolute rate coefficients for the reaction of no_3 radicals with simple dienes, *Chem. Phys. Lett.*, *145*(1), 67–70, 1988.

Bergstrom, R. W., P. Pilewskie, P. B. Russell, J. Redemann, T. C. Bond, P. K. Quinn, and B. Sierau, Spectral absorption properties of atmospheric aerosols, *Atmospheric Chemistry and Physics*, *7*(23), 5937–5943, 2007.

Berndt, T., and O. Boge, Gas-phase reaction of no_3 radicals with isoprene: A kinetic and mechanistic study, *Int'l. J. Chem. Kin.*, *29*, 755–765, 1997.

Bey, I., B. Aumont, and G. Toupance, A modeling study of the nighttime radical chemistry in the lower continental troposphere 1. development of a detailed chemical mechanism including nighttime chemistry, *J. Geophys. Res.*, *106*(D9), 9959–9990, 2001.

Bossmeyer, J., T. Brauers, C. Richter, F. Rohrer, R. Wegener, and A. Wahner, Simulation chamber studies on the no_3 chemistry of atmospheric aldehydes, *Geophys. Res. Lett.*, *33*, doi:10.1029/2006GL026778, 2006.

Brimblecombe, P., and G. A. Dawson, Wet removal of highly soluble gases, *J. of Atmos. Chem.*, *2*, 95–107, 1984.

Brown, S. S., H. Stark, S. J. Circiora, and A. R. Ravishankara, In-situ measurement of atmospherc no_3 and n_2 o_5 via cavity ring-down spectroscopy, *Geophys. Res. Lett*, *28*(17), 3227–3230, 2001.

Brown, S. S., et al., Aircraft observations of daytime no_3 and n_2o_5 and their implications for tropospheric chemistry, *Journal of Photochemistry and Photobiology A: Chemistry*, *176*, 270–278, 2005.

Brown, S. S., et al., Nocturnal isoprene oxidation over the northeast united states in summer and its impact on reactive nitrogen partitioning and secondary organic aerosol, *Atmospheric Chemistry and Physics Discussions*, *9*(1), 225–269, 2009.

Bruns, E. A., V. Perraud, A. Zelenyuk, M. J. Ezell, S. N. Johnson, Y. Yu, D. Imre, B. J. Finlayson-Pitts, and M. L. Alexander, Comparison of ftir and particle mass spectrometry for the measurement of particulate organic nitrates, *Environ. Sci. Tech.*, *44*, 1056 – 1061, 2010.

Burns, E. A., V. Perraud, A. Zelenyuk, M. J. Ezell, S. N. Johnson, Y. Yu, D. Imre, B. J. Finlayson-Pitts, and M. L. Alexander, Comparison of ftir and particle mass spectrometry for the measurement of particulate organic nitrates, *Environ. Sci. Tech.*, *44*, 1056 – 1061, 2010.

Calbert, J. G., R. Atkinson, J. A. Kerr, S. Madronich, G. K. Moortgat, T. J. Wallington, and G. Yarwood, *The Mechanisms of Atmospheric Oxidation of the Alkenes*, Oxford University Press, 2000.

Canagartna, M., et al., Chemical and microphysical characteriation of ambient aerosols with the aerodyne aerosol mass spectrometer, *Mass Spectrometry Reviews*, *26*, 185–222, 2007.

Cappa, C. D., A model of aerosol evaporation kinetics in a thermodenuder, *Atmospheric Measurement Techniques Discussions*, *2*(5), 2749–2779, 2009.

Cappa, C. D., and J. L. Jimenez, Quantitative estimates of the volatility of ambient organic aerosol, *Atmospheric Chemistry and Physics Discussions*, *10*(1), 1901–1938, 2010.

Chameides, W. L., R. W. Lindsay, J. Richardson, and C. S. Kiang, The role of biogenic hydrocarbons in urban photochemical smog: Atlanta as a case study, *Science*, *241*(4872), 1473–1475, 1988.

Chang, R. Y.-W., J. G. Slowik, N. C. Shantz, A. Vlasenko, J. Liggio, S. J. Sjostedt, W. R. Leaitch, and J. P. D. Abbatt, The hygroscopicity parameter (κ) of ambient organic aerosol at a field site subject to biogenic and anthropogenic influences: Relationship to degree of aerosol oxidation, *Atmospheric Chemistry and Physics Discussions*, *9*(6), 25,323–25,360, 2009.

Chapman, S., and T. G. Cowling, *The mathematical theory of non-uniform gases; an account of the kinetic theory of viscosity, thermal conduction and diffusion in gases*, Caimbridge University Press, 1970.

Charlson, R. J., J. Langer, H. Rodhe, C. B. Leovy, and S. G. Warren, Perturbation of the northern hemisphere radiative balance by backscattering from anthropogenic sulfate aerosols, *Tellus A*, *43*, 152–163, 1991.

Cleary, P. A., J. G. Murphy, P. J. Wooldridge, D. A. Day, D. B. Millet, M. McKay, A. H. Goldstein, and R. C. Cohen, Observations of total alkyl nitrates within the sacramento urban plume, *Atmospheric Chemistry and Physics Discussions*, *5*(4), 4801–4843, 2005.

Clegg, S. L., M. J. Kleeman, R. J. Griffin, and J. H. Seinfeld, Effects of uncertainties in the thermodynamic properties of aerosol components in an air quality model - part 2: Predictions of the vapour pressures of organic compounds, *Atmospheric Chemistry and Physics*, *8*(4), 1087–1103, 2008.

Coakley, J. A., Jr., and R. D. Cess, Response of the ncar community climate model to the radiative forcing by the naturally occurring tropospheric aerosol, *Journal of the Atmospheric Sciences*, *42*(16), 1677–1692, 1985.

Cohen, A. J., et al., The global burden of disease due to outdoor air pollution, *Journal of Toxicology and Environmental Health*, *68*(13), 2005.

Cottrell, L., R. Griffin, J. Jimenez, U. I. Z. L. Zhang, Q., P. Beckman, B. Sive, and R. Talbot, Submicron particles at thompson farm during icartt measured using aerosol mass spectrometry, *Journal. of Geophysical Research*, p. 113, 2008.

Crowley, J. N., and T. J. Dillon, Direct detection of oh formation in the reactions of ho_2 with $ch_3c(o)o_2$ and other substituted peroxy radicals, *Atmos. Chem. Phys.*, *8*, 4877–4889, 2008.

D'Anna, B., O. Andresen, Z. Gefen, and C. J. Nielsen, Kinetic study of oh and no_3 radical reactions with 14 alihatic aldehydes, *Phys. Chem. Chem. Phys.*, *3*, 3057–3063, doi:10.1039/b103623h, 2001.

D'Anna, B., A. Wisthaler, Ø. Andreasen, A. Hansel, J. Hjorth, N. R. Jensen, C. J. Nielsen, Y. Stenstrøm, and J. Viidanoja, Atmospheric chemistry of c_3-c_6 cycloalkanecarbaldehydes, *J. Phys. Chem. A.*, *109*, 5104 – 5118, doi:10.1021/jp044495g, 2005.

Day, D. A., P. J. Wooldridge, M. Dillon, J. A. Thornton, and R. C. Cohen, A thermal dissociation laser-induced fluorescence instrument for in situ detection of no_2, peroxy nitrates, alkyl nitrates, and hno_3, *J. Geophys. Res.*, *107*, 2002.

Day, D. A., M. B. Dillon, P. J. Wooldridge, J. A. Thornton, R. S. Rosen, E. C. Wood, and R. C. Cohen, On alkyl nitrates, o_3, and the "missing no_y", doi:10.1029/2003JD003685, 2003.

de Gouw, J. A., et al., Budget of organic carbon in a polluted atmosphere: Results from the new england air quality study in 2002, *J. Geophys. Res.*, *110*, D1630S, 2005.

DeCarlo, P. F., et al., Field-deployable, high-resolution, time-of-flight aerosol mass spectrometer, *Anal. Chem.*, *78*, 8281–8289, 2006.

Dlugokencky, E. J., and C. J. Howard, Studies of no_3 radical reactions with some atmospheric organic compounds at low pressures, *J. Phys. Chem*, *93*, 1091–1096, 1989.

Dockery, D. W., C. A. Pope, X. Xu, J. D. Spengler, J. H. Ware, M. E. Fay, B. G. Ferris, and F. E. Speizer, An association between air pollution and mortality in six u.s. cities, *The New England Journal of Medicine*, *329*(24), 1753–1759, 1993.

Donahue, N. M., C. O. S. A. L. Robinson, and S. N. Pandis, Coupled partitioning, dilution, and chemical aging of semivolatile organics, *Environ. Sci. Technol.*, *40*, 2635 – 2643, 2006.

Dorn, H.-P., et al., Intercomparison of no_3 measurement techniques at the simulation chamber saphir, in preparation, 2009.

Dubé, W. P., S. S. Brown, H. D. Osthoff, M. R. Nunley, S. J. Circiora, M. W. Paris, R. J. McLaughlin, and A. R. Ravishankara, Aircraft instrument for simultaneous, in situ measurement of no_3 and n_2 o_5 via pulsed cavity ring-down spectroscopy, *Rev. Sci. Inst.*, *77*, 2006.

Dzepina, K., et al., Detection of particle-phase polycyclic aeromatic hydrocarbons in mexico city using and aerosol mass spectrometer, *Int'l. J. Mass. Spec.*, *263*, 152–170, 2007.

Epstein, S. A., I. Riipinen, and N. M. Donahue, A semiempirical correlation between enthalpy of vaporization and saturation concentration for organic aerosol, doi:10.1021/es902497z, 2009.

Farmer, D. K., and R. C. Cohen, Observations of hno_3, σan, σpn and no_2 fluxes: evidence for rapid ho_x chemistry within a pine forest canopy, *Atmospheric Chemistry and Physics*, *8*(14), 3899–3917, 2008.

Farmer, D. K., A. Matsunga, K. S. Docherty, J. D. Surratt, J. H. Seinfeld, P. J. Ziemann, and J. L. Jimenez, Response of an aerosol mass spectrometer to organonitrates and organosulfates and implications for atmospheric chemistry, *Proc. Natl. Acad. Sci. USA*, *xx*, xx, 2010.

Fiore, A. M., L. W. Horowitz, D. W. Purves, H. I. Levy, M. J. Evans, Y. Want, Q. Li, and R. M. Yantosca, Evaluating the contribution of changes in isoprene emissions to surface ozone trends over the eastern united states, *J. Geophys. Res.*, *110*, doi:10.1029/2004JD005485, 2005.

Forster, P., et al., *Climate Change 2007: The Physical Science Basis. Contribution of Working Group I to the Fourth Assessment Report of the Intergovernmental Panel on Climate Change*, 129-234 pp., Caimbridge University Press, 2007.

Fountoukis, C., et al., Thermodynamic characterization of mexico city aerosol during milagro 2006, *Atmospheric Chemistry and Physics*, *9*(6), 2141–2156, 2009.

Fry, J. L., et al., Organic nitrate and secondary organic aerosol yield from no_3 oxidation of -pinene evaluated using a gas-phase kinetics/aerosol partitioning model, *Atmospheric Chemistry and Physics*, *9*(4), 1431–1449, 2009.

Fuchs, H., W. Dubé, S. Ciciora, and S. Brown, Determination of inlet transmission and conversion efficiencies for in situ measurements of the nocturnal nitrogen oxides, no_3, n_2o_5 and no_2 via pulsed cavity ring-down spectroscopy, *Anal. Chem.*, *80*(15), 6010–6017, 2008.

Fuchs, H., et al., Intercomparison of measurements of no_2 concentrations in the atmosphere simulation chamber saphir during the no3comp campaign, *Atmospheric Measurement Techniques*, *3*(1), 21–37, 2010.

Fuentes, J. D., D. Wang, D. R. Bowling, M. Potosnak, R. K. Monson, W. S. Goliff, and W. R. Stockwell, Biogenic hydrocarbon chemistry within and above a mixed desciduous forest, *J. Atmos. Chem.*, *56*, 165–185, doi:10.1007/s10874-006-9048-4, 2007.

Garland, J. A., and S. A. Penkett, Absorption of peroxy acetyl nitrate and ozone by natural surfaces, *Atmos. Environ.*, *10*, 1127–1131, 1976.

Garnes, L. A., and D. T. Allen, Size distributions of organonitrates in ambient aerosol collected in houston, texas, *Aero. Sci. Tech.*, *36*, 983 – 992, 2002.

Geyer, A., et al., Direct observations of daytime no_3: Implications for urban boundary layer chemistry, *J. Geophys. Res.*, *108*, doi:10.1029/2002JD002967, 2003a.

Geyer, A., et al., Nighttime formation of peroxy and hydroxyl radicals during the berlioz campaign: Observations and modeling studies, *J. Geophys. Res.*, *108*(D4), doi:10.1029/2001JD000656, 2003b.

Glasius, M., M. F. Carlsen, T. S. Hansen, and C. Lohse, Measurements of nitrogen dioxide on funen using diffusion tubes, *Atmospheric Environment*, *33*(8), 1177 – 1185, doi:DOI:10.1016/S1352-2310(98)00285-4, 1999.

Goldstein, A. H., and I. E. Galbally, Known and unexplored organic constituents in the earth's atmosphere, *Environ. Sci. Technol.*, *41*, 1541 – 1521, doi:10.1021/es072476p, 2007.

Gómez-González, Y., et al., Characterization of organosulfates from the photooxidation of isoprene and unsaturated fatty acids in ambient aerosol using liquid chromatography/(-) electrospray ionization mass spectrometry, *J. Mass Spectrom*, *43*, 371–382, 2008a.

Gómez-González, Y., et al., Characterization of organosulfates from the photooxidation of isoprene and unsaturated fatty acids in ambient aerosol using liquid chromatography/(-) electrospray ionization mass spectrometry, *J. Mass. Spec.*, *43*, 371 – 382, 2008b.

Grieshop, A. P., N. M. Donahue, and A. L. Robinson, Is the gas-particle partitioning in alpha-pinene secondary organic aerosol reversible?, *Geophys. Res. Lett.*, *34*, L14,810, doi:10.1029/2007GL029987, 2007.

Guenther, A., T. Karl, P. Harley, C. Wiedinmyer, P. I. Palmer, and C. Geron, Estimates of global terrestrial isoprene emissions using megan (model of emissions of gases and aerosols from nature), *Atmos. Chem. Phys*, *6*, 3181–3210, 2006.

Guenther, A., et al., A global model of natural volatile organic compound emissions, *J. Geophys. Res.*, *100*, 8873–8892, doi:10.1029/94JD02950, 1995.

Hallquist, M., et al., The formation, properties and impact of secondary organic aerosol: current and emerging issues, *Atmospheric Chemistry and Physics*, *9*(14), 5155–5235, 2009.

Hasson, A. S., G. S. Tyndall, and J. J. Orlando, A product yield study of the reaction of ho_2 radicals with ethyl peroxy ($c_2h_5o_2$), acetyl peroxy ($ch_3c(o)o_2$), and acetonyl peroxy ($ch_3c(o)ch_2o_2$) radicals, *J. Phys. Chem. A.*, *108*, 5979–5989, 2004.

Hasson, A. S., K. T. Kuwata, M. C. Arroyo, and E. B. Petersen, Theoretical studies of the reaction of hydroperoxy radicals (ho_2) with ethyl peroxy ($ch_3ch_2o_2$), acetyl peroxy ($ch_3c(o)o_2$), and acetonyl peroxy ($ch_3c(o)ch_2o_2$) radicals, *J. Photochem. and Photobio. A: Chemistry*, *176*, 218–230, 2005.

Hatakeyama, S., K. Izumi, T. Fukuyama, H. Akimoto, and N. Washida, Reactions of oh with α-pinene and β-pinene in air: estimate of global co production from the atmospheric oxidation of terpenes, *J. Geophys. Res.*, *96*(D1), 947–958, 1991.

Heald, C. L., D. J. Jacob, R. J. Park, L. M. Russell, B. J. Huebert, J. H. Seinfeld, H. Liao, and R. J. Weber, A large organic aerosol source in the free tropospher missing from current models, *Geophys. Res. Lett.*, *32*, L18,809, doi:10.1029/2005GL023831, 2005.

Henze, D. K., and J. H. Seinfeld, Global secondary organic aerosol from isoprene oxidation, *Geophys. Res. Lett.*, *33*, doi:10.1029/2006GL025976, 2006.

Hilal, S. H., L. A. Carreira, and S. W. Karickhoff, Prediction of the vapor pressure, boiling point, heat of vaporization and diffusion coefficient of organic compounds, *QSAR & Combinatorial Science*, *565*, 22, 2003.

Hilal, S. H., L. A. Carreira, and S. W. Karickhoff, Prediction of the solubility, activity coefficient, gas/liquid and liquid/liquid distribution coefficients of organic compounds, *QSAR & Combinatorial Science*, *23*, 709, 2004.

Hoffmann, T., J. R. Odum, F. Bowman, D. Collins, D. Klockow, R. C. Flagan, and J. H. Seinfeld, Formation of organic aerosols from the oxidation of biogenic hydrocarbons, *J. Atmos. Chem.*, *26*(2), 189–222, doi:10.1023/A:1005734301837, 1997.

Horowitz, L. W., J. Liang, G. M. Gardner, and D. J. Jacob, Export of reactive nitrogen from north america during summertime: Sensitivity to hydrocarbon chemistry, *J. Geophys. Res.*, *103*(D11), 13,451–13,476, 1998.

Horowitz, L. W., A. M. Fiore, G. P. Milly, R. C. Cohen, A. Perring, P. J. Wooldridge, P. G. Hess, L. K. Emmons, and J. L. Lamarque, Observational constraints on the chemistry of isoprene nitrates over the eastern united states, *J. Geophys. Res.*, 2007.

Hudman, R. C., et al., Ozone production in transpacific asian pollution plumes and implications for ozone air quality in california, *J. Geophys. Res.*, *109*, D23S10, 2004.

Huffman, J. A., et al., Chemically-resolved aerosol volatility measurements from two megacity field studies, *Atmospheric Chemistry and Physics Discussions*, *9*(1), 2645–2697, 2009.

Ingham, D. B., Diffusion of aerosols from a stream flowing through a cylindrical tube, *Aerosol Science*, *6*, 125 – 132, 1975.

Jang, M., N. M. Czoschke, S. Lee, and R. M. Kamens, Heterogeneous atmospheric aerosol production by acid-catalyzed particle-phase reactions, *Science*, *298*, 814–817, 2002.

Jenkin, M. E., M. D. Hurley, and T. J. Wallington, Investigation of the radical product channel of the $ch_3c(o)o_2$ + ho_2 reaction in the gas phase, *Phys. Chem. Chem. Phys.*, *9*, 3149–3162, doi:10.1039/b702757e, 2007.

Jerrett, M., R. T. Burnett, C. Pope, III, K. Ito, G. Thurston, D. Krewski, Y. Shi, E. Calle, and M. Thun, Long-term ozone exposure and mortality, *The New England Journal of medicine*, *360*(11), 1085–1095, 2009.

Jimenez, J. L., et al., Ambient aerosol sampling using the aerodyne aerosol mass spectrometer, *J. Geophys. Res.*, *108*, doi:10.1029/2001JD001213, 2003.

Jimenez, J. L., et al., Evolution of organic aerosols in the atmosphere, *Science*, *326*(5959), 1525 – 1529, doi:10.1126/science.1180353, 2009.

Jordan, C., P. Ziemann, R. Griffin, Y. Lim, R. Atkinson, and J. Arey, Modeling soa formation from oh reactions with c8-c17 n-alkanes, *Atmospheric Environment*, *42*(34), 8015 – 8026, doi:DOI:10.1016/j.atmosenv.2008.06.017, 2008.

Kalberer, M., et al., Identification of polymers as major components of atmospheric organic aerosols, *Science*, *303*, 1659–1662, 2004.

Kroll, J. H., and J. H. Seinfeld, Chemistry of secondary organic aerosol: Formation and evolution of low-volatility organics in the atmosphere, *Atmos. Environ.*, *42*, 3593–3624, 2008.

Kroll, J. H., N. L. Ng, S. M. Murphy, R. C. Flagan, and J. H. Seinfeld, Secondary organic aerosol formation from isoprene photooxidation under high-no_x conditions, *Geophys. Res. Lett.*, *32*, doi:10.1029/2005GL023637, 2005.

Kroll, J. H., L. N. Ng, S. M. Murphy, R. C. Flagan, and J. H. Seinfeld, Secondary organic aerosol formation from isoprene photooxidation, *Environ. Sci. Technol*, *40*(6), 1869–1877, 2006.

Kwok, E. S. C., and R. Atkinson, Estimatino of hydroxyl radical reaction rate constants for gas-phase organic compounds using a structure-reactivity relationship: an update, *Atmos. Environ.*, *29*(14), 1685–1695, 1995.

Kwok, E. S. C., S. M. Aschmann, J. Arey, and R. Atkinson, Product formation from the reaction of the no$_3$ radical with isoprene and rate constants for the reactions of methacrolein and methyl vinyl ketone with the no$_3$ radical, *Int'l. J. of Chem. Kin.*, *28*, 925–934, 1996.

Laden, F., J. Schwartz, F. E. Spelzer, and D. W. Dockery, Reduction in fine particulate air pollution and mortality: Extended follow-up of the harvard six cities study, *American Journal of Respritory and Critical Care Medicine*, *173*, 667–672, 2006.

Lanz, V. A., M. R. Alfarra, U. Baltensperger, B. Buchmann, C. Hueglin, and A. S. H. Prévôt, Source apportionment of submicron organic aerosols at an urban site by factor analytical modelling of aerosol mass spectra, *Atmoc. Chem. Phys.*, *7*, 1503–1522, 2007.

Lanz, V. A., et al., Source attribution of submicron organic aerosols during wintertime inversions by advanced factor analysis of aerosol mass spectra, *Environ. Sci. Technol.*, *42*, 214–220, 2008.

Lelieveld, J., et al., Atmospheric oxidation capacity sustained by a tropical forest, *Nature*, *452*, doi:10.1038/nature06870, 2008.

Lewis, C. W., G. A. Klouda, and W. D. Ellenson, Radiocarbon measurement of the biogenic contribution to summertime pm-2.5 ambient aerosol in nashville, tn, *Atmospheric Environment*, *38*(35), 6053 – 6061, doi:DOI:10.1016/j.atmosenv.2004.06.011, 2004.

Lim, Y. B., and P. J. Ziemann, Products and mechanism of secondary organic aerosol formation from reactions of n-alkanes with oh radicals in the presence of no$_x$, *Environ. Sci. Tech.*, *39*, 9229 – 9236, 2005.

Lippmann, M. (Ed.), *Environmental Toxicants: Human Exposures and Their Health Effects*, John Wiley & Sons, Inc., 2009.

Luxenhofer, O., M. Schneider, M. Dambach, and K. Ballschmiter, Semivolatile long chain c6-c17 alkyl nitrates as trace compounds in air, *Chemosphere*, *33*(3), 393 – 404, doi: DOI:10.1016/0045-6535(96)00205-6, 1996.

Matson, P., K. A. Lohse, and S. J. Hall, The globalization of nitrogen deposition: Consequences for terrestrial ecosystems, *Ambio*, *31*, 113–119, 2002.

Moffet, R. C., B. de Foy, L. T. Molina, M. J. Molina, and K. A. Prather, Measurement of ambient aerosols in northern mexico city by single particle mass spectrometry, *Atmospheric Chemistry and Physics*, *8*(16), 4499–4516, 2008.

Muller, L., M.-C. Reinnig, J. Warnke, and T. Hoffmann, Unambiguous identification of esters as oligomers in secondary organic aerosol formed from cyclohexene and cyclohexene α-pinene ozonolysis, *Atmos. Chem. Phys.*, *8*, 1423–1433, 2008.

Munger, J. W., S. C. Wofsy, P. S. Bakwin, S.-M. Fan, M. L. Goulden, B. C. Daube, and A. H. Goldstein, Atmospheric deposition of reactive nitrogen oxides and ozone in a temperate deciduous forest and a subarctic woodland. 1. measurements and mechanisms, *J. Geophys. Res.*, *101*, 12,639–12,657, 1996.

Murphy, D. M., et al., Single-particle mass spectrometry of tropospheric aerosol particles, *J. Geophys. Res.*, *111*, D23S32, doi:10.1029/2006JD007340, 2007.

Muthuramu, K., P. B. Shepson, and J. M. O'Brien, Preparation, analysis, and atmospheric production of multifunctional organic nitrates, *Environ. Sci. Technol.*, *27*(6), 1117–1124, doi:10.1021/es00043a010, 1993.

Mylonas, D. T., D. T. Allen, S. H. Ehrman, and S. E. Pratsinis, The sources and size distributions of organonitrates in los angeles aerosol, *Atmospheric Environment. Part A. General Topics*, *25*(12), 2855 – 2861, doi:DOI:10.1016/0960-1686(91)90211-O, 1991.

Ng, N. L., J. H. Kroll, A. W. H. Chan, P. S. Chhabra, R. C. Flagan, and J. H. Seinfeld, Secondary organic aerosol formation from m-xylene, toluene, and benzene, *Atmospheric Chemistry and Physics*, *7*(14), 3909–3922, 2007a.

Ng, N. L., et al., Effect of no_x level on secondary organic aerosol (soa) formation from the photooxidation of terpenes, *Atmospheric Chemistry and Physics*, *7*(19), 5159–5174, 2007b.

Ng, N. L., et al., Secondary organic aerosol (soa) formation from reaction of isoprene with nitrate radicals (no_3), *Atmos. Chem. Phys.*, *8*, 4117–4140, 2008.

Nichols, P. L. J., A. B. Magnusson, and J. D. Ingham, Synthesis of nitric esters by the addition of nitric acid to the ethylene oxide ring, *J. Am. Chem. Soc.*, *75*, 4255–4258, 1953.

Noda, J., G. Nyman, and S. Langer, Kinetics of the gas-phase reaction of some unsaturated alcohols with the nitrate radical, *J. Phys. Chem. A*, *106*, 945–951, 2002.

Northway, M. J., et al., Demonstration of a vuv lamp photoionization source for improved organic speciation in an aerosol mass spectrometer, *Aerosol Sci. Technol.*, *41*, 828–839, 2007.

Noziére, B., I. Barnes, and K.-H. Becker, Product study and mechanisms of the reactions of α-pinene and of pinonaldehyde with oh radicals, *J. Geophys. Res.*, *104*(D19), 23,645 – 23,656, 1999.

Odum, J. R., T. Hoffmann, F. Bowman, D. Collins, R. C. Flagan, and J. H. Seinfeld, Gas/partitioning and secondary organic aerosol yields, *Environ. Sci. Technol.*, *30*, 2580–2585, 1996.

Offenberg, J. H., C. W. Lewis, M. Lewandowski, M. Jaoui, T. E. Kleindienst, and E. O. Edney, Contributions of toluene and α-pinene to soa formed in an irradiated toluene/α-pinene/no_x/air mixture: Comparison of results using ^{14}c content and soa organic tracer methods, *Environ. Sci. Technol.*, *41*, 3972 – 3976, 2007.

Olivier, J. G. J., J. A. Van Aardenne, F. J. Dentener, V. Pagliari, L. N. Ganzeveld, and J. A. H. W. Peters, Recent trends in global greenhouse gas emissions: regional trends 1970-2000 and spatial distribution of key sources in 2000, *Environmental Sciences*, *2*, 81–99, 2005.

Palen, E. J., D. T. Allen, S. N. Pandis, S. E. Paulson, J. H. Seinfeld, and R. C. Flagan, Fourier transform infrared analysis of aerosol formed in the photo-oxidation of isoprene and [beta]-pinene, *Atmospheric Environment. Part A. General Topics*, *26*(7), 1239 – 1251, doi:DOI:10.1016/0960-1686(92)90385-X, 1992.

Pan, X. L., P. Yan, J. Tang, J. Z. Ma, Z. F. Wang, A. Gbaguidi, and Y. L. Sun, Observational study of influence of aerosol hygroscopic growth on scattering coefficient over rural area near beijing mega-city, *Atmospheric Chemistry and Physics*, *9*(19), 7519–7530, 2009.

Pandis, S. N., S. E. Paulson, J. H. Seinfeld, and R. C. Flagan, Aerosol formation in the photooxidation of isoprene and β-pinene, *Atmospheric Environment. Part A. General Topics*, *25*(5-6), 997 – 1008, doi:DOI:10.1016/0960-1686(91)90141-S, 1991.

Pankow, J. F., An absorption model of gas/particle partitioning of organic compounds in the atmosphere, *Atmospheric Environment*, *28*(2), 185 – 188, doi:DOI:10.1016/1352-2310(94)90093-0, 1994a.

Pankow, J. F., An absorption model of the gas/aerosol partitioning involved in the formation of secondary organic aerosol, *Atmospheric Environment*, *28*(2), 189 – 193, doi:DOI:10.1016/1352-2310(94)90094-9, 1994b.

Pankow, J. F., and W. E. Asher, Simpol.1: A simple group contribution method for predicting vapor pressures and enthalpies of vaporization of multifunctional organic compounds, *Atmos. Chem. Phys.*, (8), 2773–2796, 2008.

Paredes-Miranda, G., W. P. Arnott, J. L. Jimenez, A. C. Aiken, J. S. Gaffney, and N. A. Marley, Primary and secondary contributions to aerosol light scattering and absorption in mexico city during the milagro 2006 campaign, *Atmospheric Chemistry and Physics Discussions*, *8*(5), 16,951–16,979, 2008.

Paulot, F., J. D. Crounse, H. G. Kjaergaard, J. H. Kroll, J. H. Seinfeld, and P. O. Wennberg, Isoprene photooxidation: new insights into the production of acids and organic nitrates, *Atmospheric Chemistry and Physics*, *9*(4), 1479–1501, 2009.

Perring, A. E., A. Wisthaler, M. Graus, P. J. Wooldridge, A. Lookwood, L. Mielke, P. B. Shepson, A. Hansel, and R. C. Cohen, A product study of the isoprene + no_3 reaction, *Atmos. Chem. Phys. Discuss.*, *9*, 5231–5261, 2009.

Petters, M. D., and S. M. Kreidenweis, A single parameter representation of hygroscopic growth and cloud condensation nucleus activity, *Atmospheric Chemistry and Physics*, *7*(8), 1961–1971, 2007.

Pope, C. A., III, and D. W. Dockery, Health effects of fine particulate air pollution: Lines that connect, *J. Air & Waste Manage. Assoc.*, *56*, 709–742, 2006.

Presto, A. A., K. E. H. Hartz, and N. M. Donahue, Secondary organic aerosol production from terpene ozonolysis. 2. effect of no_x concentration, *Environ. Sci. Technol.*, *39*, 7046–7054, 2005.

Ramanathan, V., et al., Indian ocean experiment: An integrated analysis of the climate forcing and effects of the great indo-asian haze, *J. Geophys. Res.*, *106*(D22), 28,371–28,398, 2001.

Ridley, B. A., F. E. Grahek, and J. G. Walega, A small, high-sensitivity, medium-response ozone detector suitable for measurements from light aircraft, *J. Atmos. Oceanic Technol.*, *9*, 142–149, 1992.

Riipinen, I., J. R. Pierce, N. M. Donahue, and S. N. Pandis, Equilibration time scales of organic aerosol inside thermodenuders: Evaporation kinetics versus thermodynamics, *Atmospheric Environment*, *44*(5), 597 – 607, doi:DOI:10.1016/j.atmosenv.2009.11.022, 2010.

Rohrer, F., B. Bohn, T. Brauers, D. Bruning, F.-J. Johnen, A. Wahner, and J. Kleffmann, Characterisation of the photolytic hono-source in the atmosphere simulation chamber saphir, *Atmos. Chem. Phys.*, *5*, 2189 – 2201, 2005.

Rollins, A. W., J. L. Fry, J. F. Hunter, J. H. Kroll, D. R. Worsnop, S. W. Singaram, and R. C. Cohen, Elemental analysis of aerosol organic nitrates with electron ionization high-resolution mass spectrometry, *Atmospheric Measurement Techniques*, *3*(1), 301–310, 2010.

Rollins, A. W., et al., Isoprene oxidation by nitrate radical: alkyl nitrate and secondary organic aerosol yields, *Atmospheric Chemistry and Physics Discussions*, *9*(2), 8857–8902, 2009.

Rosen, R. S., E. C. Wood, P. J. Wooldridge, J. A. Thornton, D. A. Day, W. Kuster, E. J. Williams, B. T. Jobson, and R. C. Cohen, Observations of total alkyl nitrates during texas air quality study 2000: Implications for o3 and alkyl nitrate photochemistry, *J. Geophys. Res.*, *109*, D07,303, doi:10.1029/2003JD004227, 2004.

Saleh, R., A. Shihadeh, and A. Khlystov, Determination of evaporation coefficients of semi-volatile organic aerosols using an integrated volume-tandem differential mobility analysis (iv-tdma) method, *J. Aero. Sci.*, *40*, 1019 – 1029, 2009.

Sander, R., Compilation of henry's law constants for inorganic and organic species of potential importance in environmental chemistry (version 3), http://www.mpch-mainz.mpg.de/ sander/res/henry.html#4, 1999.

Sandu, A., and R. Sander, Technical note: Simulating chemical systems in fortran90 and matlab with the kinetic preprocessor kpp-2.1, *Atmospheric Chemistry and Physics*, *6*(1), 187–195, 2006.

Saunders, S. M., M. E. Jenkin, R. G. Derwent, and M. J. Pilling, Protocol for the development of the master chemical mechanism, mcm v3 (part a): tropospheric degradation of non-aromatic volatile organic compounds, *Atmospheric Chemistry and Physics*, *3*(1), 161–180, 2003.

Schneider, M., O. Luxenhofer, A. Deissler, and K. Ballschmiter, C_1-c_{15} alkyl nitrates, benzyl nitrate, and bifunctional nitrates: Measurements in california and south atlantic air and global comparison using c_2cl_4 and $chbr_3$ as marker molecules, *Environ. Sci. Technol.*, *32*, 3055–3062, 1998.

Seinfeld, J. H., and S. N. Pandis, *Atmospheric Chemistry and Physics: From Air Pollution to Climate Change*, 1998.

Shepson, P. B., K. G. Anlauf, J. W. Bottenheim, H. A. Wiebe, N. Gao, K. Muthuramu, and G. I. Mackay, Alkyl nitrates and their contribution to reactive nitrogen at a rural site in ontario, *Atmospheric Environment. Part A. General Topics*, *27*(5), 749 – 757, doi:DOI:10.1016/0960-1686(93)90192-2, 1993.

Shepson, P. B., E. Mackay, and K. Muthuramu, Henry's law constants and removal processes for several atmospheric β-hydroxy alkyl nitrates, *Environ. Sci. Technol.*, *30*, 3618–3623, 1996.

Skov, H., J. Hjorth, C. Lohse, N. R. Jensen, and G. Restelli, Products and mechanisms of the reactions of the nitrate radical (no_3) with isoprene, 1,3-butadiene and 2,3-dimethyl-1,3-butadiene in air, *Atmos. Environ.*, *26A*(15), 2771–2783, 1992.

Song, C., K. Na, and D. R. C. III, Impact of the hydrocarbon to no_x ratio on secondary organic aerosol formation, *Environ. Sci. Technol.*, *39*, 3143–3149, 2005.

Spittler, M., Untersuchungen zur troposphärischen oxidation von limonen: Produktanalysen, aerosolbildung und photolyse von produkten, Ph.D. thesis, 2001.

Starn, T. K., P. B. Shepson, S. B. Bertman, D. D. Riemer, R. G. Zika, and K. Olszyna, Nighttime isoprene chemistry at an urban-impacted forest site, *J. Geophys. Res.*, *103*, 22,437–22,447, 1998.

Steinbacher, M., J. Dommen, C. Ordonez, S. Reimann, F. C. Grüebler, J. Staehelin, S. Andreani-Aksoyoglu, and A. S. H. Prevot, Volatile organic compounds in the po basin. part b: Biogenic vocs, *J. Atmos. Chem.*, *51*, 293–315, doi:10.1007/s10874-005-3577-0, 2005.

Stroud, C. A., et al.

Suh, I., W. Lei, and R. Zhang, Experimental and theoretical studies of isoprene reaction with no_3, *J. Phys. Chem. A*, *105*, 6471–6478, 2001.

Surratt, J. D., et al., Chemical composition of secondary organic aerosol formed from the photooxidation of isoprene, *J. Phys. Chem. A*, *110*, 9665–9690, 2006.

Surratt, J. D., et al., Organosulfate formation in biogenic secondary organic aerosol, *J. Phys. Chem. A*, *112*, 8345–8378, 2008.

Szidat, S., et al., Radiocarbon (14c)-deduced biogenic and anthropogenic contributions to organic carbon (oc) of urban aerosols from zrich, switzerland, *Atmospheric Environment*, *38*(24), 4035 – 4044, doi:DOI:10.1016/j.atmosenv.2004.03.066, includes Special Issue Section on Results from the Austrian Project on Health Effects of Particulates (AUPHEP), 2004.

Thornton, J., P. Wooldridge, R. Cohen, E. Williams, D. Hereid, F. Fehsenfeld, J. Stutz, and B. Alicke, Comparisons of in situ and long path measurements of no_2 in urban plumes, *J. Geophys. Res.*, *108*(D16), 4496, doi:10.1029/2003JD003559, 2003.

Thornton, J. A., P. J. Wooldridge, and R. C. Cohen, Atmospheric no_2: In situ laser-induced fluorescence detection at parts per trillion mixing ratios, *Anal. Chem.*, *72*, 528–539, 2000.

Thornton, J. A., et al., Ozone production rates as a function of no_X abundances and ho_X production rates in the nashville urban plume, *J. Geophys. Res.*, *107*, doi:10.1029/2001JD000932, 2002.

Tobias, H. J., P. M. Kooiman, K. S. Docherty, and P. J. Ziemann, Real-time chemical analysis of organic aerosols using a thermal desorption particle beam mass spectrometer, *Aerosol Sci. Tech.*, *33*, 170–190, 2000.

Treves, K., and Y. Rudich, The atmospheric fate of c_3 - c_6 hydroxyalkyl nitrates, *J. Phys. Chem. A.*, *107*, 7809–7817, 2003.

Treves, K., L. Shragina, and Y. Rudich, Henry's law constants of some β-, γ-, and δ-hydroxy alkyl nitrates of atmospheric interest, *Environ. Sci. Technol.*, *34*, 1197–1203, 2000.

Turnipseed, A. A., et al., Eddy covariance fluxes of peroxyacetyl nitrates (pans) and no_y to a coniferous forest, *J. Geophys. Res.*, *111*, doi:10:1029/2005JD006631, 2006.

Vaughan, S., C. Canosa-Mas, C. Pfrang, D. Shallcross, L. Watson, and R. Wayne, Kinetic studies of reactions of the nitrate radical (no_3) with peroxy radicals (ro_2): an indirect source of oh at night?, *Phys. Chem. Chem. Phys.*, *8*, 3749–3760, doi:10.1039/b605569a, 2006.

Volkamer, R., et al., Secondary organic aerosol formation from anthropogenic air pollution: Rapid and higher than expected, *Geophys. Res. Lett.*, *33*, L17,811, doi:10.1029/2006GL026899, 2006.

von Kuhlmann, R., M. G. Lawrence, U. Poschl, and P. J. Crutzen, Sensitivities in global scale modeling of isoprene, *Atmos. Chem. Phys.*, *4*, 1–17, 2004.

Weber, R. J., et al., A study of secondary organic aerosol formation in the anthropogenic-influenced southeastern united states, *J. Geophys. Res.*, *112*, D13,302, 2007.

Wegener, R., T. Brauers, R. Koppmann, S. R. Bares, F. Roher, R. Tillmann, A. Wahner, A. Hansel, and A. Wisthaler, Simulation chamber investigation of the reactions of ozone with short-chained alkenes, *J. Geophys. Res.*, *112*, doi:10.1029/2006JD007531, 2007.

Wille, U., E. Becker, R. N. Schindler, I. T. Lancer, G. Poulet, and G. Le Bras, A discharge flow mass-spectrometric study of the reaction between the no_3 radical and isoprene, *J. Atmos. Chem*, *13*, 183–193, 1991.

Williams, B. J., A. H. Goldstein, N. M. Kreisberg, and S. V. Hering, An in-situ instrument for speciated organic composition of atmospheric aerosols: Thermal desorption aerosol gc/ms-fid (tag), *Aero. Sci. Tech.*, *40*, 627–638, 2006.

Wolfe, G. M., R. L. N. Yatavelli, J. A. Thornton, M. McKay, A. H. Goldstein, B. LaFranchi, K.-E. Min, and R. C. Cohen, Eddy covariance fluxes of acyl peroxy nitrates (pan, ppn, and mpan) above a ponderosa pine forest, *Atmospheric Chemistry and Physics Discussions*, *8*(5), 17,495–17,548, 2008.

Wooldridge, P. J., et al., Total peroxy nitrates (σpns) in the atmosphere: the thermal dissociation-laser induced fluorescence (td-lif) technique and comparisons to speciated pan measurements, *Atmospheric Measurement Techniques Discussions*, *2*(6), 3055–3097, 2009.

Wu, S., L. J. Mickley, D. J. Jacob, J. A. Logan, R. M. Yantosca, and D. Rind, Why are there large differences between models in global budgets of tropospheric ozone?, *J. Geophys. Res.*, *112*, doi:10.1027/2006JD007801, 2007.

Yu, H., et al., A review of measurement-based assessments of the aerosol direct radiative effect and forcing, *Atmospheric Chemistry and Physics*, *6*(3), 613–666, 2006.

Yu, Y., et al., Photooxidation of α-pinene at high relative humidity in the presence of increasing concentrations of no_X, *Atmospheric Environment*, *42*(20), 5044 – 5060, doi: DOI:10.1016/j.atmosenv.2008.02.026, 2008.

Zelenyuk, A., J. Yang, C. Song, R. Zaveri, and D. Imre, A new real-time method for determining particles' sphericity and density: Application to secondary organic aerosol formed by ozonolysis of α-pinene, *Environ. Sci. Technol.*, *42*(21), 8803 – 8038, doi:10.1021/es8013562, 2008.

Zhang, J., K. E. H. Hartz, S. N. Pandis, and N. M. Donahue, Secondary organic aerosol formation from limonene ozonolysis: Homogeneous and heterogeneous influences as a function of no_x, *J. Phys. Chem. A*, *110*, 11,053–11,063, 2006.

Zhang, Q., M. R. Alfarra, D. R. Worsnop, J. D. Allan, H. Coe, M. R. Canagaratna, and J. L. Jimenez, Deconvolution and quantification of hydrocarbon-line and oxygenated organic aerosols based on aerosol mass spectrometry, *Environ. Sci. Technol.*, *39*, 4938–4952, 2005.

Zhang, Q., et al., Ubiquity and dominance of oxygenated species in organic aerosols in anthropogenically-influenced northern hemisphere midlatitudes, *J. Geophys. Res.*, *34*, L13,801, doi:10.1029/2007GL029979, 2007a.

Zhang, S.-H., M. Shaw, J. H. Seinfeld, and R. C. Flagan, Photochemical aerosol formation from α-pinene and β-pinene, *J. Geophys. Res.*, *97*(D18), 20,717–20,729, 1992.

Zhang, Y., J. P. Huang, D. K. Henze, and J. H. Seinfeld, Role of isoprene in secondary organic aerosol formation on a regional scale, *J. Geophys. Res.*, *112*(D20207), doi:10.1029/2007JD008675, 2007b.